UNIVERSITY OF CALGARY

Probing Humics: New Methods and New Models

by

Joseph Robert Melton

A THESIS

SUBMITTED TO THE FACULTY OF GRADUATE STUDIES

IN PARTIAL FULFILLMENT OF THE REQUIREMENTS FOR THE

DEGREE OF MASTER OF SCIENCE

DEPARTMENT OF CHEMISTRY

CALGARY, ALBERTA

June, 2004

UNIVERSITY OF CALGARY

FACULTY OF GRADUATE STUDIES

The undersigned certify that they have read, and recommend to the Faculty of Graduate Studies for acceptance, a thesis entitled "Probing Humics: New Methods and New Models" submitted by Joseph Robert Melton in partial fulfillment of the requirements for the degree of Master of Science.

_____

Supervisor, Dr. C.H. Langford, Department of Chemistry

_____

Dr. E.A. Dixon, Department of Chemistry

_____

Dr. A. S. Hinman, Department of Chemistry

_____

Dr. A. Kantzas, Department of Chemical and Petroleum Engineering

_____

Date

ABSTRACT

Humics substances (HS) are formed by the degradation of organic matter and are ubiquitous in soil and water in the environment. Only recently available evidence provided by state of the art sample interrogation techniques [1-3] shows HS to be a collection of monomers, oligomers, and polymers interacting in a complex pattern of labile aggregational and conformational equilibria under the influence of weak forces (H-bonding, hydrophobic interaction, charge transfer complexing). This structural paradigm shift then demands a similar shift in present thought on binding of contaminants to humics.

Borrowing from combinatorial chemistry, a dynamic combinatorial system (DCS) contains building blocks that are in constant flux, continuously able to form and break new members as they form supramolecular units held together by non-covalent interactions. With the recent structural evidence, it is a natural progression to envision HS as a DCS.

Light scattering experiments and a novel Low-field Nuclear Magnetic Relaxometery (NMR) technique were conducted on a well characterized Laurentian humic acid (LHA) with copper (II) ions in solution. The results from both experiments were comfortably interpreted as that of a DCS.

ACKNOWLEDGEMENTS

First I would like to thank my supervisor, Dr. Cooper H. Langford. Dr. Langford has mastered the deft art of how to guide (not push, pressure or belittle) a graduate student for results. I am very grateful for the experience and for his knowledge, enthusiasm, and understanding. Thank-you.

A lot of people at the University have helped me over the course of this thesis. From the start, Tiona Todoruk was instrumental in getting me started in our lab, as well as guiding me towards this thesis topic and answering my pesky questions. Dr. Dixon, has been a wealth of advice and assistance since her days as my undergraduate program director to her role on my supervisory committee. I am grateful for my exposure to such a helpful and selfless professor. Florence Manalo from TIPM was great for answering any (and many) NMR questions. Dr. Kantzas is due thanks for permitting me use of his NMR and ICP, without which I would not have a thesis, and for sitting on my examining committee. Dr. Hinman greatly helped me out by agreeing to sit on my examining committee as well. Dorothy Fox helped me understand the EPR. Dr. Liu and Xiahou Yan were very gracious is letting me use their laser light scattering apparatus as well as training me on the instrument. As can be seen I used pretty much any instrument that was not ours. Once my data were collected, Dr. Tak Fung gracefully guided me through the world of fitting procedures (whether my ideas were realistic or not). Dr. Gamble provided the calculations that appear in the discussion for copper hydrolysis. The many support staff at the Uni are deserving of my gratitude, especially Bonnie King and Ed DeBruyn. I

really must thank Mark Ritchie for huge help with diagrams and with Microsoft Word. Without his help I would probably still be trying to properly insert figures and getting very frustrated while doing it.

The Langford group mainstays; Elena Vaisman, Yanjun Chang, and Heather Reader, are worthy of medals for putting up with my music and making me feel welcome and looking forward to coming in each day. My friends in Calgary were wonderful for pretending to listen when I described my work to them. Their support and friendship made my time in Calgary for both undergraduate and this thesis, an incredible time in my life.

To my Mom and Dad,

my brother Todd,

and the memory of my Grandpas,

Art Kennedy and Bob Melton.

TABLE OF CONTENTS

LIST OF TABLES

LIST OF FIGURES

CHAPTER ONE: INTRODUCTION

1.1. Natural Organic Matter

Natural organic matter (NOM) is comprised of all material of biotic origin. Highly degraded NOM, that is recalcitrant to further degradation, can be classified as a humic substance (HS).

HSs are found in aquatic, soil, and sediment environments and are of paramount importance for sustaining plant growth and controlling both the fate of environmental pollutants, and the biogeochemistry of organic carbon (OC) in the global ecosystem [4]. HSs are known to play many roles in different agronomic, geochemical and environmental processes including; reservoirs for micronutrient retention in soil while making these nutrients available for plant root hairs, acid-base buffering of soils, and contributions to soil structure and water regime [5]. Additional HS influenced processes include the dissolution of minerals [6], electron shunting in microbial and abiotic redox reactions [7], immobilization and transport of anthropogenic chemicals and heavy metals [8, 9], and global carbon cycling. Additionally HSs have uses in environmental engineering, industry and even medicine [10]. For further information, Tipping [5] has compiled an extensive list of environmental issues involving humic substances.

Despite their importance to sustainability, agriculture and environmental stewardship, these compounds still remain relatively poorly understood.

1.2. Humic Substances

In most environments the majority of dead biomass is transformed into carbon dioxide through the process of mineralization. Mineralization is rarely one hundred

percent efficient and as a result a small amount of biomass is retained in solid form as humic material. This humic material is developed from a myriad of processes during the decay of plant tissues, microbial metabolism or catabolism, or from both [11]. Thus the nature of HSs and extent of their accumulation is dependent upon many factors including climatic conditions, turnover times, vegetation, parent mineral material, cropping, and topography [12].

The processes that create HSs quite naturally create very diverse and heterogeneous mixtures. Recent advances in mass spectrometry (MS) and nuclear magnetic resonance (NMR) have demonstrated that humic mixtures are extremely complex. Stenson *et al.* [1] used an extremely high field (9.4 T) Fourier transform ion cyclotron resonance mass spectrometer (FT-ICR-MS) to elucidate 4626 individual ions from a Suwannee River fulvic acid. These ions were then assigned to one of 266 distinct homologous series (differing in oxygen content and double bond equivalence) (Figure 1.2.1. and 1.2.2.)

Additional evidence of the super-mixture nature of humics was provided by Cook *et al.* [2] who analyzed a Laurentian fulvic acid (LFA) in solution. The fulvic acid was interrogated using state of the art heteronuclear and 2D high resolution NMR techniques. Cook and co-workers were able to observe a proton coupled system of up to seven bonds in a TOCSY spectrum and 329 narrow peaks in the ^{1}H, ^{13}C-HSQC spectrum (Figure 1.2.3.). The new knowledge of humics as this type of mixture requires a different interpretation with regards to binding behaviour than has been previously postulated. An

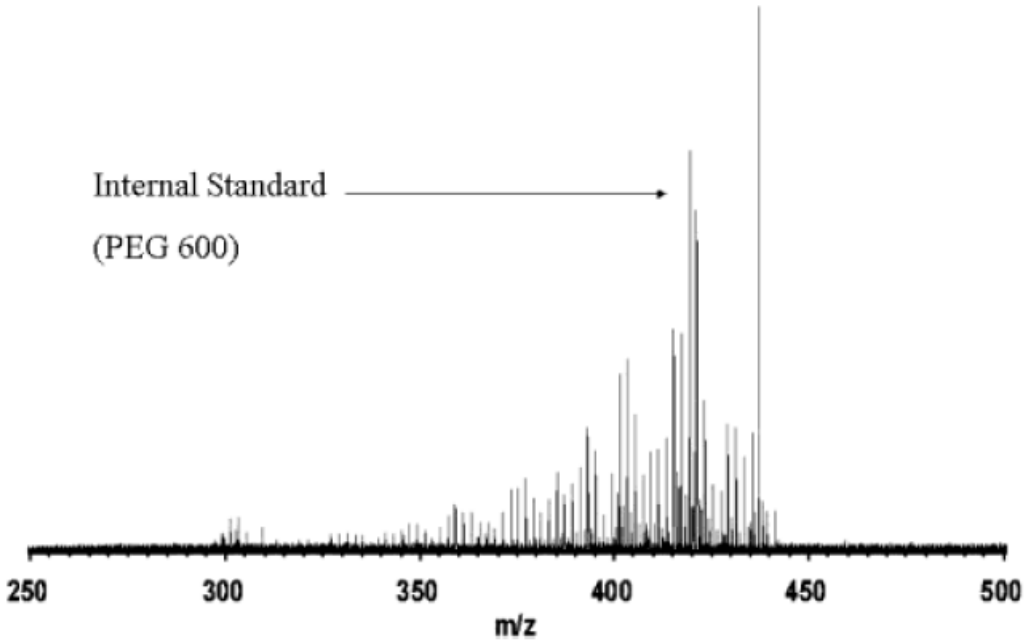

Figure 1.2.1. Suwannee River Fulvic Acid electrospray ionization FT-ICR mass spectrum after quadrupole isolation of the low *m/z* fraction with PEG 600 internal standard (1000 coadds). Reprinted with permission from [1]. Copyright 2003 American Chemical Society.

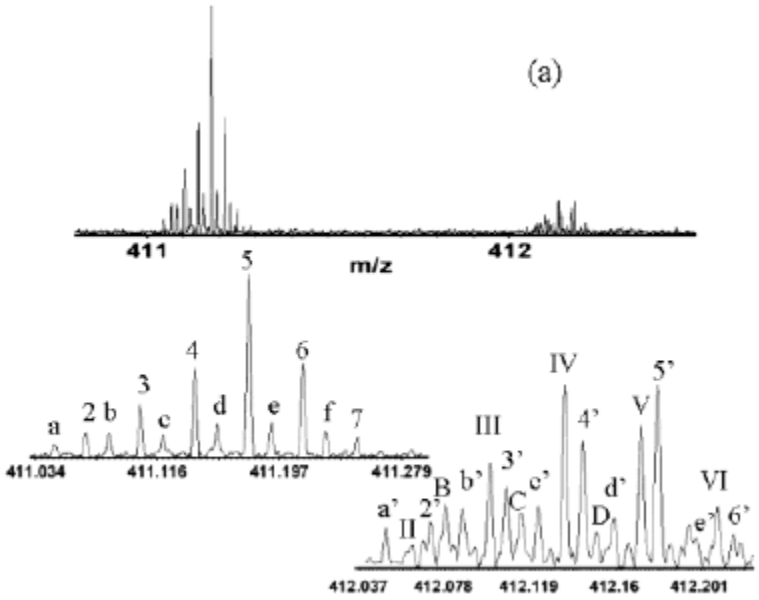

Figure 1.2.2. Electrospray ionization FT-ICR mass spectrum of Suwannee Rive FA ion at 410 and 411 actual mass. Reprinted with permission from [1]. Copyright 2003 American Chemical Society.

interpretation of copper-humic acid binding based upon a dynamic combinatorial chemistry approach will be presented in Chapter Five.

It is readily apparent that humic substances are not classifiable in unambiguous structural terms. Additionally, HSs cannot be defined in terms of any specific biological or biochemical function. Thus the most convenient and simple classification scheme utilizes solubilities in aqueous acids and bases. Humic substances have therefore been divided into three fractions; humic acid (HA), fulvic acid (FA) and humin [13].

Humic acids consist of the fraction of HS that is precipitated from aqueous solutions when the pH is decreased below 2 [14]. Fulvic acids are soluble under all

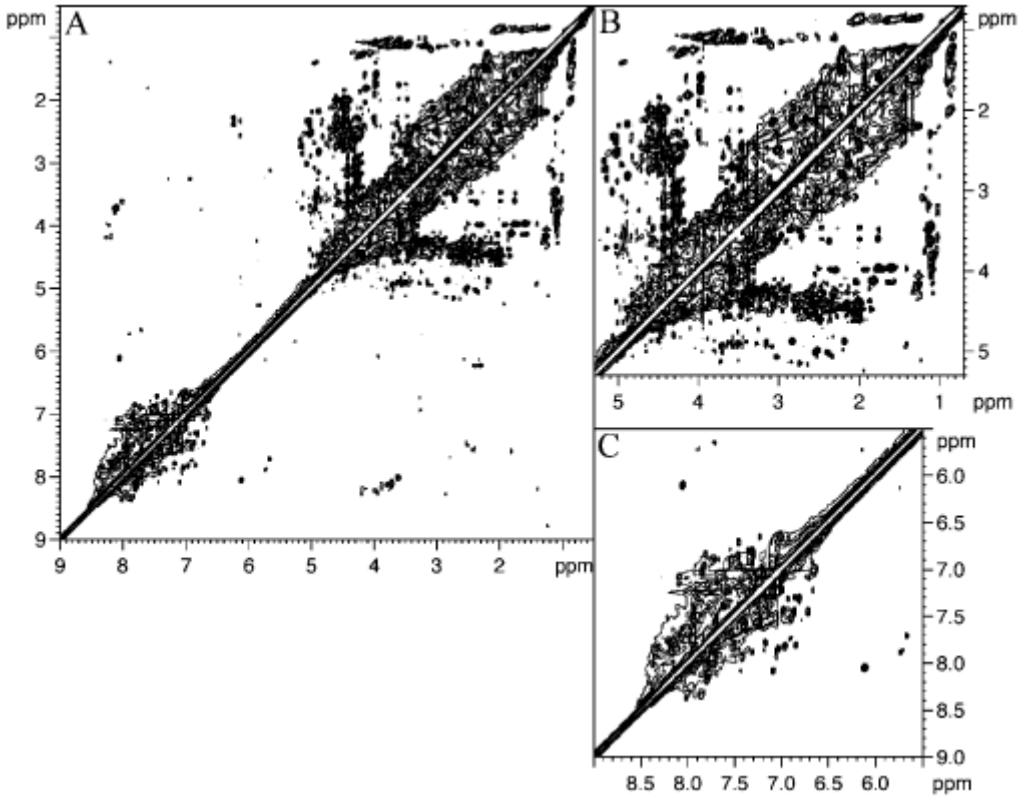

Figure 1.2.3. A TOCSY spectrum of LFA (A), enlarged in the aliphatic/carbohydrate region (B) and the amine/aromatic region (C). Reprinted with permission from [2]. Copyright 2003 American Chemical Society.

conditions of pH, while humin is the fraction insoluble in water at any pH value. Humin is thought to consist of HA in strong association with mineral matter, highly condensed insoluble humic matter, fungal melanins, and paraffinic substances [12].

The distribution of these species in natural systems is affected by their physical properties. Humin and HA are more commonly found in soils and sediments as part of the solid phase while the more mobile FA is a major part of the dissolved organic matter (DOM) in natural waters [5].

Table 1.2.1. Approximate concentrations for HS in different environmental compartments. These values are subject to large site specific differences. Data adapted from Tipping, 2002 [5]

Environmental Compartment	Sub-compartment	Concentration of HS (approximate)
Soils	Peat	50 g/ L
	B horizons of forest soils	60 g/L
	Mineral horizons of sandy soils	>1% (by weight)
Subsurface waters	Soil waters	1 – 70 mg/L
	Organic rich soil waters	~ 400 mg/L
	Deep groundwater	0.2 – 100 mg/L (median of 0.7mg/L)
Surface waters	Freshwater lakes	0.5 – 100 mg/L
	Major rivers	~ 5 mg/L
	Open ocean surface water	1 mg/L
	Open ocean deep water	~ 0.5 mg/L
Aquatic sediments	Interstitial waters of sediments	4 – 20 mg/L (oxic) 10 – 390 mg/L (anoxic)

It is important to remember that these compounds are not pure compounds and that the distinctions are purely operational by nature.

Characterization of humic substances is hampered not only by their large chemical heterogeneity but also from variability caused by different source locations and extraction and fractionation techniques [15, 16]. Regardless, definitive compositional differences are evident for HA and FA, whether from soil, stream, or marine environments.

The most commonly varied moieties within HA derived from different sources include differing amounts and compositions of ‘carbohydrate’, phenolic, methoxyl, aromatic, hydrocarbon, amino acid, and nitrogen containing groups [15].

The most frequently found functional groups within HSs include: carboxylic acids, phenolic hydroxyls, carbonyls, and hydroxyl groups as well as ‘carbohydrates’ and some amino acids [17]. This heterogeneity of the HS is hypothesized by MacCarthy and Rice [18] to disallow the evolution of appropriate degrading enzymes and is the primary cause of a resistance to degradation.

The recent work utilizing highly precise MS has lead to postulation of a few of the humic substances base monomer units in the mixtures (Figure 1.2.4.).

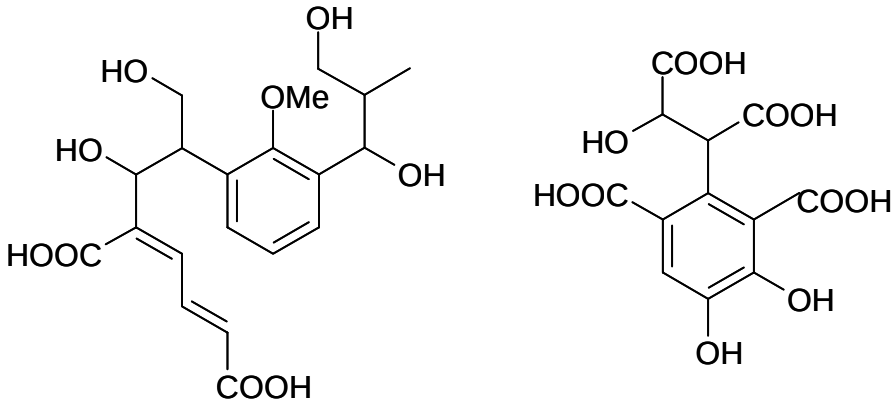

Figure 1.2.4. Postulated monomer components of a fulvic acid drawn from recent ultra high resolution MS studies. Structure from Reemstma (R) and Cooper (L) [3, 19].

1.3. Environmental Metal Speciation

Metals in the environment exist in many forms dependant upon the environmental conditions the metal is exposed to. The most common metals in fresh water systems by concentration include $Fe^{(III)}$, $Mn^{(IV)}$, $Mn^{(II)}$, $Cu^{(II)}$, $Ni^{(II)}$, $Zn^{(II)}$, $Al^{(III)}$, $Cd^{(II)}$, V and

$Pb^{(II)}$[20, 21]. Many of these metal species are introduced into the environment through anthropogenic processes such as mining, smelting, oil production and land disturbances.

Once metal species are in the environment large amounts of naturally occurring ligands can influence the apparent toxicity, mobility, and bioavailability of the metal [22]. The influence of ligands is felt through both thermodynamic and kinetic processes which affect the metal ion speciation [23]. Not only are the types of metal-ligand complexes formed significant, but information about the strength of association, kinetics of formation, complex aggregation, etc. are important to gain an adequate understanding of dynamics within a system.

Humic substances, amino acids in proteins and extra cellular products are the most common natural organic ligands that are capable of complexing trace metals [24]. Humic substances are thus believed to play an important role in the speciation, fate, and transport of metals in many aqueous environments. Indeed, humic substances are some of the most powerful metal-binding agents among natural organic substances [25]. HS ubiquity, and high concentration of functional groups known to interact with metals (total acidity is typically between 5 and 15 equivalents/kg of humic), demonstrates the likelihood of metal-humic interaction [26]. In soils and natural waters trace metal ions such as Cu^{2+} or Pb^{2+}, may exist predominantly in complexes with humic ligands [12].

1.4. Research Objectives / Thesis Outline

Due to the importance of humic substances, and relative lack of understanding, this project was initiated to achieve some novel insight into humic-metal interactions.

Drawing upon previous work utilizing low-field nuclear magnetic relaxometry (NMR), within our research group on soils [27, 28], low-field NMR was used to investigate solution-phase binding interactions of Cu^{2+} ions and Laurentian humic acid (LHA). The results of this work dictated the further directions that the project then took.

This thesis is set out in six chapters and attempts have been made to have the order as logical as possible. Chapter One is an introduction to the world of humic substances and the classifications therein. The chapter also details the phenomenon of metal speciation in the environment, and its importance to biota as well as interactions with HSs. Chapter Two is a review of the techniques used in the creation of this thesis. The chapter details the theoretical and historical (within the HS literature) basis for the work to set context. The techniques covered will include, in this order: dynamic light scattering (DLS), electron paramagnetic resonance (EPR), competing ligand exchange method (CLEM) using Chelex ion exchange resin, and low-field nuclear magnetic relaxometry. The order of techniques remains the same for the remaining chapters. This chapter is not meant to be exhaustive in either theory or history but to serve as a primer on the work to follow. Chapter Three lists the experimental procedures followed for all the techniques utilized. Replication of the work presented should be possible using the information presented in this chapter for any interested parties. Chapter Four presents the experimental results. Chapter Five is the discussion of the experimental results and where the concept of humics as a dynamic combinatorial system is introduced. Chapter Six presents conclusions on the work conducted as well as suggestions for further work.

CHAPTER TWO: THEORETICAL AND HISTORICAL PERSPECTIVES

The work contained in this thesis used several different analytical methods. This chapter is provided as a primer to the relevant theoretical and historical perspectives of the techniques utilized. The order of presentation, which at first may seem haphazard, is to coincide with the requirements of the discussion in Chapter Five.

Experiments with dynamic light scattering (section 2.1) were performed to test a novel binding model introduced in Section 5.1. The experimental core of the thesis is, however, based in low-field nuclear magnetic relaxometry, which is presented here last (Section 2.4). Analysis of the NMR data set required the use of electron paramagnetic resonance (EPR) and a competing ligand exchange method (CLEM), which are presented in Sections 2.2 and 2.3 respectively.

2.1. Laser Light Scattering

2.1.1. Theoretical and Historical Background

Electromagnetic radiation is one of the most important probes of the structure and dynamics of matter. Light is electromagnetic radiation in the frequency range from approximately 10^{13} Hz (infrared) to 10^{17} Hz (ultraviolet) or the wavelength range from 3 nm to 30,000 nm.

When a light beam illuminates a piece of matter possessing a dielectric constant different from unity, light will be absorbed or scattered, or both, depending on the wavelength of light and the optical properties of the material. The net result of the absorption and scattering caused by the material is known as the extinction of incident

light. When light impinges on matter, the electric field of the light induces an oscillating polarization of the electrons in the molecules. The molecules then serve as secondary sources of light and subsequently radiate (scatter) light. The frequency shifts, angular distribution, polarization and the intensity of the scattered light are determined by the size, shape, and molecular interactions in the scattering material. Thus from the light scattering characteristics of a given system it should be possible, with the aid of electrodynamics and the theory of time-dependent statistical mechanics, to obtain information about the structure and molecular dynamics of the scattering medium.

Detected scattering is dependant upon the particle(s) within a scattering volume, which is the cross section between the beam and the detection cone. The absorbed light energy that becomes the excitation energy of the particles within the scattering volume will be dissipated mostly through thermal degradation (i.e., converted to heat) or lost through a radiative decay producing fluorescence or phosphorescence depending on the electronic structure of the material. Scattering is also only observed from material that is in itself heterogeneous, in the case of isotropic material the radiation scattered by individual molecules interferes destructively and no scattering is observed. Since many materials exhibit strong absorption in the infrared and ultraviolet regions, which greatly reduces scattering intensity, most light scattering measurements are performed using visible light.

The earliest experimental studies were by Tyndall in 1869 on light scattering of aerosols and the initial theoretical work of Rayleigh (1871, 1881) laid the groundwork for studies of a variety of physical phenomena concerning assemblies of non-interacting particles sufficiently small, compared to the wavelength of light, to be regarded as point-

dipole oscillators. Subsequent papers produced by Rayleigh derived the full theory for spheres of arbitrary size. Debye (1915) made further contributions to the theory of these larger particles and extended the calculations to particles of non-spherical shape. While Rayleigh's formula performed well for gases, it required some alterations for condensed phases. These were provided by Smoluchowski (1908) and Einstein (1910) [29].

Introduction of laser techniques has allowed the measurement of very small frequency shifts in the light scattered from gases, liquids, and solids. Moreover, because of the high intensities of laser sources it is possible to measure even weakly scattered light. Thus the main difficulties encountered in the past are eliminated when lasers are used. The structure and dynamics of such diverse systems as solids, liquid crystals, gels, solutions of biological macromolecules, simple molecular fluids, electrolyte solutions, dispersions of micro-organisms, solutions of viruses, membrane vesicles, protoplasm in algae, and colloidal dispersions have now all been studied by laser light scattering techniques as early as the 1970s [29].

Dynamic light scattering (DLS) is an effective and straightforward technique for determining the hydrodynamic size of species from large polymer chains to micelles and microspheres, among others [30]. DLS depends on correlation of the light scattered from particles as they randomly diffuse through a solution. In principle, the light scattered at a given time, t, is correlated with the light scattered at $t \pm \Delta t$, typically Δt is of the order of milliseconds; the degree of correlation then depends on how fast the particles move and hence can be used to give a diffusion co-efficient, D, from which a particle size can be estimated.

The output of this technique is then the scattered intensity autocorrelation function, $C(\tau)$, for correlation time, which is given by

$$C(\tau) = A\left(1 + \beta \int_0^\infty P(\Gamma)\exp(-\Gamma t)d\Gamma\right) \quad (2.1.1.1)$$

where A is a baseline value, β is an instrumental constant and Γ is the characteristic line width of the distribution function $P(\Gamma)$. Γ contains information about the diffusion co-efficient D of the scattering species, and are related by

$$\Gamma = Dq^2 \quad (2.1.1.2.)$$

where q is the scattering vector, which is constant for a given observation angle, incident light angle, etc. Additionally, if it is assumed that the scattering species can be roughly taken as spheres, then the apparent hydrodynamic diameter, d_h can be calculated through the Stokes-Einstein equation:

$$d_h = k_B T / (3\pi\eta D) \quad (2.1.1.3.)$$

where k_B is the Boltzmann constant, T is the absolute temperature and η is the viscosity.

2.1.2. Distribution Analysis

When dynamic light scattering results are obtained in the form of equation 2.1.1.1. a fitting procedure is required for analysis. The simplest fitting procedure makes an initial assumption of one type of scattering species, and fits the data to a single exponential expanded as a Taylor series, commonly referred to as the Cumulants method. This limitation, of assuming only one type of scattering species, can be avoided in well-behaved systems by inversion through a proper Laplace inversion algorithm. An example of this is the CONTIN model [31, 32]. This method has some limitations as it can be sensitive to experimental noise and the results attained are dependent upon the inversion

limits. It does, however, avoid the limitation of the Cumulants method and can be very reliable in appropriate systems.

2.1.3. Dynamic Light Scattering and Humic Substances - Historical Background

There are at present relatively few reports of light scattering measurements of humic materials. Black and Christman [33] reported the detection of scattering signals from aquatic fulvic acid solutions using 436 and 546 nm light with secondary filters to prevent fluorescent emissions from reaching the detector. It was noted early on that the strong absorbance of UV light and fluorescence in the visible region of humics is a major problem for visible light scattering experiments. This led to the use of longer wavelengths that resulted in greatly reduced scattering intensity due to the dependence of scattering on a $1/\lambda^4$ relation.

Upon the introduction of laser-based instrumentation operating at higher wavelengths, an increase in literature reports using DLS has been evident. Some early studies from our lab by Underdown *et al.* [34] and Gamble *et al.* [35] on an Armdale fulvic acid investigated the effects of metal binding. Since those early studies an assortment of literature reports on HSs and metal interactions has developed. The range of reported diameters for unbound HA ranges from (436 $\pm$ 36) nm [36] to a lower limit of approximately 20 nm [37]. The size of a HS has been reported to vary depending upon ionic strength, pH, temperature, metal cation properties and concentration, degree of HS fractionation, and method of sample preparation [37-40].

Wagoner and Christman investigated a bulk NOM and found low pH promotes aggregation, with generally larger particle sizes found as pH was lowered [37]. Reid and coworkers [41] examined peat HA, surface water HA and fulvic acid extracted from

Whitray Beck in North Yorkshire, UK. From DLS measurements their humic acids were found to have aggregates present. They also found evidence of reversible aggregation with fulvic acid as determined by static light scattering, sedimentation velocity measurements, and use of detergents to promote dissociation. High ionic strength was correlated to aggregation in humic acids by Pinheiro *et al.* [39], who also found a strong influence of the solution preparation to the final properties of the humic material. Palmer and Wandruszka performed temperature and cation effects experiments on aqueous humic and fulvic acids [42]. They discovered an increase in temperature generally led to an increase in particle sizes. Addition of cations led to either contraction or expansion depending on the charge and concentration of the ion, and the nature of the humic material.

2.2. Electron Paramagnetic Resonance

2.2.1. Historical Perspective

The electron paramagnetic resonance (EPR) and NMR effect were both conceived and discovered around the same time. It was in 1945, however that the first observed electron spin phenomenon was published by Zavoisky [43]. Electron spin echoes were then observed in 1958 by Blume in a relaxation study of trapped electrons in liquid ammonia [44].

The first pulsed EPR studies were confined to compounds with long relaxation times and small line widths. This was principally due to the large energies involved with electron spin interactions giving rise to spectral widths in the order of 10-25% of the carrier frequency, as opposed to the ppm scale that applies to NMR, as well electron-spin

relaxation times are orders of magnitude shorter than NMR relaxation times. The last few decades have seen microwave equipment improve and the application of pulsed EPR has spread to biological systems, polymers, catalysts, short lived radicals, transition metal complexes and photo-excited triplets [45].

A fairly large body of EPR work studying humic substances and metals is available in the literature [46-53]. A large amount of this stems from the fact that humic substances often contain a measure of stable radical species allowing ease of measurement.

The occurrence of stable free radicals in humic acids was first observed by Rex in 1960 [54]. Rex believed that the radicals were semiquinones (Figure 2.2.1) formed by the dehydrogenation or oxidative removal of hydrogen from the aromatic –OH, -NH_2, and/or –SH groups.

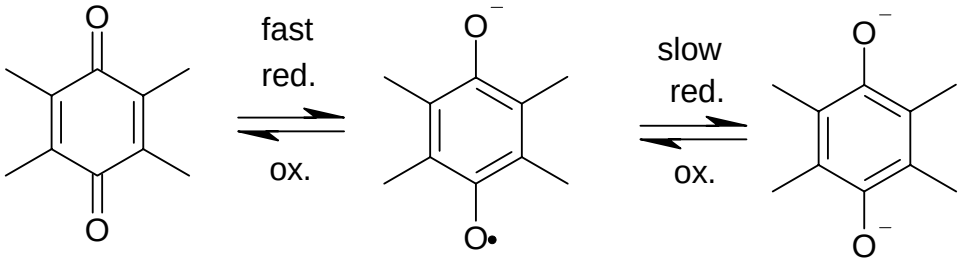

Figure 2.2.1. Diagrams of benzoquinone (L), semi-quinone (centre), and hydroquinone (R).

Steelink and Tollin [55] agreed with Rex in 1962 and postulated that the humic acid is a mixture of free radicals of the semi-quinone type, also noting the high resistance and perseverance of the radicals. Termination of various free radical reactions proceeding during the decomposition of organic matter leads to the formation of the EPR- detectable stable radicals from such compounds as polyphenols, melanins, melanoidins, and other

Maillard polymers [56]. The polyphenolic and/or melanoid character of the materials undergoing degradation effectively stabilizes the organic free radicals [57].

Most EPR work on humics is done in the solid state. A typical spectrum consists of a single peak devoid of any hyperfine splitting attributed to the high complexity of the material. Some liquid samples have been analysed and exhibit similar peaks albeit with lower intensity.

A number of studies involving humic acid interactions with metals have been published [46, 48, 49]. The majority utilize the effect of paramagnetic metal species on the EPR spectrum of the humic mixture to investigate the metal humic interactions.

2.2.2. Electron Paramagnetic Resonance Principles

Electron paramagnetic resonance (EPR), also known as electron spin resonance (ESR), relies upon the same principles as NMR. However, in EPR, it is an unpaired electron that possesses spin rather than nuclear magnetic dipoles. This leads to differences in the magnitudes and signs of the magnetic interactions involved which naturally leads to divergences in the experimental techniques employed. EPR measurements are commonly taken in the X band of the microwave spectrum.

Paramagnetism arises from the circulation of charge on an atomic scale. The magnetic moment of an unpaired electron, μ_e, is given by the relation,

$$\mu_e = -g\beta S \qquad (2.2.2.1.)$$

where g is the spectroscopic splitting factor, or g-value, β is the Bohr magneton and S is the spin angular momentum vector of the electron. Equation 2.2.2.1. is analogous to that of a nucleus but with opposite sign. EPR experiments are based upon the interaction of μ_e and an external magnetic field, B_o, which can be described by,

$$E = -\mu_e B_o = g\beta B_o M_Z \qquad (2.2.2.2.)$$

where E is the energy of the unpaired electron, and M_Z may assume values of +1/2 and –1/2, which correspond to the two allowed orientations of the electron spin in the magnetic field. Note that due to the negative charge of the electron, μ_e in equation 2.2.2.2. is negative and that β is defined as positive.

Within an EPR experiment it is possible that nuclear spin and nuclear motion associated with rotation of molecules can be dropped from consideration. This is due to the ratio of 10^3 to 10^5 in the masses of nuclei and electrons. If the angular momentum arises from electronic motion only, then for a given angular momentum the angular frequency will be much greater than for nuclear motion [58].

Application of an oscillating field perpendicular to B_o induces transitions provided that the frequency, *v,* is such that the resonance condition

$$h\nu = g_e \beta B_o \qquad (2.2.2.3.)$$

is satisfied [59]. This is completely equivalent to equation 2.4.3.1. in the NMR section.

2.3. Competing Ligand Exchange Method using Chelex Resin

2.3.1. Historical Perspective

Simultaneous kinetic analysis of multi-component systems is well established [60, 61] and extensively used [62, 63]. The basis of the competing ligand exchange method (CLEM) was introduced by our lab in 1992 [64], as a reaction to the abundance of papers in the literature based upon equilibrium studies. The relevance of equilibrium speciation studies is limited to instances where the equilibria are established rapidly with respect to the time scale of uptake [65]. Additionally a heterogeneous polyelectrolytic ligand

system, such as a humic system, can depart considerably in kinetic behaviour from simple ligands and may result in systems that are dynamic and far removed from equilibrium; hence equilibrium speciation methods may not apply [66]. Further theoretical work that was introduced by Langford and Gutzman is presented in the following section.

The CLE method has been highly favoured by the lab of C.L. Chakrabarti who has published several papers using the CLE method to investigate metal speciation in both lab and environmental samples [67-70]. The most powerful technique utilizing CLEM was then developed by Chakrabarti and associates involving the use of a Chelex 100 ion-exchange resin. Chelex-100 resin is composed of a copolymer of styrene and divinylbenzene that has attached iminodiacetic acid chelating groups (Figure 2.3.1). Chelex is very useful for chemical speciation due to its two properties; moderate ion-exchange reactivity and exclusion of large molecules and colloidal particles by virtue of the size of its beads (200 – 400 mesh) [68].

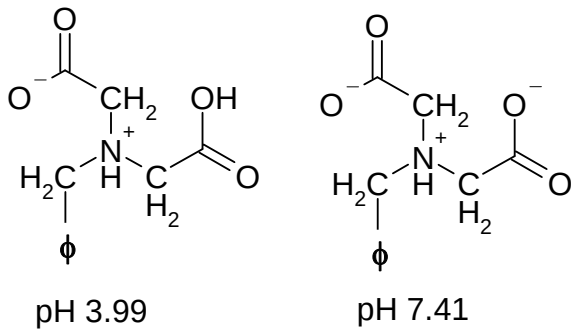

Figure 2.3.1. Chelex-100 resin metal chelating ligands affixed to a copolymer of styrene and divinylbenzene. The protonation is pH dependant as is demonstrated above.

The application of Chelex resin to the problem of metal speciation dates from the late 1970s when T.M. Florence [71] used an ion-exchange resin to determine metal

speciation of copper, lead, cadmium, and zinc in four natural waters and a tap water. Resins have since been widely used to distinguish between resin exchangeable (labile) and non-exchangeable metal forms.

Some of the earlier studies used batch techniques [72], different types of ion-exchange resins [73], and different metal quantifying apparatus [70]. However, Chakrabarti's lab has developed a method that utilizes ICP-MS allowing for highly sensitive measurement of a wide range of metals in a continuous flow system [69, 70]. Initial papers investigated the effects of different resin particle sizes, loading, wetting, and concentration, as well as optimization of experimental procedure [67, 68, 70]. Several model solutions of fulvic acids and various metals have been analysed as well as snow and water samples.

The interactions of copper and humic substances has been repeatedly investigated by Chakrabarti and co-workers. A selection of their results is summarized in Table 2.3.1.

2.3.2. Theoretical Background

It is now widely recognized [64, 69, 74, 75] that consideration of dynamic processes are vital for estimates of metal bioavailability to aquatic organisms. With this in mind, kinetic approaches for chemical speciation are required to appropriately observe the realities of natural systems. The competing ligand exchange method (CLEM), developed by Langford and Gutzman [64] is particularly well suited to the study of dynamic processes in a humic environment.

Table 2.3.1. Dissociation kinetics of copper complexes as determined by the Competing Ligand Exchange Method utilizing Chelex-100 cation exchange resin. Uncertainties represent the 95% confidence limits from linear regression analysis.

Ref.	Sample	$\%C_1$	k_1 ($10^{-1}s^{-1}$)	$\%C_2$	k_2 ($10^{-3}s^{-1}$)	$\%C_3$	k_3 ($10^{-4}s^{-1}$)	$\%C_4$	k_4 ($10^{-5}s^{-1}$)
[69]	LFA[a]	---	---	0.2	0.80±0.13	---	---	99.8	1.3±4.0
	River water[b]	0.01	3.6±0.1	<0.01	41±4	0.01	83±9	100	1.8±2.7
[68]	Rain water[c]	---	---	80.0	2.3±0.1	5.6	33±3	17.4	0.85±0.02
	Snow[d]	50.0	0.31±0.05	14.6	1.6±0.1	18.8	0.62±0.11	16.7	0.88±0.03
[66]	LFA[e]	---	---	---	---	32	0.24±0.03	68	1.3±0.1
	Rideau River[f]	---	---	47	0.9±0.2	51	1.0±0.2	---	---
	Moose Lake[g]	---	---	8.4	2.0±0.1	---	---	88	7.1±0.1

[a] c_M/c_{FA} = 0.056, pH 5.0 ± 0.1, I = 6 x 10^{-6} M, 23 ± 2 °C; [b]Sample collected June 23, 2002, DOC 14.9 ± 0.4 mg/L, pH 7.9 ± 0.1, I = 6 x 10^{-3} M, 23 ± 2 °C; [c]Sample collected August 26, 1992, pH 5.3; [d]Sample collected January 10, 1992, pH 3.9; [e]pH 5.0 ± 0.1, I = 4.2 x 10^{-5}M, c_M/c_{FA} = 0.8; [f]Sample collected on June 13, 1996, pH 5.0 ± 0.1, DOC = 7.7 mg/L, I = 4.9 x 10^{-3} M; [g]Sample collected on October 27, 1998, pH = 6.9 ± 0.1, DOC = 1.5 mg/L, I = 2.4 x 10^{-2} M

Within the competing ligand exchange method, a sample of *n* components in which each component, ML_i, exists in equilibrium with its dissociation products: the free metal ion (i.e. a metal aqua complex, for eg. $[Cu(H_2O)_6)]^{2+}$), M^{x+} , and a naturally occurring heterogeneous complexant, L (charge is omitted for clarity of presentation), is considered.

$$ML \underset{k_f}{\overset{k_d}{\rightleftharpoons}} M^{x+} + L \qquad (2.3.2.1.)$$

Within the system considered free ligand, and free metal, as well as complexes of the two are present. The complexes present in the sample can be in several forms from a single ligand (or site on a ligand) bound to a single metal ion, *ML,* to complexation with several ligands (or sites on one or several ligands), ML_2, $ML_3 \ldots ML_i$. The subscript, *i*, refers to different binding sites on L_i.

For free metal ions complexation by a competing ligand, such as Chelex resin, is straight forward, and with a large excess of Chelex resin, can be considered as pseudo first order (this applies to the complexes ML_i as well).

$$M^{x+} + Chelex \xrightarrow{k_{f,chelex}} M - Chelex \text{ (fast)} \qquad (2.3.2.2.)$$

Here the rate constant is determined by the speed of uptake of the metal into the resin. However for the complexed metal the picture is more complex.

$$ML_i \underset{k_{f,i}}{\overset{k_{d,i}}{\rightleftarrows}} M^{x+} + L_i \text{ (slow)}$$

$$M^{x+} + Chelex \xrightarrow{k_{f,chelex}} M - Chelex \text{ (fast)} \qquad (2.3.2.3.)$$

where the overall formation, k_f, and dissociation, k_d, rate constants are coupled by the stability constant, $K = k_f / k_d$, through the principle of microscopic reversibility [76]. Since $k_{f,chelex}$ is much faster than $k_{d,i}$, the rate of uptake into the resin is determined by the initial slow step (dissociation of the metal ligand complex).

If each complex, ML_i dissociates simultaneously and independently (at a rate that depends on the nature of the functional group, the residual charge, and the position within the humic complex), the total concentration of all complexes, c_{ML}, at any time, t, is given by the sum of the exponentials.

$$c_{ML}(t) = \sum_{i=1}^{n} c^{o}_{ML_i} \cdot \exp(-k_{d,i} \cdot t) \qquad (2.3.2.4.)$$

where $c^{o}_{ML_i}$ is the initial concentration of ML_i and $c_{ML,i}(t)$ is the concentration of ML_i at any time, t.

Due to the chemical and physical heterogeneity inherent in humic substances, a continuous distribution of binding sites is expected [62, 69]. Thus the summation in Equation (2.3.2.4.) can be replaced by an integral

$$c_{ML}(t) = S\oint H(k)\cdot\exp(-k_{d,i}\cdot t)d[\ln k] \qquad (2.3.2.5.)$$

In equation 2.3.2.5, $H(k)\cdot\exp(-k_{d,i}\cdot t)d[\ln k]$ is the probability of finding a site with a rate constant in the range from ln (k) to ln (k) + d[ln (k)] in molar concentration units. Second order approximate solutions can be obtained using the first and second derivative of $c_{ML}(t)$ and the approximate inversion of a Laplace transform expression equivalent to 2.3.2.5., where the integral is taken with respect to ln (k) in place of k [64]. The resulting expressions are then:

$$S = \frac{4C_{ML}(t)}{\sum C_{ML}(0,i)} \qquad (2.3.2.6.)$$

$$H(k) = \frac{d^2C_{ML}(t)}{d(\ln t)^2} - \frac{dC_{ML}(t)}{d(\ln t)} \qquad (2.3.2.7.)$$

The value of S depends on whether the first, second or nth derivative was taken in the approximation.

A simple determinant of rate constants is then a plot of $H(k)$ against ln t which yields a series of peaks that correspond to kinetically distinguishable components. A distribution of rate constants is then displayed around the ln t peak values. The area under the peak is proportional to the concentration of the complexes, since the constrain requires that the integral over the entire range of $H(k)$ adds to the sum of all initial concentrations.

Rate constants from Equations 2.3.2.6. - 2.3.2.7. arise from the spontaneous process of dissociation of the metal-ligand complexes. The dissociation of the metal-

ligand complex followed by subsequent complexation with the competing ligand is termed the disjunctive pathway [77]. An alternative pathway is the adjunctive,

$$ML + R \rightarrow RML \rightarrow MR + L \qquad (2.3.2.8.)$$

In the adjunctive pathway, the incoming ligand, *R*, first complexes the *ML* complex to form *RML*, which then dissociates. Forcing the disjunctive pathway, through separation of phases or choice of ligand, is highly preferred for determining rate constants compared to the adjunctive, which is difficult to interpret due to rate constants being influenced by the nature (e.g. steric and electrostatic factors and protonation) of the probe ligand [62].

2.4. Low-Field Nuclear Magnetic Relaxometry

2.4.1. Low-Field NMR Historical Perspective

Nuclear magnetic resonance (NMR) is a phenomenon that occurs when the nuclei of certain atoms are immersed in a static magnetic field and then exposed to a second oscillating magnetic field [78]. The actual resonance occurs as the nuclei relax back to equilibrium. The physics behind resonance were derived long before the first successful experiments were carried out independently in 1946 by Bloch *et al.* at Stanford, [79] and Purcell *et al.* at Harvard [80]. Since those pioneering papers, NMR has quickly developed into one of the most powerful non-destructive analytical methods in many fields including medicine, chemistry, and the petroleum industry. The non-invasive and non destructive nature of the probe was first illustrated in 1967 by Jackson measuring signals from a live animal [81].

Between 1950 and 1970, NMR experienced rapid development in the fields of chemical and physical molecular analysis. This period sparked the refinement of many aspects of solid and liquid state NMR such as data acquisition and analysis tools.

NMR work on natural organic matter did not begin until 1963 when a very poorly resolved ^{1}H NMR liquid state spectrum of methylated humic acid was reported by Barton and Schnitzer [82]. Spectra remained quite poor until 1977 when Lentiz *et al.* [83] used Fourier Transform (FT) techniques to collect spectra. Since that work by Lenitz *et al.* the field has shown rapid advancement. In the last twenty years NMR has become a viable tool for HSs study combining the use of FT, high field strength and novel pulse sequences to derive large amounts of information.

A recent paper by Cook *et al.* [2] that was introduced in Section 1.2., effectively illustrates the huge volume of information available from state of the art heteronuclear and 2D high resolution NMR techniques (See figure 1.2.3.). Excellent reviews of additional high-field NMR work on humic substances can be found elsewhere [84, 85].

2.4.1.1. Low-field Nuclear Magnetic Relaxometry

While high-field proton NMR (field strengths giving proton resonance on the order of 200-800 MHz) is very useful for elucidating structural data, studies of relaxation time can be difficult and time consuming. Alternatively, low-field Nuclear Magnetic Relaxometry (NMR) (~1MHz) allows for the measurement of relaxation time, (but not chemical shifts) while ensuring high data quality and a simplification of dynamic problems. This allows for a very complex system to be studied without risk of an overwhelming amount of data being generated.

Low-field proton NMR is commonly utilized in petroleum exploration, examining fluids in porous media in rock formations and drill cores [86, 87]. Additional applications have included studies of food water content [88, 89], and relaxation time of water in soils [28].

Low-field NMR has, to this author's knowledge, never been applied to the question of effects of humic-metal binding on solvent water NMR signals. However, solvent water NMR has been utilized to investigate humic-metal binding on a few occasions.

The first investigations of the utility of solvent NMR relaxation times for the study of the binding of paramagnetic ions was with deoxyribonucleic acid in 1961 [90]. Within Eisinger and co-workers' report they comment that a T_2 or transverse relaxation time should be of use for other problems of paramagnetic ion binding to large molecules. This then led to two papers from our lab investigating the use of solvent proton NMR to investigate humic-metal interactions.

The first paper by Gamble *et al.* in 1976 [91] utilized a 60 MHz continuous wave instrument. Gamble and co-workers studied the interaction of manganese and fulvic acid through the manual measurement of line widths. Earlier work using ion exchange equilibrium had confirmed binding. An outer sphere electrostatic structure of the complex was proposed from the observation of minimal change in the presence of fulvic acid of the effect of paramagnetic Mn^{2+} on the NMR water spectra. Additional comparison with measurements of Mn^{2+} complexes with simple ligands and contrast with NMR measurements of Fe^{3+} - fulvic acid complexation strengthened the interpretation. Fe^{3+} - fulvic acid interaction is known to be inner sphere. The second paper by Deczky and

Langford provided supporting evidence to the earlier findings on Mn^{2+} and Fe^{2+} complexes and also provided evidence for Cu^{2+} forming inner sphere complexes [92].

2.4.2 Principles of Low-field NMR

The nuclear magnetic resonance (NMR) phenomenon is based upon the absorption and emission of energy in the radio frequency domain of the electromagnetic spectrum [78]. For NMR to occur a nucleus must possess spin (I), an intrinsic characteristic of the nucleus correlating to the atomic mass and atomic number. Nuclear spin is a quantized vector with discrete values that can be half-integral or integral values. A nucleus with a half-integral value for nuclear spin (i.e., I = 1/2, 3/2…etc.) has an odd atomic weight due to an unpaired proton [93]. NMR practitioners commonly exploit nuclei with I = 1/2 (i.e., ^{1}H, ^{31}P, ^{15}N, ^{19}F and ^{13}C) due to the complex coupling and relaxation effects that arise from nuclei with integral spins. Nuclei with half-integral spins (greater than ½) are also rarely measured as quadrupolar effects increase line width and make signal collection and interpretation challenging. The hydrogen atom is thus the most attractive nucleus due to its half integral spin, large abundance, and magnetic moment, which allows for a strong signal [81].

In the absence of an external magnetic field, the magnetic moments of magnetic nuclei are oriented randomly producing a net magnetization of zero (M = 0). Upon application of an external magnetic field, a magnetic torque is applied to the nuclei causing their spins to tend to align with the applied field. A nucleus of spin ½ will align either parallel or anti-parallel with respect to the applied field (B_o). Parallel alignment is the lower energy state thus there is a slight excess of nuclei oriented parallel to the field

direction resulting in a net magnetization vector, M. This nucleus orientation produces the NMR signal and is arbitrarily chosen as the z-direction [78].

Classically, nuclei aligned in a magnetic field continue dynamic processes, continually spinning around their own axes. The torque applied to the spinning nuclei by the external magnetic field causes the spin axes of the nuclei to shift perpendicular to the torque, or precess [94]. The observed precession occurs because of interaction between the mobile nucleus and the magnetic field [93], and causes the magnetic moment

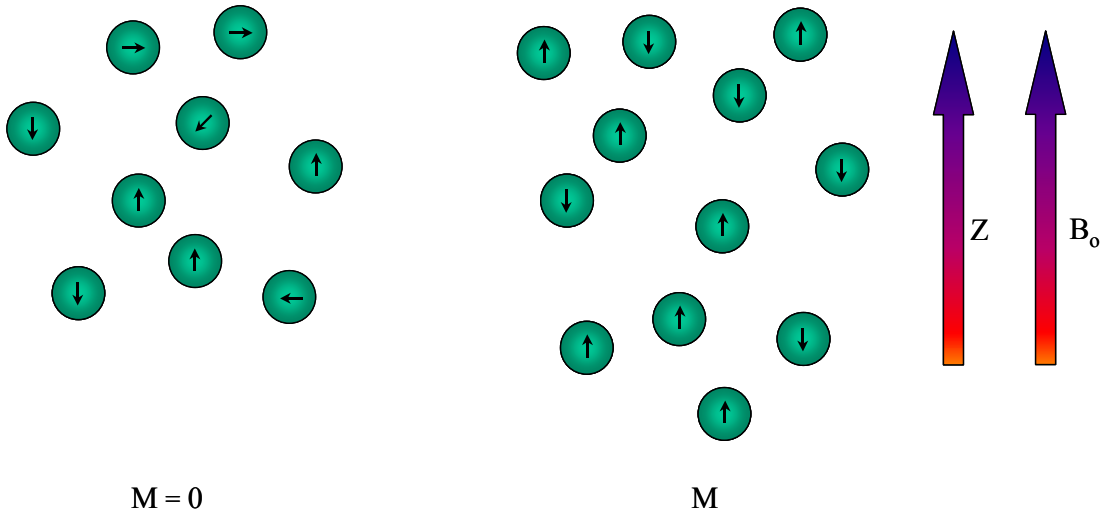

Figure 2.4.2.1. Prior to application of an external magnetic field, protons are aligned randomly for a net magnetization of zero. Application of the magnetic field aligns the protons both parallel and anti-parallel to the field with a slight excess in the parallel alignment.

to tilt slightly away from the axis of the magnetic field. The axis of rotation, however, remains parallel to B_o resulting in a periodic rotational motion of the nucleus spin vector about the direction of the external field B_o. The frequency of the nuclear precession or Larmor frequency, is directly dependant on the strength of the magnetic field, B_o and can be related by the Larmor equation [93]

$$\omega = \gamma B_o \qquad (2.4.2.1)$$

where ω is the resonance frequency, and γ is the gyromagnetic ratio. The gyromagnetic ratio is unique for each NMR active nucleus and field strength allowing for nuclei of a specific element to be selectively chosen for measurement in NMR. For example, ^{1}H possesses a gyromagnetic ratio of 26.8 x 10^{7} $T^{-1}s^{-1}$ at field strength of 1 Tesla (T), corresponding to a Larmor frequency of 42.58 MHz [93].

It can be useful at this point to assume a coordinate system that rotates at the Larmor frequency. Due to the frame of reference rotation, the transverse component (the magnetization vector lying in the transverse plane) appears stationary while the remainder of the system rotates about this point [81]. The utility of this system is a simplified description that allows the splitting of M into two components; one along the Z-axis, M_Z or longitudinal magnetization occurring in the direction of the field, B_o, and one in the x-y plane, M_{XY} or transverse magnetization occurring perpendicular to the field.

At equilibrium, M_{XY} is zero and M_Z is equal to M. With the nuclei aligned with the static magnetic field, B_o, a second magnetic field can be applied as a radio frequency (RF) pulse perpendicular to B_o. Pulse application causes the M to precess away from the z-axis toward the x-y plane, thus decreasing M_Z and increasing M_{XY} proportionally. The angle of M deflection depends primarily on the duration and amplitude of the applied RF pulse. Thus a RF pulse at an appropriate amplitude and period of time will rotate M until the vector is oriented 90^{o} from its initial position, commonly termed a 90^{o} or A pulse. A B or 180^{o} pulse will completely invert M. Once the RF pulse is turned off the system decays to equilibrium with M_Z increasing to its original value, M, and M_{XY} decaying back to zero [95].

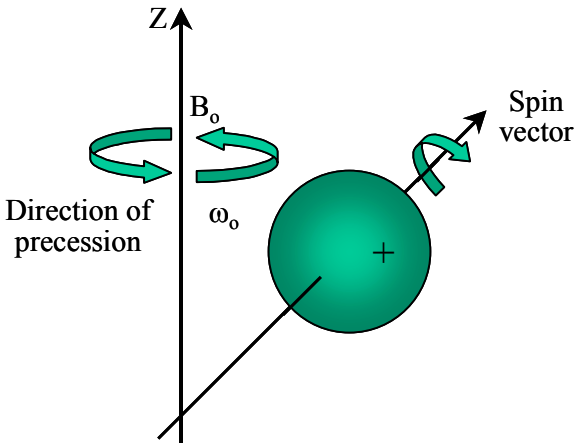

Figure 2.4.2.2. A nucleus under the applied magnetic field, B_o, which is parallel to the primary magnetic field, Z, will precess in that field direction. The frequency of precession is determined by equation 2.4.2.1.

2.4.3. Relaxation Processes

When the nuclei and RF pulse have the same frequency, energy exchange is possible from the RF pulse to the nuclei [96]. The frequency, v, required for energy exchange can be found by [59],

$$hv=g_N\beta_N B_o \qquad (2.4.3.1.)$$

where h is Planck's constant, g_N is a dimensionless constant called the nuclear g factor, and β_N is the nuclear magneton. β_N is equal to $e\hbar/2Mc$, where e and M are respectively the charge and mass of the proton, c is the velocity of light, and $\hbar$ is Planck's constant divided by 2π.

Thus application of an RF pulse gives rise to an excited state with a finite lifetime. The excited state lifetime is determined by the excited protons precessing out of alignment due to molecular interactions and inhomogeneities in B_o [95]. Excess energy emitted from the nuclei is dissipated by RF emission and by transferring energy to the surrounding molecules. This process of energy transfer is termed relaxation [97]. These

relaxation processes; spin-lattice or longitudinal relaxation and spin-spin or transverse relaxation, are exponential in nature and independent of each other.

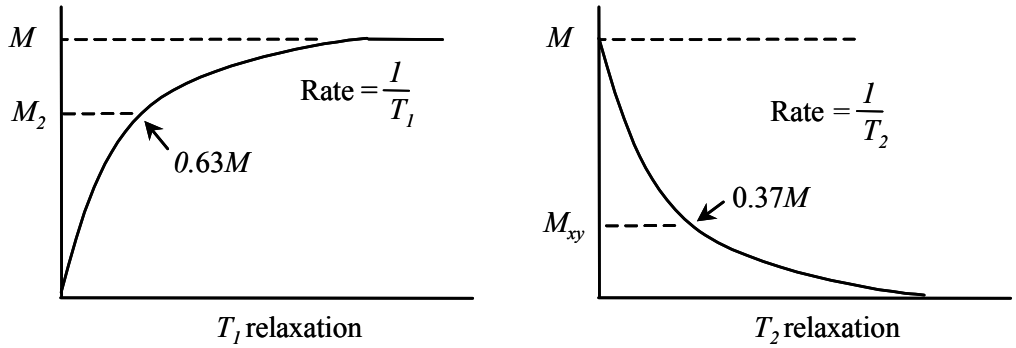

Figure 2.4.3.1. T_1 relaxation (L) as the increase in M_Z, or longitudinal component of M, as a function of time. T_2 relaxation (R) as the decrease in M_{XY}, or transverse component of M, as a function of time.

2.4.3.1. T_1 – Spin- Lattice Relaxation

Spin-lattice, or longitudinal, relaxation dissipates the energy of the nucleus to the surrounding "lattice". The term 'lattice' is a convenient, if somewhat loose, term to describe all the degrees of freedom associated with our system other than those directly concerned with spin. Longitudinal relaxation occurs with a time constant, T_1, describing the return of M_Z to equilibrium. T_1 also determines the difference between M_Z and M_o, the equilibrium net magnetization [81]. The equation governing this behaviour is,

$$M_Z = M_o(1 - e^{(-\frac{t}{T_1})}) \qquad (2.4.3.2.)$$

The characteristic time constant, T_1, is thus the time required for the Z component of M to return to 63% of its initial value following an excitation pulse (See Figure 2.4.3.1.) [96].

T_1 relaxation can occur via six different mechanisms. For further description of the mechanisms, the reader is referred to Martin *et al.* [93], however in our case only one

of the six types of relaxation occurs, allowing for quantitative interpretation of the data. This predominant T_1 relaxation mechanism is a result of paramagnetic impurities.

2.4.3.2. T_2- Spin-Spin relaxation

A nucleus undergoing spin-spin or transverse relaxation exchanges its energy with other nuclei during decay back to equilibrium. Thus no energy is transferred from, or to the lattice. This process can be described as a loss of phase coherence, or randomization of the spins, in the transverse (XY) direction. The following equation describes the decay, [95]

$$M_{XY} = M_{XY_o} e^{(\frac{-t}{T_2})} \qquad (2.4.3.3.)$$

where M_{XYo} is the equilibrium magnetization in the x-y plane and T_2 is the spin-spin relaxation time constant. The T_2 time constant is the time required for the transverse component (M_{XY}) of M to decay to 37% of its initial value (See Figure 2.4.3.1). All mechanisms that lead to T_1 relaxation will also lead to T_2 relaxation thus the T_2 value is always less than, or equal to, T_1[81, 95]. These processes of decay are irreversible [98].

The exponential decay curve of a transverse relaxation, T_2^*, is much faster than in pure T_2 processes and is termed the effective transverse relaxation time [81]. Two factors contribute to this effective transverse relaxation time: molecular interactions and variations in B_o. Magnetic field imperfections and intrinsic differences in local fields within the sample itself cause the nuclei to precess at slightly different rates gradually producing an irreversible loss of phase coherence of the spins. The value of M_{XY} thus decreases and approaches zero.

The mechanism of spin-spin relaxation is sensitive to interactions with magnetic fields caused by adjacent spins with low or zero reorientation rates (i.e. spins that are

bound at surfaces or within rigid solids). T_2 relaxation is thus more efficient in large molecules. Water molecules strongly bound to macromolecules lead to rapid T_2 relaxation of the water protons and the T_2 for free water is much longer than that of bound water. Bound waters can be taken as waters that are almost completely immobilized because of attachment to a macromolecule by 1 – 2 hydrogen bonds. Free waters are located at a distance from the macromolecules and retain the 3-dimensional hydrogen bond network present in the bulk water[99]. Additionally, relaxation mechanisms are highly sensitive to the presence of paramagnetic or ferromagnetic impurities due to the large local magnetic field inhomogenieties caused by the impurities [81, 95, 97].

The relaxation times of systems of interest determine the maximum time available for data acquisition. Signals may be observable for times ranging from a few microseconds to a few seconds with the longer relaxation times desirable due to increased acquisition time.

2.4.3.3. Pulse sequences

Since both spin-lattice and spin-spin relaxation processes occur simultaneously, modifications in the sample stimulation are necessary to allow for specific measurement of T_1 or T_2. Thus pulse sequences are designed to selectively interrogate a sample [81].

Singular pulses can be used to attain hydrogen concentration information within a system but for measurement of T_1 and T_2 relaxation, two or more pulses are required in quick succession. Parameters such as pulse number and strength, and interpulse spacing can be tailored to monitor various specific aspects of the system.

2.4.3.4. Spin Echo Pulse Sequence

The most basic pulse sequence contains two pulses, an initial A pulse to rotate the magnetization vector to the Y axis, followed by a B pulse after some time interval, τ, to rotate the magnetization vector 180^{o}. An echo signal, referred to as the spin-echo, then develops and reaches a maximum after time, τ. The time period between the A pulse and the corresponding echo is the echo time, TE.

After a 90^{o} pulse, free induction decay (FID) lasts for approximately a few milliseconds. In this small time interval between the A and B pulse, minimal T_1 decay, some T_2 dephasing, and substantial T_2^* dephasing occurs. Dephasing of T_2^* occurs at a constant rate due its dependence on the field inhomogeneity that the sample is exposed to, while pure T_2 dephasing is a random fluctuation resulting from the interactions among the nuclei themselves. As a result of these combined dephasing processes almost complete disappearance of the signal prior to the start of the second pulse is observed.

If a B pulse is applied at time τ, (τ = TE/2) after the A pulse, then phase coherence can be re-established at some time, τ, following the second pulse [100]. Since T_2^* dephasing is constant, all nuclei can be perfectly refocused and M_{XY} will equal its original value (immediately after the A pulse). While T_2^* dephasing is constant, T_2 dephasing is random and causes the nuclei to retain some randomness thus the echo is weaker than the initial signal. With this in mind, the time interval, τ, is varied and the period of free precession of the nuclei dephases irreversibly through spin-spin relaxation processes resulting in an amplitude decrease of the maximum echo with increasing TE/2.

A sequence was developed to attain the relaxation times without requiring a large amount of information on the system being studied, first by Carr and Purcell [101] and

later modified by Meiboom and Gill [102]. The resulting sequence is called the Carr-Purcell-Meiboom-Gill (CPMG) pulse sequence.

2.4.3.5. Carr-Purcell-Meiboom-Gill Pulse Sequence (CPMG)

CPMG involves the transmission of a sequence of 180^o pulses with echo measurement after each pulse, yielding the true relaxation of the magnetization vector in the transverse plane. The series of 180^o pulses are applied at evenly spaced intervals, τ, 3τ, 5τ, 7τ, etc., following the initial 90^o pulse. Echoes are then observed during the intervals, 2τ, 4τ, 6τ, 8τ, etc. [78]. Diffusional effects that lead to a decrease in echo amplitude are minimized by ensuring the time intervals between pulses (2τ) are small [103]. T_2 can now be readily found using the decrease in echo amplitude,

$$M = Ae^{(-TE/T_2)} \qquad (2.4.3.4.)$$

where M is the signal strength and A is the relative population constant for each value of τ. The relaxation time is now readily available.

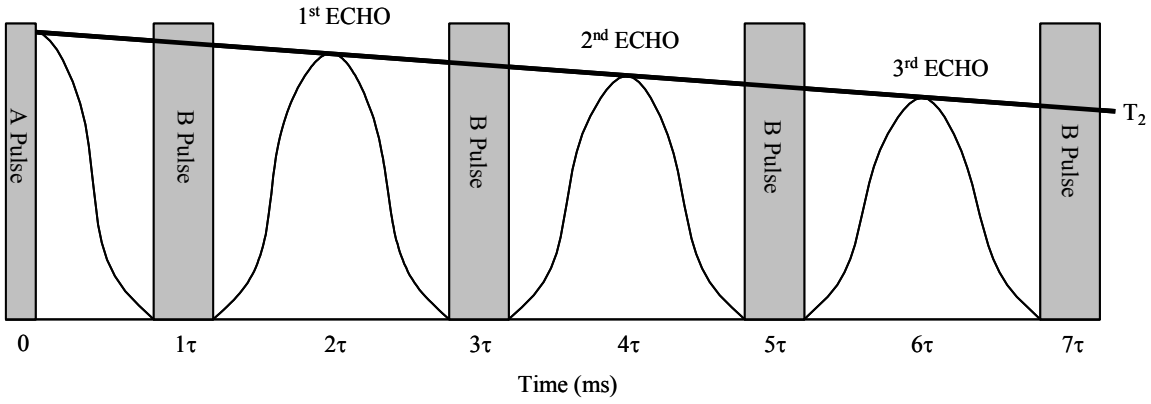

Figure 2.4.3.5. CPMG Pulse Sequence diagram.

CHAPTER THREE: EXPERIMENTAL PROCEDURE

3.1. Sample and Solution Preparation

3.1.1. Soil Sample

Laurentian soil (LAUR) was fractionated to obtain a representative humic acid sample. LAUR is an organic rich forest podzol, from the Laval University forest reserve in Quebec, Canada, and is well characterized [27, 104-107]. The soil sample used in this study was collected by Dr. Don Gutzman.

Table 3.1.1. Podological Properties of LAUR Soil (mean values are in brackets) [108]

Particle Size	Total Sand (50 - 2mm) 50 – 69 %	Total Silt (2 - 0.05mm) 18 – 33 %	Total Clay (0.05 - 0mm) 6 – 25 %
pH	3.8 – 4.3 (4.1) in H_2O (1:1)		
Organic Carbon	0.3 – 13.2 % (12 %)		
Nitrogen	0.28 – 0.9 % (0.54%)		
Exchangeable Cations (meq / 100g)	Ca: 0.0 – 4.1	Al: 1.0 – 10.7	
	K: 0.03 – 0.21	Mg: 0.04 – 0.2	
	Na: 0.0 – 0.1		
Cation Exchange Capacity (CEC) (meq / 100g)	44.2 – 75.8		
Total Elemental Analysis	(%)	Al: 6.6, Fe: 6.1, Ti: 1.8, Ca: 1.8, Mg: 0.42, K: 1.8, Na: 0.65	
	(ppm)	Mn: 518 $\pm$ 28, Zn: 89 $\pm$ 3.9, Cu: 7 $\pm$ 2.2, Pb: 26 $\pm$ 2.4, Co: 18 $\pm$ 2.2, Ni: 4 $\pm$ 1.0, Cr: 16 $\pm$ 1.4, Sr: 300 $\pm$ 32, Hg: 0.166, Se: 0.710	

3.1.2. Humic Acid Extraction

One kilogram of LAUR was stirred in 0.1M NaOH (BDH Scientific) solution under a blanket of N_2 gas for 5 hours. The liquid was collected and centrifuged on a rotary spinner for 25 minutes. The supernatant was then acidified to pH 2.0 with 1.0M HCl (EM Science) and left to settle. The solution was decanted and the collected solid

was put through repeated cycles of washing with 1.0M HCl solution followed by centrifugation under an N_2 blanket. After ten cycles, the solid was washed with ultrapure water (Millipore Milli-Q) (18MΩ) then centrifuged. Washings were discarded and after four cycles, the solid was dried in a desiccator under vacuum.

3.1.3. Humic Characterization

This particular humic acid is, as stated previously, well characterized, however to ensure the extraction process was efficient, a few characterization tests were performed. The final Laurentian Humic Acid (LHA) was tested for levels of ash, sodium and iron to ensure; a high organic carbon content, sample is fully protonated, and low total metals, respectively.

Iron, as well as mercury, are typically the most strongly bound of metals to humic ligands [109]. A low iron concentration is therefore conveniently used as an indicator of a low total metals concentration (mercury is usually in very trace concentrations which are more difficult to quantify). Iron was analyzed using a Thermo-Jarrel Ash Inductively Coupled Plasma (ICP) with an atomic emission spectrometer controlled by ThermoSpec v. 5.06 software. Solution concentration was 150 mg/ L LHA. Iron concentration was 1.7 $\pm$ 0.5 ppm based upon the solid. For reference LHA has been described in previous work as 51.9% C, 5.5% H, 2.3% N, 39.9% O, and 0.26% S with 6 ppm Na and 2 ppm Fe (as determined by elemental analysis and atomic adsorption) [106, 108].

To test for ash content, a crucible of known weight, containing a known amount of LHA was partially covered and heated till no more vapours were observed. The crucible was then cooled in a desiccator and reweighed. The remaining mass of LHA was

taken as ash and constituted 4.51% of the LHA total mass, presumably mainly aluminosilicate material. This indicates a soil with a high organic content.

The absence of sodium was confirmed using a flame test. The solutions analysed were 150 mg/L and no sodium was detected. Thus the sample is > 99% in the proton form.

3.1.4. Solution Preparation

All containers used in this project were pre-cleaned with a 0.1% ethylenediamine tetraacetate (EDTA) solution (BDH Scientific) followed by triplicate rinses with ultrapure water. LHA solutions were prepared by weighing out the appropriate amount of LHA and dissolving it in a solution of NaOH (pH ≅ 10). The solution was stirred till no visible solid remained. A buffer was then added at a concentration of 15 mM to ensure stable pH values. pH 4.0 and 5.0 used a sodium acetate buffer (pKa 4.76) (BDH) while pH 6.0 and 7.0 used a potassium dihydrogen orthophosphate buffer (pKa 7.20) (BDH). The pH values were chosen to mimic environmental values. An additional benefit of the buffer solutions is an ionic strength buffering as well. The LHA solutions were then adjusted to the appropriate pH ($\pm$ 0.01 pH units) using either HCl or NaOH. The solutions were then transferred to pre-cleaned, aluminium foil wrapped Nalgene® HDPE screw top bottles and refrigerated in the dark. The solutions were not used if they were older than one month.

Copper solutions were created by dissolving solid copper sulphate (MCB Reagents) in ultrapure water and storing in Nalgene® HDPE screw top bottles

3.2 Laser Light Scattering Experimental Procedure

3.2.1. Sample Preparation

The light scattering cells were rigorously cleaned prior to use to ensure no dust or metal contamination. The cells were first soaked in a warm Extran® 300 solution (EM Science) overnight, rinsed with ultrapure water, 1% EDTA solution, then followed by three rinses of 0.2 μm filtered ultrapure water. The cells were then immediately wrapped in tinfoil and dried in a desiccator under vacuum. All cleaned cells were protected from dust prior to analysis.

LHA solutions were filtered with 1.2 μm Acrodisc® 32 mm Supor® membrane syringe filters prior to analysis. The more common 0.45 μm filters were not used for the LHA solutions due to literature reports of HA of diameters up to 436±36 nm [36], and a desire to not bias the samples towards the smaller diameter HA species. LHA filtered and non-filtered solutions were checked by absorbance to ensure no LHA was lost to the filter. No difference between the solutions was detected. All copper solutions were filtered with 0.45 μm nylon syringe filters (MSI). The LHA and copper were mixed 35 minutes prior to analysis and capped to avoid contamination. Prior to analysis, the cells were wiped down with KimWipes® and introduced into the light scattering apparatus. A diffraction matching liquid was pumped around the cell for one minute to ensure no air bubbles, then left to settle for a further minute prior to analysis. The samples were analyzed at room temperature.

3.2.2. Instrument Parameters

A PMT Hamatsu HC 120 with a BI-9025 AT system made by Brookhaven fitted with a BI-200 SM collector was used for all runs. Software used to collect the light

scattering data was BI-2P v. 4.3 manufactured by Brookhaven. The detector was set to 90^{o} to minimize effects of flare, dust and misalignment. The viscosity was 1.005, refractive index 1.333, and $\lambda = 632.8$ nm. Detector aperture was set to 400 nm.

3.2.3. Data Analysis

All results were analysed using a CONTIN model. The measured baseline was used and the software suggested particle size range was accepted. The results were transferred to a spreadsheet. Particle sizes were summed from 1-50, 51-120, 121-250, 251-400, and 401-9000 nm. Within each pH value and copper concentration, the largest detector response of particle diameter was given a value of 100 and the remaining data normalized to that point. This ensures that the data presents the distribution accurately, however the values cannot be quantitatively compared from one copper concentration to another. Instead the distribution of particle sizes is available for comparison qualitatively through plots of detector response as a function of particle size. Confidence intervals were calculated for both 95% and 90% and are presented in Appendix One.

3.3 EPR Experimental Procedure

3.3.1. Sample Preparation

Samples were run at room temperature in either 4 mm diameter quartz (solid samples) or capillary tubes (liquid samples). Solid LHA samples were run in three different ways: “dry”, “moist” and “sludge”. “Dry” samples were dried in a desiccator for 12 days before being weighed and placed in a 4 mm sample tube, sealed from the atmosphere, and analysed. LHA placed on an elevated open dish inside a sealed container with water in the bottom allowed the LHA to equilibrate with atmospheric water content

for 12 days. These samples were termed “moist”. After this wetting period the sample was quickly weighed and transferred to a 4 mm tube, sealed, and analyzed. For “sludge” samples, dry LHA was wetted until the water to LHA ratio was approximately 1:4 (w/w) and left for 4 hours to equilibrate prior to analysis (Todoruk *et al.* found 3 hours is sufficient to ensure full wetting [27]).

A “liquid” LHA sample was also prepared at a high pH (~10) and a high concentration (greater than 1000 mg/L LHA). High pH is implicated in promotion of radicals in HS [110], as well a high concentration will increase any signal. This sample was placed into a capillary cell which is advantageous to minimize dielectric microwave dissipation by water [111]. An additional sample of 500 mg/L LHA at a pH of approximately 10 was run in a capillary tube. Each sample was analyzed in triplicate.

3.3.2. Instrument Parameters

Experiments were run on a Bruker ER083CS with an ER 041 XG MW bridge X band. The detector was a Bruker EMX EPR Spectrometer. Ten scans were performed for each experiment with sweep width varying between 100 and 25 G. The microwave field frequency was 9.771 GHz with a power of 12.660 mW. The receiver gain was 1.59×10^4 with a modulation frequency of 100 kHz and amplitude of 1 G. The signal channel had a conversion of 20.480 ms with a time constant of 0.320 ms and a sweep time of 20.972 s. The microwave power was always kept as low as possible to avoid saturation effects due to oxygen from the air, which can become significant when high microwave power is employed [112]. The instrument was calibrated with a Strong Pitch standard (Bruker).

3.4 Competing Ligand Exchange Method Experimental Procedure

3.4.1. Sample Preparation

Buffered humic acid-copper solutions were analyzed at room temperature (concentrations of 50, 150, and 250 mg/L LHA with the full range of copper concentrations in this study) for pH 4.0 and 7.0 as well as some runs of pH 5.0 and 6.0. Copper ions were introduced to the humic solutions 35 minutes prior to the initiation of each run to allow for binding to occur. The experimental cell was custom made from glass (10 cm tall and 6 cm in diameter). An outlet on the bottom edge allowed solution to flow into a fitted Acrodisc® Supor® membrane syringe filter (Pall Gelman). The filter, either 0.45 μm or 1.2μm pore sizes, was attached to Tygon® tubing leading to the ICP pump and from there into the ICP nebulizer (Figure 3.4.1). The cell was placed on a heat-insulated stirrer with a Teflon™ coated stir bar placed inside the cell, stirring at a moderate rate over the course of the experiment.

The ion exchange resin used was a Chelex 100 molecular biology grade resin of 200-400 mesh size in the sodium form (corresponding to a resin size range of 75 – 150 μm) (Bio-Rad). The resin was pre-treated to appropriate pH by soaking in buffer until the supernatant of the resin was within $\pm$ 0.02 pH units of the desired pH. The resin was weighed prior to runs to ensure a 1% (w:w) loading and used moist. It was important that the resin be used moist as the drying of the resin has been found to impact upon the metal binding properties [67]. A loading of 1% (equivalent to a Chelex to metal ratio of 100 or higher, depending on the metal concentration within the sample) was used to ensure that the change in the sample volume over the course of the experiment has negligible effect

[70]. Any grinding of the resin by the stir bar is taken to be insignificant with regards to changes in resin surface area [70].

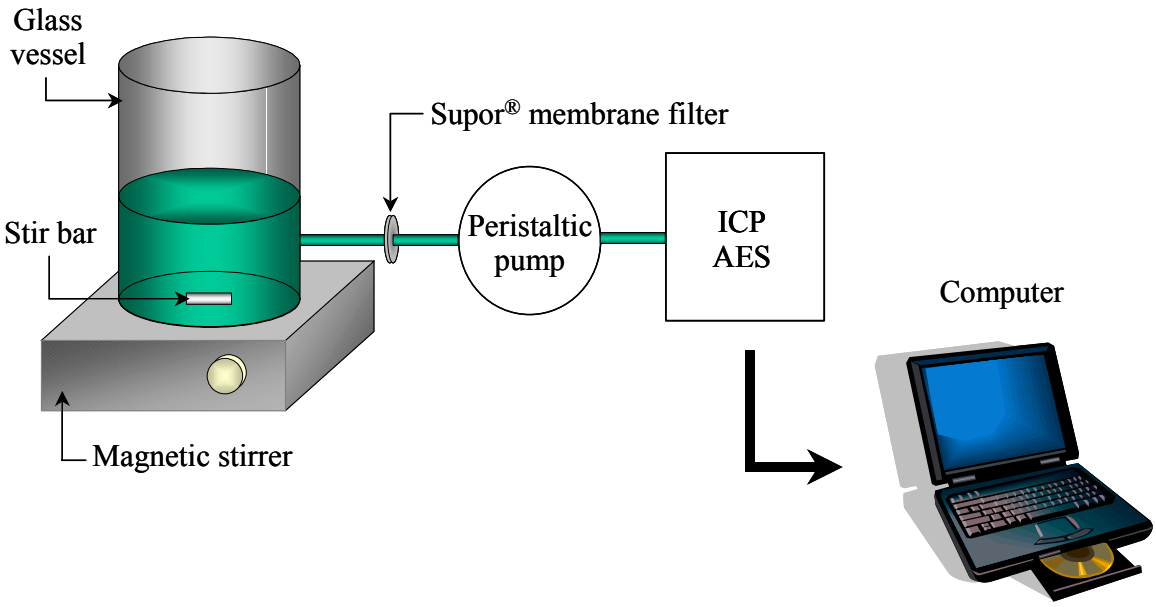

Figure 3.4.1. Schematic of CLE Method using Chelex-100 resin instrumental setup.

3.4.2. Instrument Parameters

A Varian Liberty RL Sequential ICP-OES was used for all runs and controlled by ICP Expert software for Liberty. Copper was analyzed in triplicate at the 324.754 nm wavelength with a plasma flow rate of 15.0 L/min, and nebulizer pressure of 200 kPa. Prior to each data point acquisition, a fast pump rate was held for 10 seconds to flush out the previous sample, a stabilization period of 15 seconds was then initiated at a pump rate of 15 rpm. A final period of 5 seconds was used for sample measurement for a total single datum point measurement time of 30 seconds. A solution of 5% HNO_3 was used to flush the system prior to each experiment. Instrument output was time of measurement completion and copper concentration in ppm.

3.4.3. Experimental Procedure

Calibration of the ICP was accomplished by 1.005 mg/L and 10.05 mg/L standards, prepared fresh daily from a certified 1005 mg/L standard (SCP Science).

Prior to the introduction of the Chelex resin, several readings were taken of the sample solution to get an accurate reading of the solution copper concentration. Once a stable copper concentration was recorded, the resin was introduced and measurements were begun immediately. Measurement was then repeated every 30 seconds till a total of approximately forty were completed.

3.4.4. Data Analysis

Data were inputted into Excel® spreadsheets and plotted. The data analysis method for determination of rate constants follows from the work of Shuman and co-workers involving a Laplace transform [113, 114]. The plots were first fitted to a sixth degree polynomial fit (Excel) to smooth the data. The first and second derivatives of the polynomial were then taken and *H(k)* was calculated (from equation 2.3.2.7.) and plotted against ln *t*. The peaks in the plot then corresponded to the number, relative abundance and rate constants of the components present in the system. These values were used as initial guesses to treat unsmoothed data by a minimization of equation 2.3.2.4. through a Marquardt algorithm (statistical software SAS 8.2). One advantage of this method of component elucidation is that the Laplace transform provides an objective choice of the number of components and approximate concentrations, which can then provide initial guesses that will be optimized by the Marquardt algorithm.

3.5. Low-field NMR Experimental Procedure

3.5.1. Sample Preparation

Sample cells were cylindrical glass vessels 3.5cm in diameter and 5cm in height. The cells had round glass lids that were secured in place with Teflon™ tape. Auto pipettes were used to deliver 9.90 ml of buffered LHA solution and 0.10 mL of the copper solution. The cell was sealed and placed into a 30 $\pm$1 ^{o}C water bath for 35 minutes prior to analysis. A standard of 1.0 x 10^{-4} M copper solution was run as a measure of day to day instrumental fluctuation. (Appendix Two).

3.5.2. Instrument Parameters

The low-field NMR experiments were performed on a CoreSpec-1000™ (NUMAR Corp.) relaxometer at a frequency of 1 MHz (field strength of 0.024 T) with a Teflon™ tube sample holder thermostated at 30^{o}C. The T_2 relaxation time distributions were recorded using the CPMG pulse sequence as introduced in Section 2.4.3.5. [78, 103]. Spectra were optimized with the best program found at an inter-echo spacing of 0.6 ms, with a signal to noise (S/N) ratio of at least 225. A recovery time of 5500 ms was allowed for a series of 5000 echoes. System gain was set to 400 with the number of trains (discrete pulses) at 16. Each run took three minutes and fifty-six seconds. Prior to analysis the instrument was tuned to ensure accurate performance.

3.5.3. Data Processing

The data were processed using EchoFit v.3.02 (NUMAR Corporation), a software package created for relaxometry that utilizes non-negative least squares methods to create the T_2 distributions. The T_2 geometric mean was used for further data analysis.

Independent analysis demonstrated that a single exponential provided a good fit of the data.

CHAPTER FOUR: EXPERIMENTAL RESULTS

Over the course of the experiments required for this thesis, several techniques were required. Analysis of the NMR experiments highlighted the necessity for the EPR and CLEM experiments which will be presented in Sections 4.2 and 4.3., respectively. The information from these sections is used in Section 4.4 where it is integrated into calculations of the low field NMR system.

The formation of some visible aggregates in some concentrated LHA and copper solution led to an interest in dynamic light scattering (DLS) to investigate the conformational changes that occur upon binding. DLS also provides an attractive test for our binding model (introduced in section 5.1). The first section of this chapter is the DLS that was performed.

4.1. Laser Light Scattering Results

Light scattering is an attractive tool to investigate aggregation behaviour in humic mixtures. The binding concept that will be introduced in Section 5.1., will give aggregation a central role. Therefore, DLS was measured on a subset of samples (25 mg/L, 125 mg/L, and 225 mg/L LHA) to obtain information about the changes that occur for the LHA particles upon binding of copper for various levels of copper loading.

For all pH values the major particle diameter was between 121-250 nm, with smaller amounts of the larger and smaller particles as well. The mixtures displayed a heterogenous size distribution. Results were not attainable for 1.0×10^{-3} M Cu^{2+} due to excessive noise from aggregates that had formed in the solutions.

Some representative plots for pH 7.0 are shown in Figures 4.1.1. – 4.1.4. The data shows the predominance of different size components of the LHA solutions. As the copper concentration was increased from 0 to 1.0 x 10^{-4} M the distribution of 25 mg/L LHA shifted from a large amount in the lower diameter divisions (1-50 and 51-120 nm) to the larger diameter (401- 9000 nm). The pattern was less apparent for 125 mg/L LHA and not resolvable at 225 mg/L LHA.

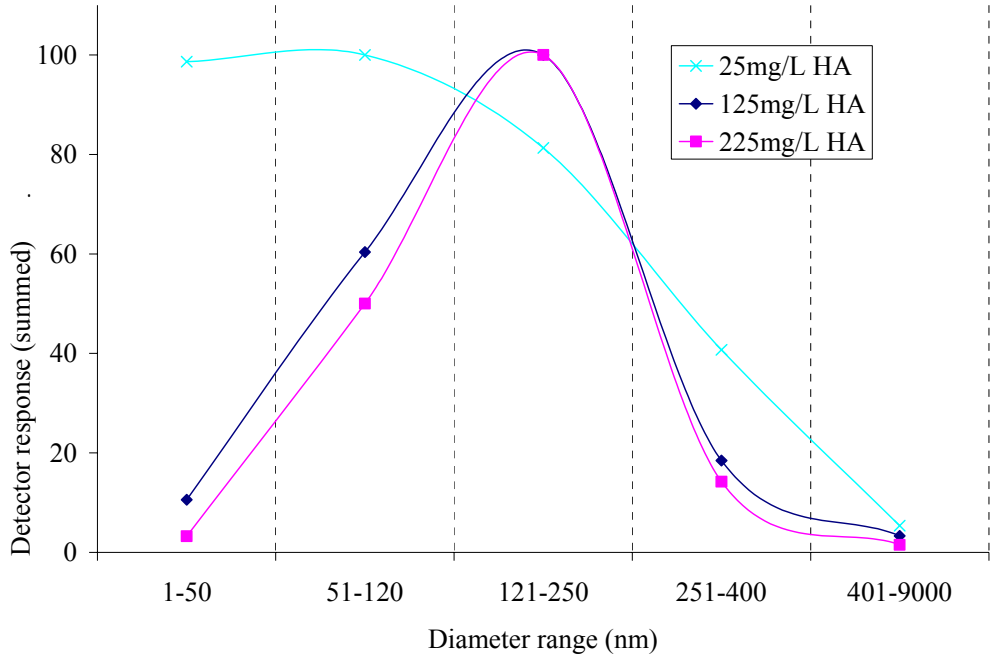

Figure 4.1.1. DLS plot of summed size distributions for pH 7.0 25 mg/L, 125 mg/L, and 225 mg/L LHA with no Cu^{2+} added. (Error analysis is in Appendix One)

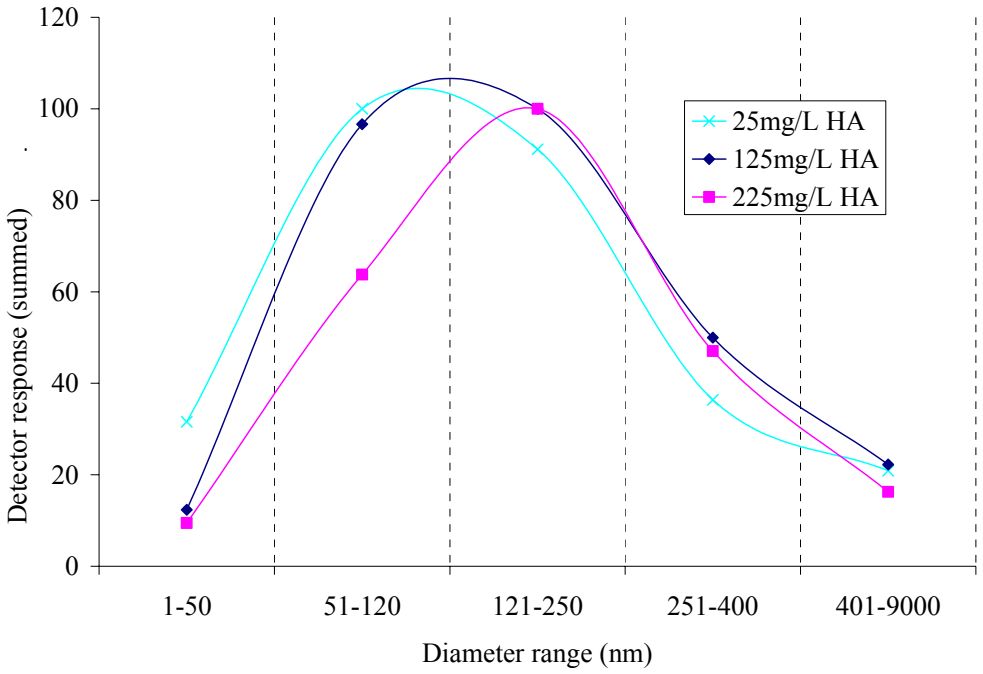

Figure 4.1.2. DLS plot of summed size distribution for pH 7.0 25 mg/L, 125 mg/L, and 225 mg/L LHA with 1.0 x 10^{-6} M Cu^{2+}. (Error analysis is in Appendix One)

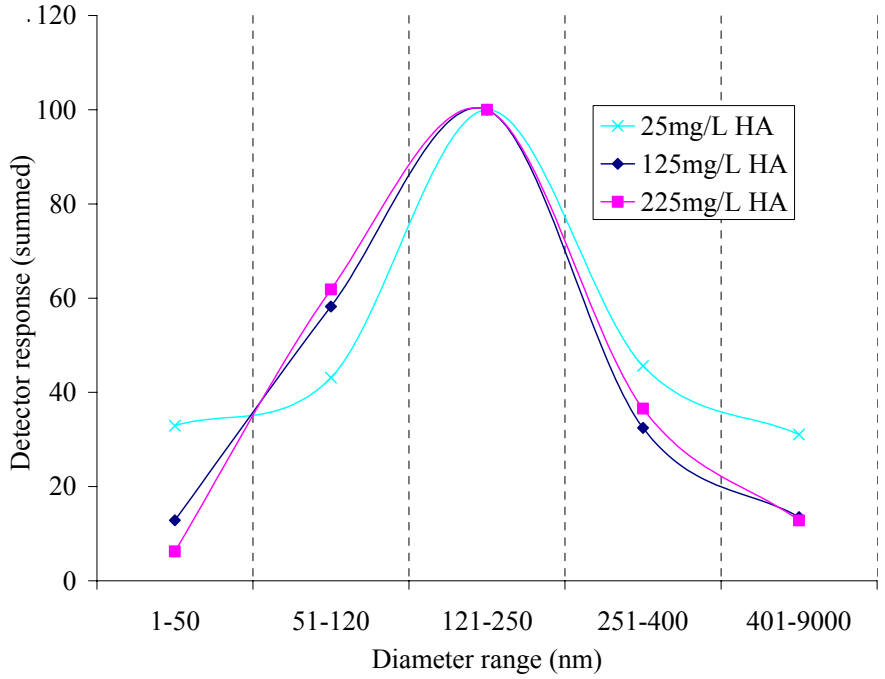

Figure 4.1.3. DLS plot of summed size distributions for pH 7.0 25 mg/L, 125 mg/L, and 225 mg/L LHA with 1.0 x 10^{-5} M Cu^{2+}.(Error analysis is in Appendix One)

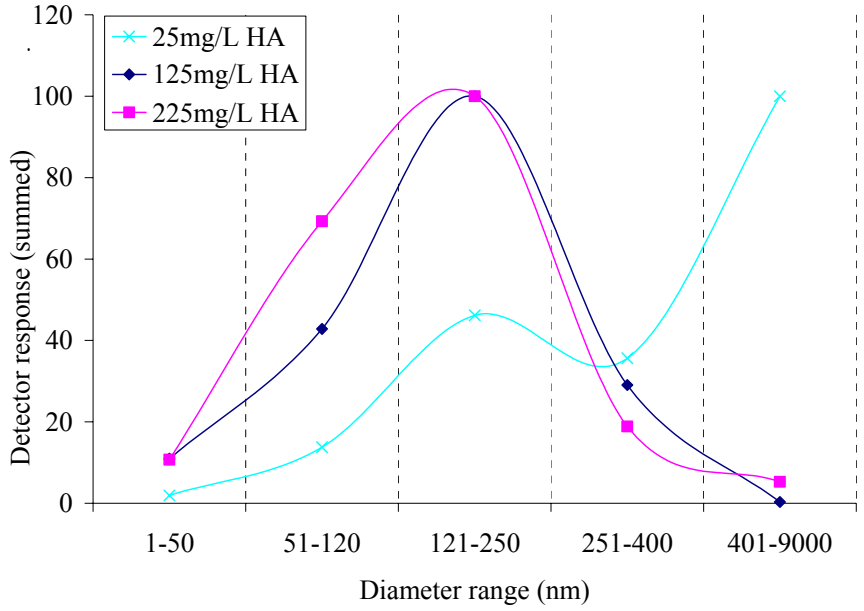

Figure 4.1.4. DLS plot of summed size distributions for pH 7.0 25 mg/L, 125 mg/L, and 225 mg/L LHA with 1.0 x 10^{-4} M Cu^{2+}. (Error analysis is in Appendix One)

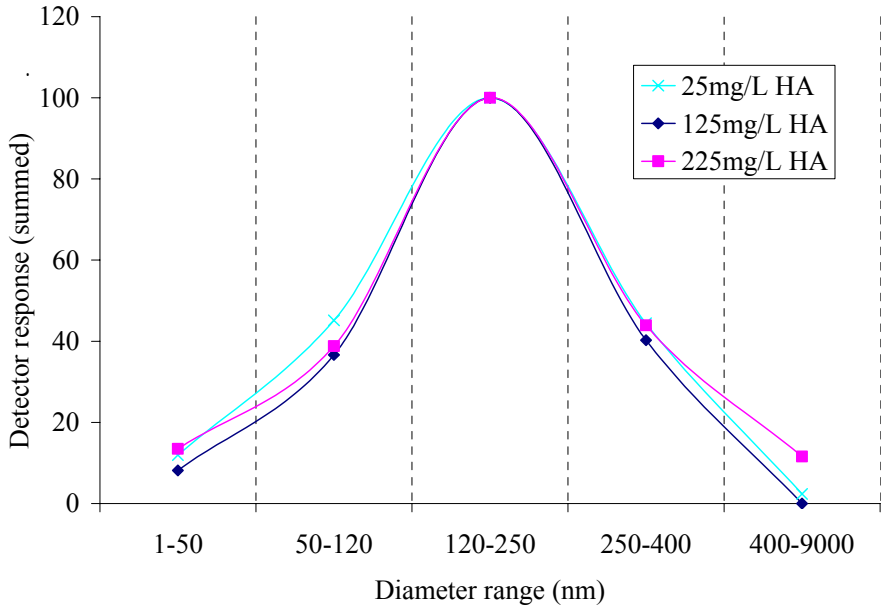

Figure 4.1.5. DLS plot of summed size distributions for pH 4.0 25 mg/L, 125 mg/L, and 225 mg/L LHA with no Cu^{2+} added. (Error analysis is in Appendix One)

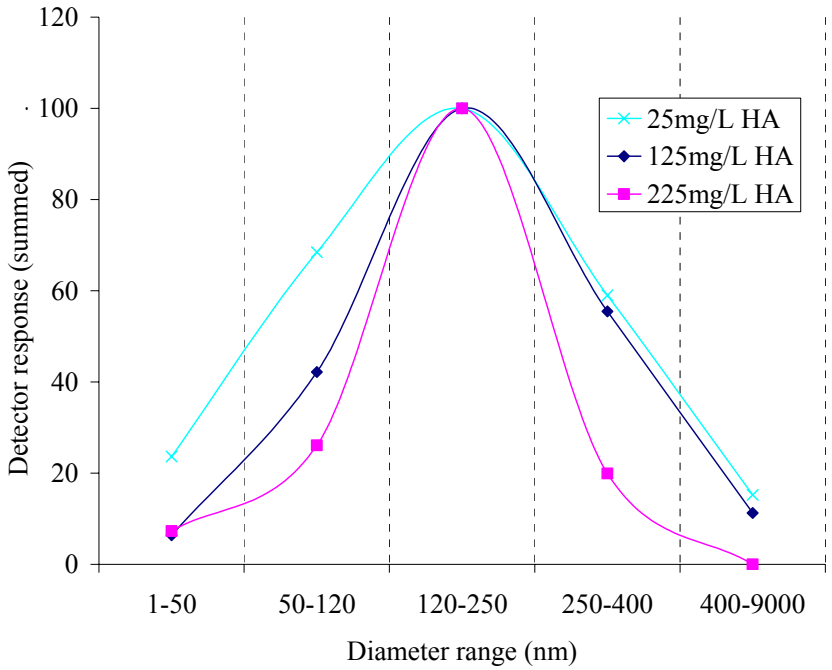

Figure 4.1.6. DLS plot of summed size distributions for pH 4.0 25 mg/L, 125 mg/L, and 225 mg/L LHA with 1.0 x 10^{-6} M Cu^{2+}. (Error analysis is in Appendix One)

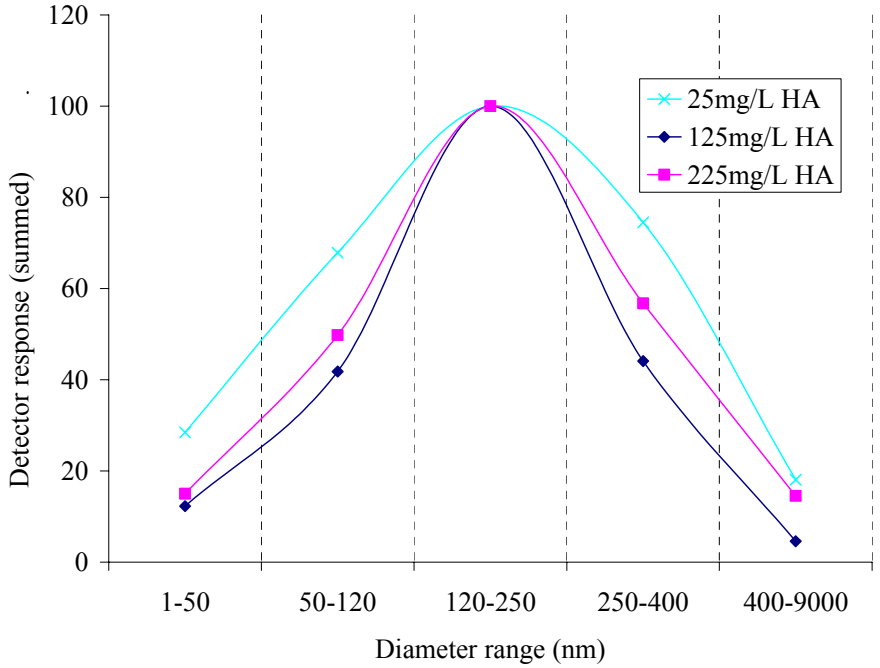

Figure 4.1.7. DLS plot of summed size distributions for pH 4.0 25 mg/L, 125 mg/L, and 225 mg/L LHA with 1.0 x 10^{-5} M Cu^{2+}. (Error analysis is in Appendix One)

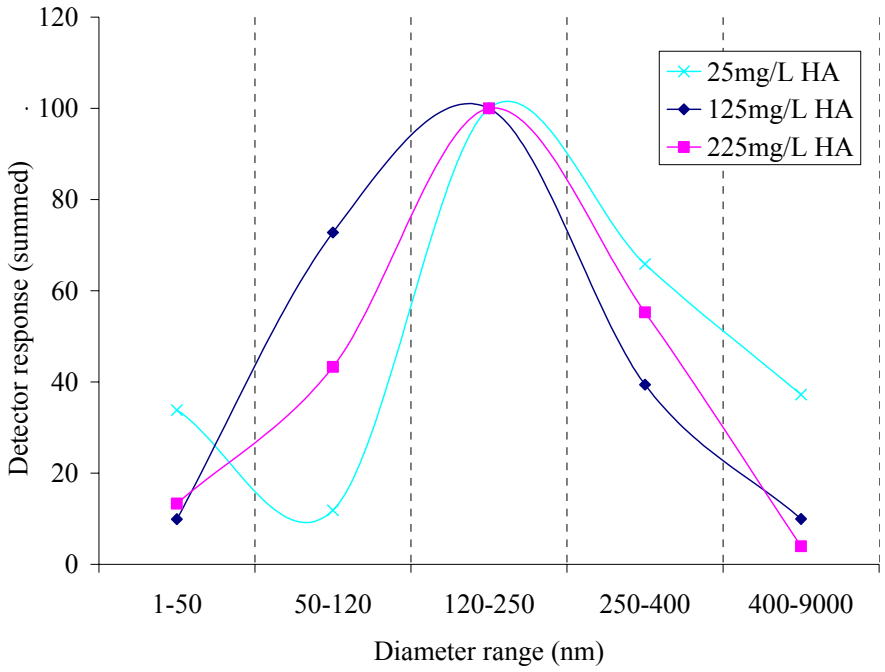

Figure 4.1.8. DLS plot of summed size distributions for pH 4.0 25 mg/L, 125 mg/L, and 225 mg/L LHA with 1.0 x 10^{-4} M Cu^{2+}. (Error analysis is in Appendix One)

Results of pH 4.0 (Figures 4.1.5-4.1.8.) underline the promotion of a similar degree of aggregation as the carboxylate groups of LHA are protonated. Generally, they also showed a slight shift towards larger particle size. This was apparent for 25 mg/L but could not be easily identified for 125 mg/L. The 225 mg/L again shows very little shifts. The shift towards a larger diameter particle size is less apparent for pH 4.0 than pH 7.0. Samples of pH 5.0 and 6.0 were also measured and demonstrated patterns that generally coincided with that seen in pH 4.0 and 7.0 (Appendix Three). The patterns evident in the pH 5.0 and 6.0 are more complex with some deviations, however the main conclusions drawn from the pH 4.0 and 7.0 are still evident.

4.2 EPR Results

Five LHA samples were analyzed; 'dry' (dried 12 days in desiccator), 'moist' (12 days equilibration with atmospheric water in sealed environment), 'sludge' (1:4 (w/w) water to LHA ratio with 4 hours of equilibration), and 'wet' (approx. 1000 mg/L, pH ~10), as well as a 500 mg/L LHA solution (pH ~10).

The solid samples showed the strongest signals with the signal diminishing with increasing water content. "Dry" samples (Figure 4.2.1.) showed a spectrum consisting of a single symmetrical line devoid of any fine structure. The peak is centred at 3486.4 G and has amplitude of 30 x 10^3. The "moist" (Figure 4.2.2.) spectrum also possessed a single line devoid of any fine structure. This peak was centred at the same point as the "dry" sample yet the amplitude decreased to approximately 6.5 x 10^3. The spectrum also shows a higher noise in the signal line as the intensity of the main signal drops. Further wetting of the LHA to form the "sludge" sample, with a water/LHA ratio of 1:4, causes the spectrum peak to decrease greatly in amplitude (Figure 4.2.3.) to a value of roughly 0.90 x 10^3 with a band centre at 3445.0 G. This peak shift is slightly downfield. The "liquid" LHA spectrum continues the pattern of diminished peak height (Figure 4.2.4.). The peak has a height of approximately 0.35 x 10^3. The peak is also much noisier as the signal is getting closer to the background noise level. The 500 mg/L LHA solution did not give any detectable signal. The 'wet' and 500 mg/L sample were run in capillary tubes to minimize the dielectric absorption of microwave radiation by water molecules [115]. While the 'wet' sample did display a slight signal, none was detected for the 500 mg/L solution. Both solutions concentrations were far greater than that of any experimental runs in the low-field NMR Cu – LHA titrations.

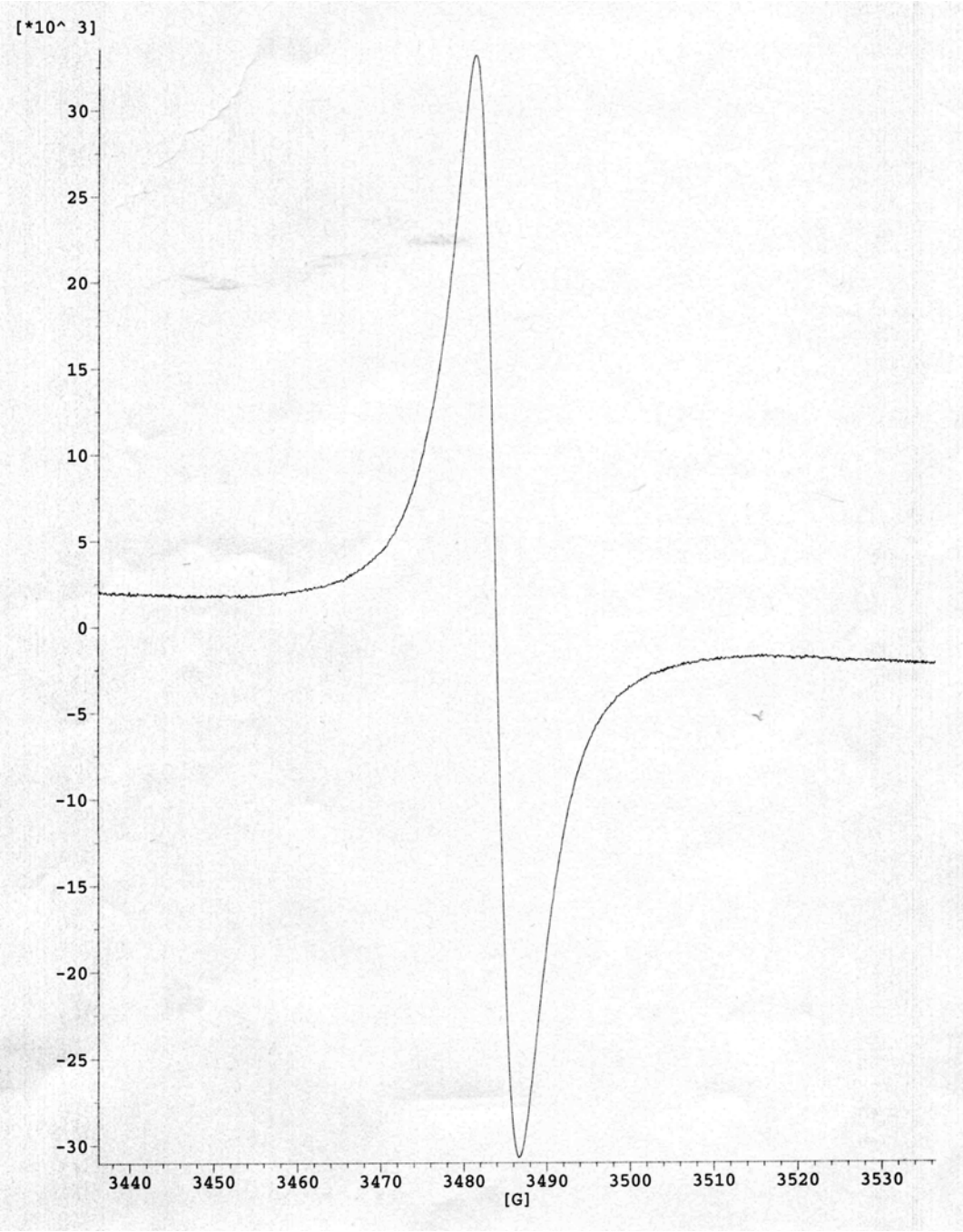

Figure 4.2.1. EPR Spectra of 'dry' sample run in 4 mm quartz tube. y axis is signal intensity (unspecified units).

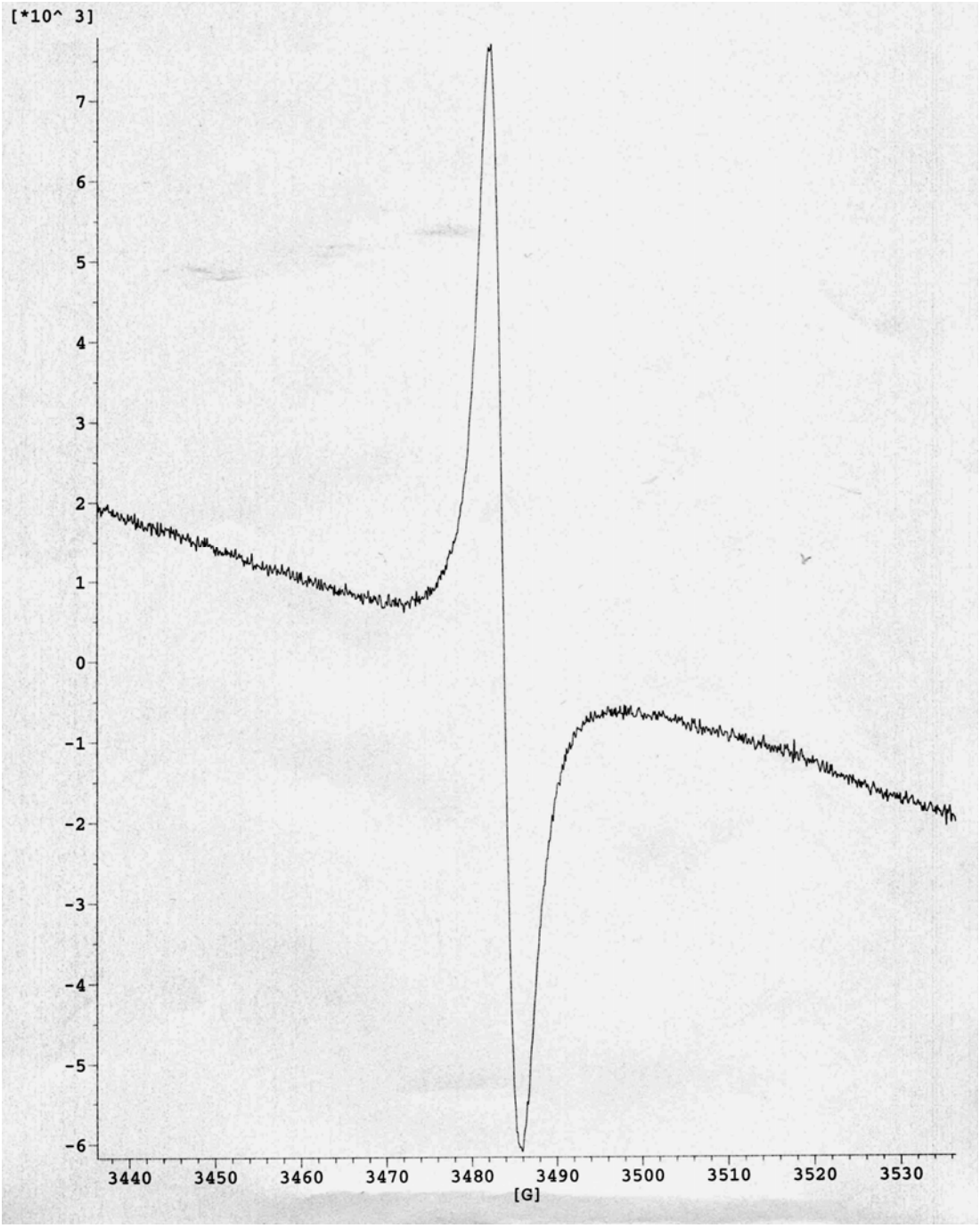

Figure 4.2.2. EPR spectra of 'moist' sample run in 4 mm quartz tube. y-axis is signal intensity (unspecified units).

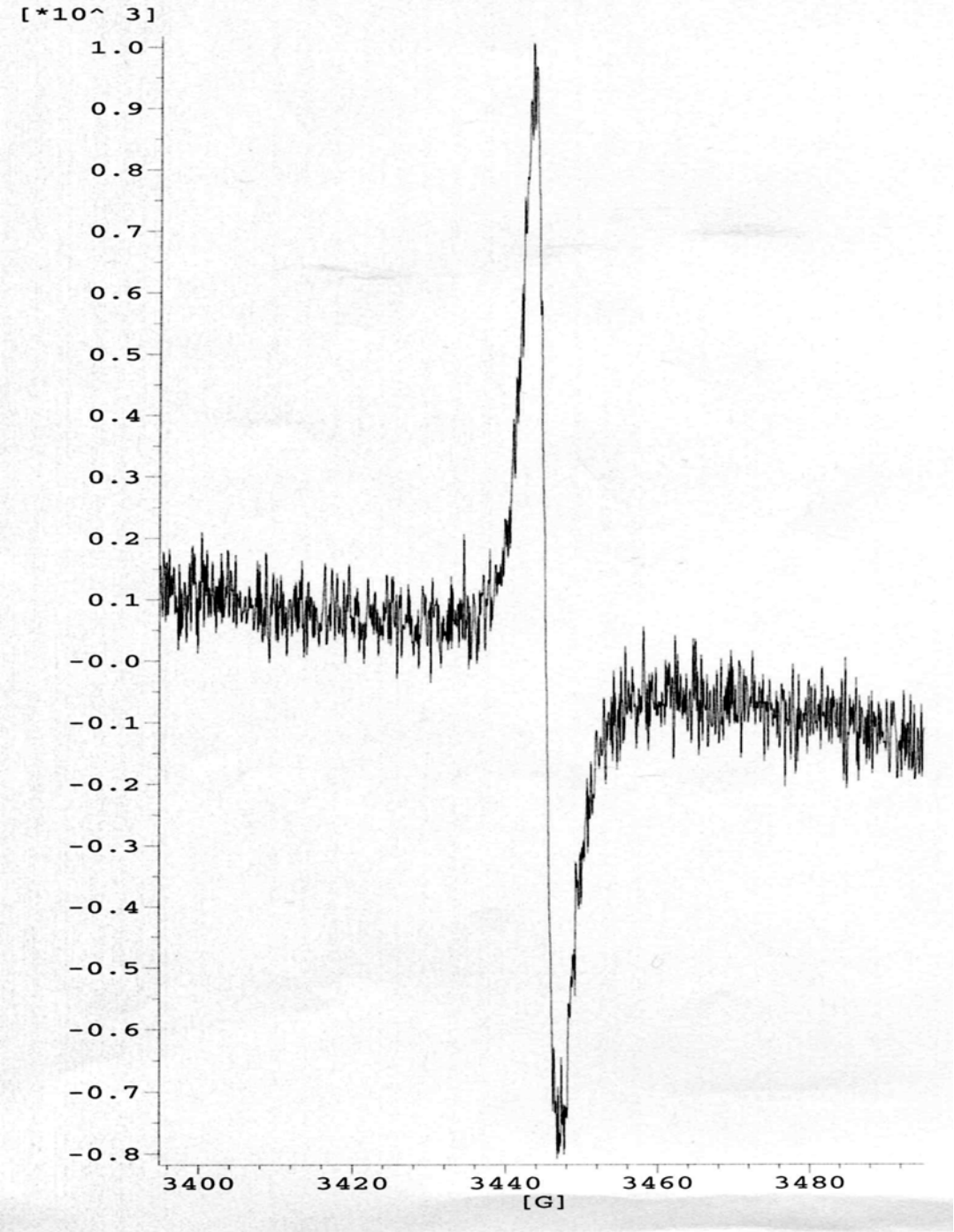

Figure 4.2.3. EPR spectra of 'sludge' sample run in 4 mm tube. y-axis is signal intensity (unspecified units).

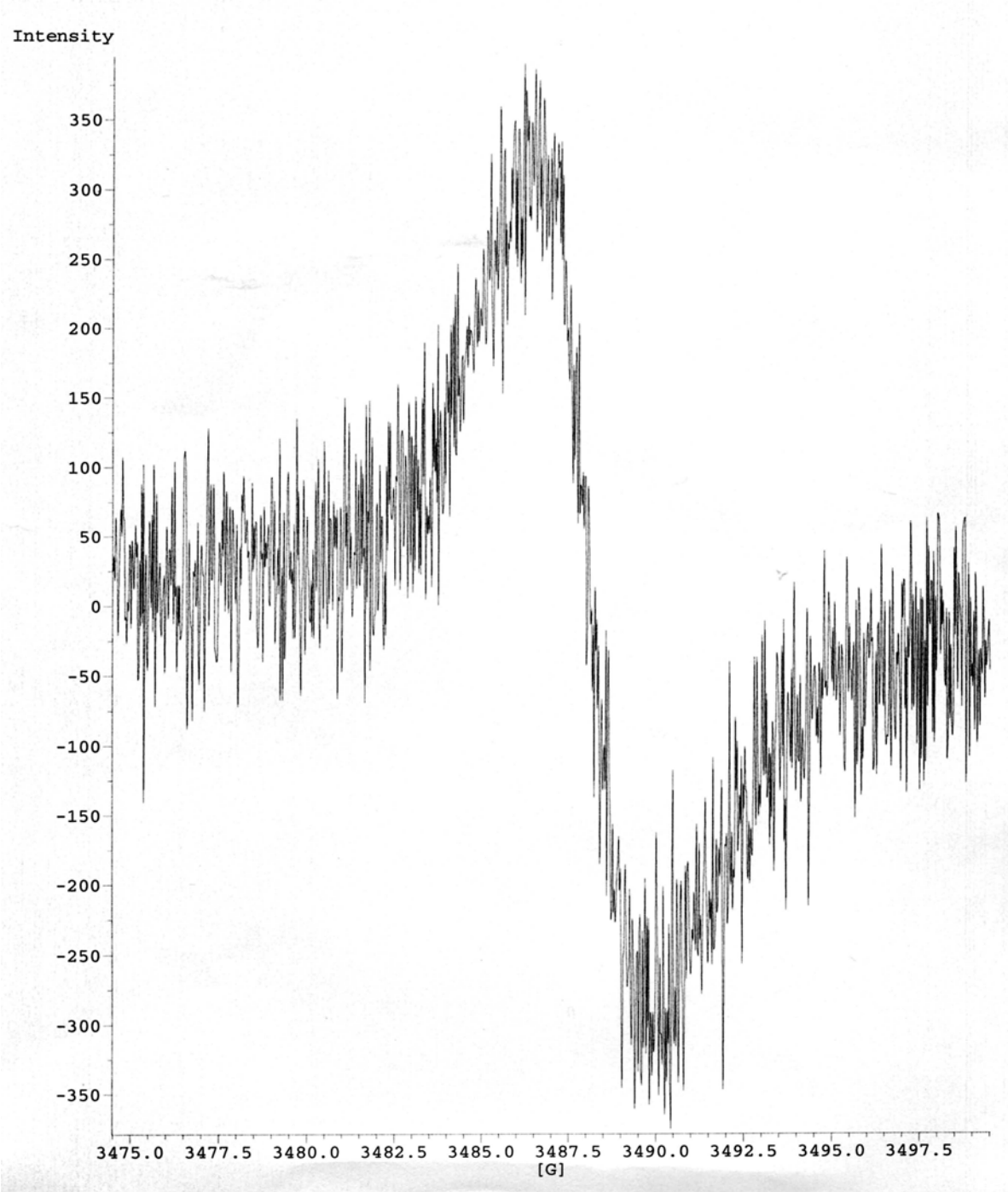

Figure 4.2.4. EPR spectra of 'wet' sample in capillary tube. y-axis is signal intensity (unspecified units).

4.3. CLEM Results

4.3.1. CLEM results

The uptake of Cu^{2+} into the Chelex resin in the absence of LHA (buffered to pH 4.0) is shown below. The rate constant for copper uptake into the resin is approximately 0.019 $\pm$ 0.002 s^{-1}. The decay curves of pH 4.0 and 7.0 for 150 mg/L LHA and 5.0 x 10^{-5} M Cu^{2+} are provided in Figures 4.3.2. and 4.3.3., respectively. The decay curves for all data were fitted as per the procedure described in Section 3.4.4., and from the Marquardt non-linear fitting applied to the sum of first order kinetic terms, the number and concentration of components was found.

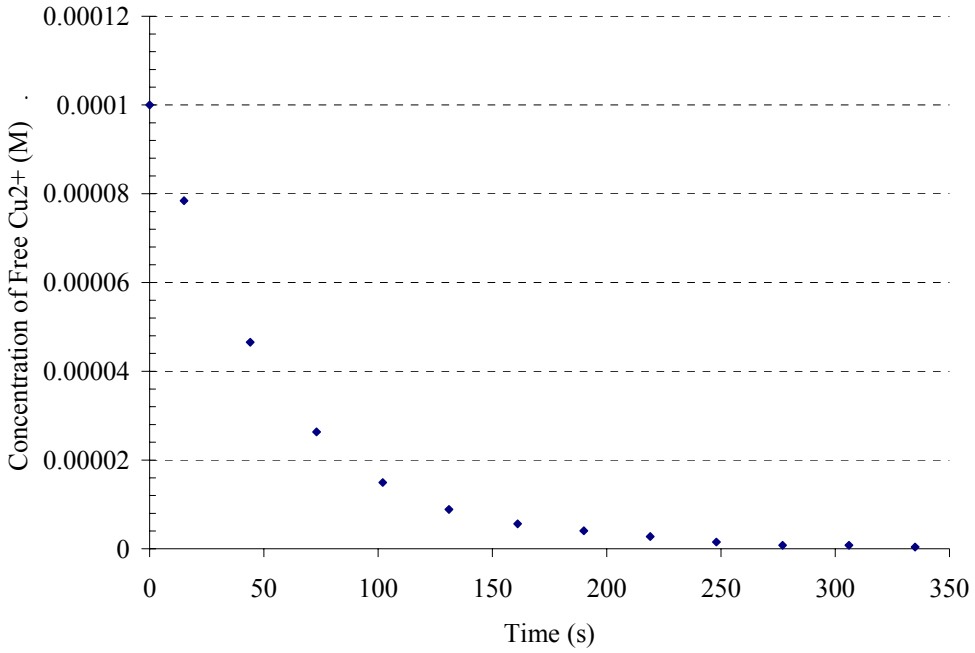

Figure 4.3.1. Chelex-100 experimental blank of 1.0 x 10^{-4} M Cu^{2+} buffered to pH 4.0 (15 mM acetate buffer) in the absence of LHA.

4.3.2. Marquardt fitting results

The data from all runs were fitted to the optimal number of components, (from one to four were attempted). The vast majority required two components, Table 4.3.2.1. lists a summary of the results for the 1st component and Table 4.3.2.2. for the 2nd component.

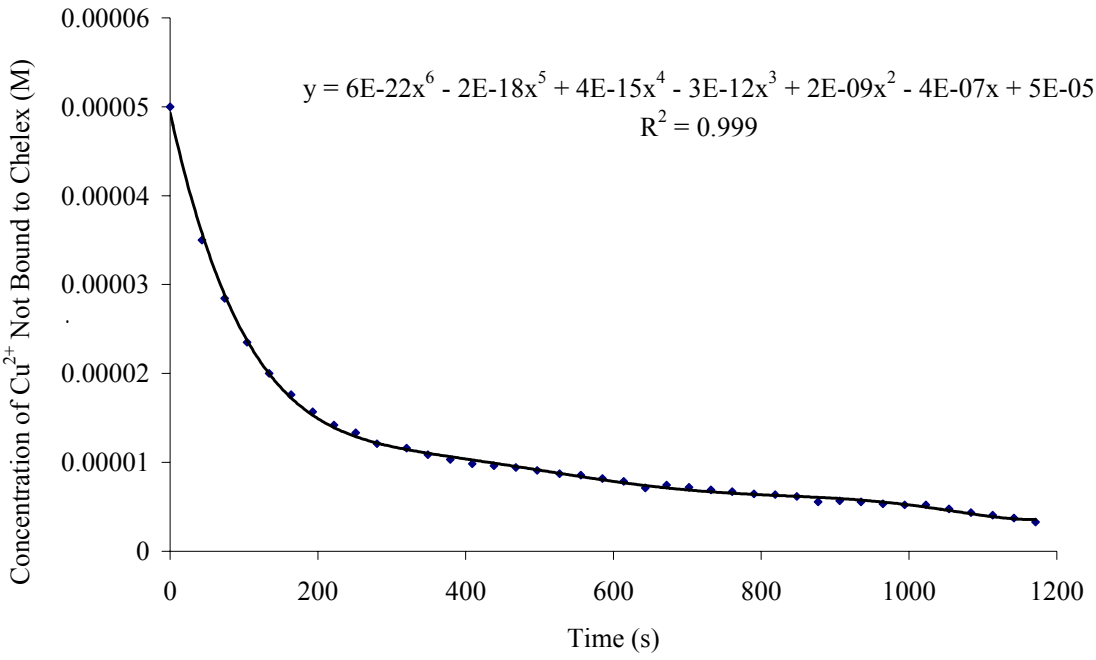

Figure 4.3.2. Decay of copper concentration as a function of time, pH 4.0 150 mg/L LHA, 5.0 x 10^{-5} M Cu^{2+} with 1% Chelex-100 resin

The results from the Marquardt non-linear fitting showed several patterns. Within each LHA concentration, as the copper concentration increased so did the percent of component 1 (with the corresponding decrease in percentage of component 2). As the LHA concentration increased, for each respective copper concentration, the percent of component 1 decreased. Additionally, pH 4.0 displayed larger percentages of component 1 for respective LHA and copper concentration than pH 7.0. The average rate constants for component 1 were 0.0145 s^{-1} for pH 4.0 and 0.0180 s^{-1} for pH 7.0, while component 2 was 0.00184 s^{-1} for pH 4.0 and 0.00120 s^{-1} for pH 7.0.

Table 4.3.1.1. Results from CLEM Chelex-100 resin experiments fit using a Marquardt non-linear algorithm for the 1st component and first rate constant with standard deviations.

pH	LHA conc. (mg/L)	Cu2+ conc. (M)	1st component (%)	SD (%)	k1 (s-1)	SD (s-1)
4	50	5.00E-06	38.32	1.71	0.016	0.0015
		1.00E-05	60.32	4.75	0.014	0.0017
		5.00E-05	83.10	1.14	0.016	0.00040
		1.00E-04	97.38	1.55	0.012	0.00029
4	150	5.00E-06	34.46	2.02	0.035	0.0050
		1.00E-05	47.04	2.06	0.026	0.0024
		5.00E-05	69.69	0.45	0.012	0.00015
		1.00E-04	84.90	2.32	0.011	0.00030
4	250	5.00E-06	28.14	1.44	0.014	0.0013
		1.00E-05	44.09	12.02	0.0085	0.0016
		5.00E-05	62.00	3.28	0.0075	0.00030
		1.00E-04	76.33	2.78	0.0096	0.00029
7	50	5.00E-06	0.00	0.00	---	---
		1.00E-05	27.87	1.68	0.016	0.0019
		5.00E-05	43.68	1.99	0.022	0.0020
		1.00E-04	86.67	3.04	0.0051	0.00026
7	150	5.00E-06	0.00	0.00	---	---
		1.00E-05	23.31	1.38	0.012	0.0018
		5.00E-05	36.34	1.51	0.027	0.0030
		1.00E-04	45.13	1.93	0.019	0.0019
7	250	5.00E-06	0.00	0.00	---	---
		1.00E-05	0.00	0.00	---	---
		5.00E-05	22.42	0.76	0.017	0.0067
		1.00E-04	39.78	1.91	0.024	0.0026

Table 4.3.1.2. Results from CLEM Chelex-100 resin experiments fit using Marquardt non-linear algorithm for the 2nd component and second rate constant with standard deviations

pH	LHA conc. (mg/L)	2nd component (%)	SD (%)	k2 (s-1)	SD (s-1)
4	50	60.08	0.99	0.0013	0.00010
		36.81	3.95	0.0021	0.00036
		31.88	0.87	0.0023	0.00012
		3.82	1.55	0.0020	0.00068
4	150	65.15	1.14	0.0014	0.000036
		42.02	1.49	0.0024	0.00015
		30.25	0.41	0.0011	0.000022
		15.84	2.38	0.0027	0.00025
4	250	70.81	7.96	0.00056	0.00020
		56.07	11.60	0.0031	0.00043
		24.87	2.69	0.0017	0.00029
		23.39	2.35	0.0023	0.00032
7	50	99.61	2.65	0.0017	0.000088
		72.12	0.78	0.0017	0.000097
		55.70	1.50	0.0026	0.00014
		15.38	3.13	0.0008	0.00018
7	150	98.64	1.56	0.00072	0.0000048
		76.33	10.31	0.00055	0.00014
		63.54	1.27	0.0018	0.00015
		54.06	1.01	0.0014	0.00012
7	250	99.71	2.02	0.00042	0.00025
		99.90	0.43	0.00041	0.0000074
		77.58	0.03	0.0010	0.000015
		59.57	0.99	0.00089	0.000025

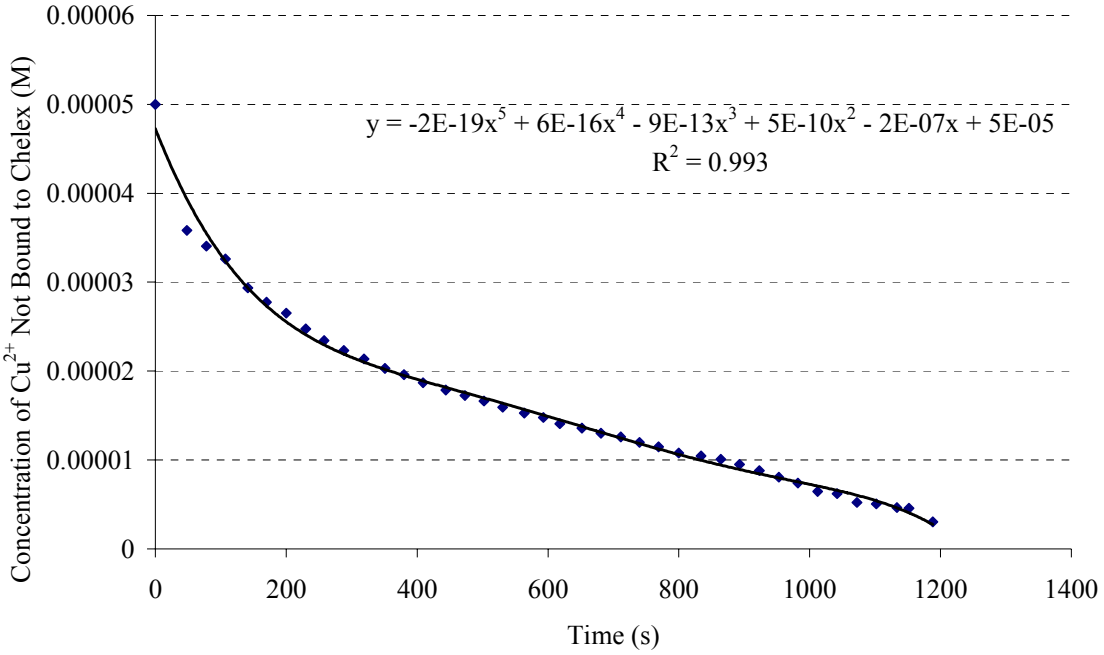

Figure 4.3.3. Decay of copper concentration as a function of time, pH 7.0 150 mg/L LHA, 5.0 x 10^{-5} M Cu^{2+} with 1 % Chelex-100 resin 4.4 Low-field NMR Results

4.4.1. Low-field NMR Results

Replicate NMR runs of ultrapure water showed a relaxation time of 2932 $\pm$ 20 ms, which was taken as the T_2 relaxation time of bulk water.

Blanks were also performed on buffered LHA solutions. Relaxation time was shown to decrease from a value ranging between 2917 to 2792 ms (pH dependant) for a concentration of 25 mg/L LHA to a value ranging from 2346 to 2290 ms for the highest concentration of 250 mg/L LHA (Figure 4.4.1.1.). The decrease in relaxation time was fitted with a second-degree polynomial and manually inspected to ensure good fit. The relations are given in Table 4.4.1.1

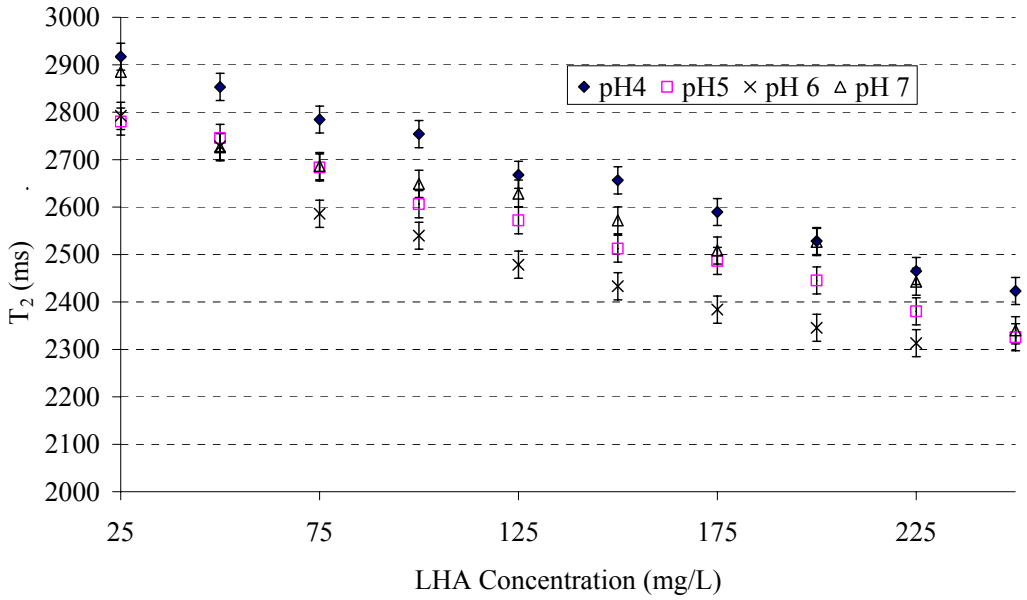

Figure 4.4.1.1. T_{2GM} vs. LHA concentration buffered at pH 4.0, 5.0, 6.0 &7.0 (15mM $NaCH_3COOH$ or KH_2PO_4), no copper added.

Table 4.4.1.1. LHA Low-field NMR blank runs for pH 4.0, 5.0, 6.0, and 7.0 second order polynomial regression equations and correlation co-efficients

pH	Equation of linear regression	Correlation Co-efficient (R^2)
4.00	$y = 0.0002x^2 - 2.2311x + 2965.2$	0.9941
5.00	$y = 0.0009x^2 - 2.2391x + 2840.8$	0.9936
6.00	$y = 0.0086x^2 - 4.5071x + 2905.1$	0.9923
7.00	$y = 0.0012x^2 - 2.3137x + 2885.2$	0.9433

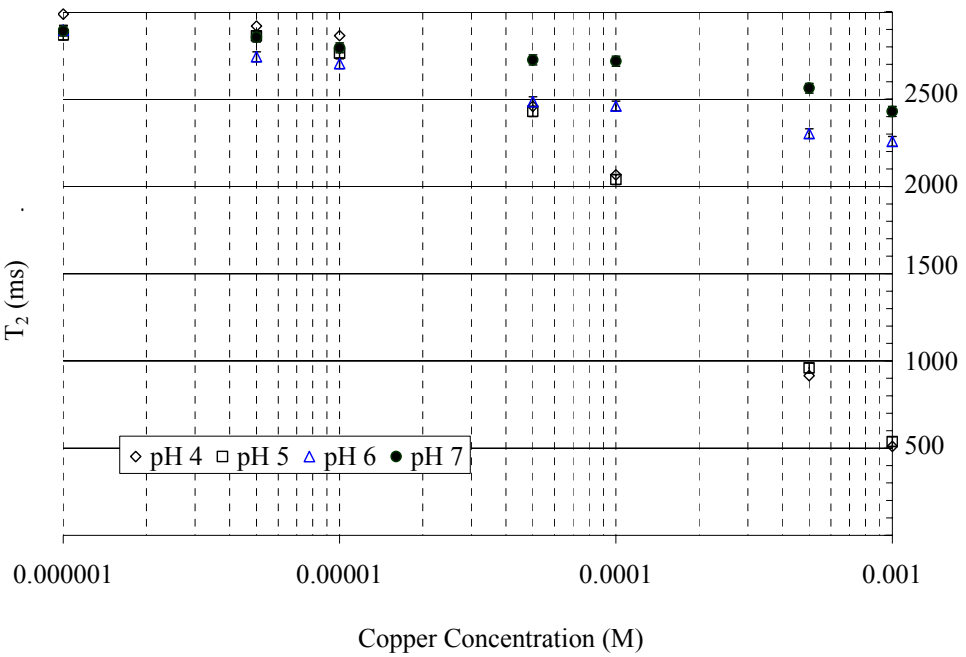

Figure 4.4.1.2. Plot of T_2 vs. copper concentration for buffered copper blank solutions at pH values of 4.0, 5.0, 6.0, and 7.0

Copper blanks were also analyzed in solutions of buffer and ultrapure water (Figure 4.4.1.2.). pH 6.0 and 7.0 experienced moderate shortening in T_2 relaxation time as copper concentration increased, with the slope of falling T_2 remaining relatively constant closely following a logarithmic curve . This was not evident for pH 4.0 and 5.0 where the slope follows a nearly exponential decrease in T_2 as log copper concentration is increased.

After the blanks, a titration of LHA with copper was performed. The data displayed several patterns with regard to pH, and concentrations of LHA and copper. A general trend of decreasing T_2 relaxation time with increasing LHA concentration, as well as with increasing copper concentration was evident. In general, as the pH decreased so did the relaxation time, however there was some grouping of the pH 4.0 and 5.0 samples distinct from the pH 6.0 and 7.0. The pH 4/5 trends were for a smaller slope for

T_2 relaxation time plotted against copper concentration than pH 6/7 (see for example, Figures 4.4.1.3. and 4.4.1.4.). The lowest and highest T_2 values were found at the pH 4.0 and 7.0 pH values, respectively with pH 5.0 and 6.0 values in between.

4.4.2. Low-field NMR Data Analysis

Low-field NMR results can not give information on binding without some secondary input. Interpretation of the NMR signal therefore requires a more in-depth approach. This will be done using a variant on the Bloch equation [79]. Some background is required before proceeding with further data presentation.

In 1970, Mildvan and Cohn successfully used line broadening, as a result of coordination of an organic ligand to a paramagnetic Mn^{2+} ion, in the solvent (water)

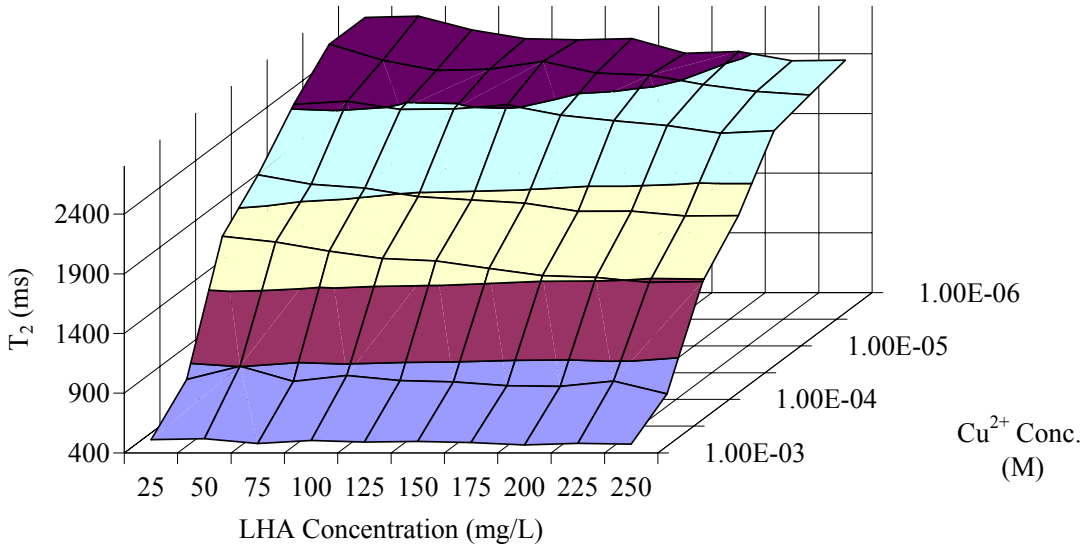

Figure 4.4.1.3. LHA and copper low-field NMR titration. Buffered at pH 5.0

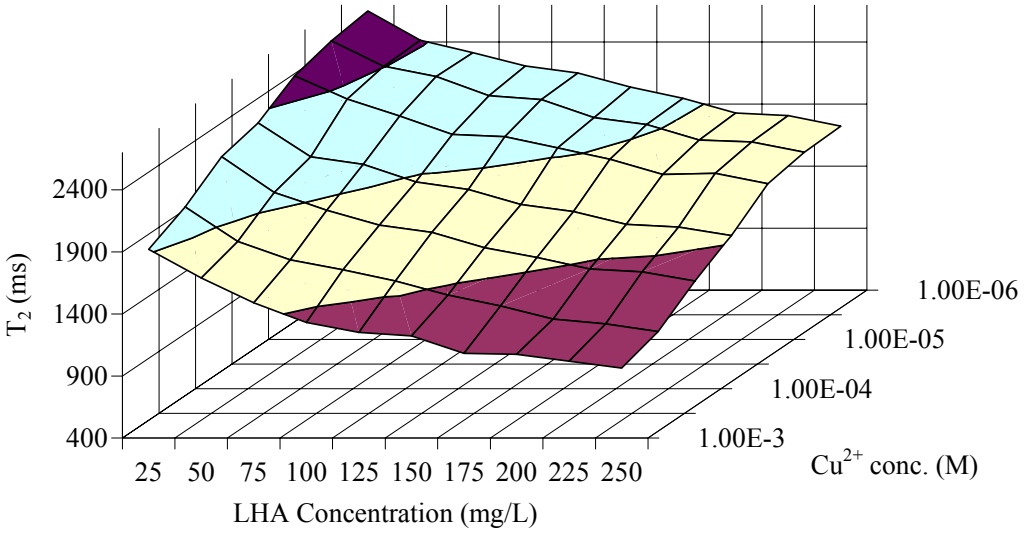

Figure 4.4.1.4. LHA and copper low-field NMR titration. Buffered at pH 6.0.

NMR signal to explore manganese binding to enzymes [116]. This line broadening, or diminished measured $T_{2,}$ is a result of faster relaxation of protons in the close vicinity (approximately the inner coordination sphere [91]) of a paramagnetic ion, due to the large local magnetic field present.

When exchange is very fast compared to the NMR time scale, using McConnell's equation (Equation 4.4.2.1.) as a starting point [117], the relaxation times in two different environments; protons in the inner co-ordination sphere of a paramagnetic ion, M, and protons in the free bulk water, B, is completely averaged and a single line is obtained of width [118],

$$1/T_{2(obs)} = P_M / T_{2M} + P_B / T_{2B} \qquad (4.4.2.1.)$$

where $1/T_{2(obs)}$ is the experimentally observed transverse relaxation time. T_{2M} and T_{2B} are the transverse relaxation times of the paramagnetic ion co-ordination sphere protons and bulk water protons respectively. P_M and P_B are probabilities that a proton will be found in the specific environment. The two term partitioning is usually justified by the fact that a r^{-6} dependence ensures rapid falloff of paramagnetic effects [119]. In the case of copper, the previously stated, fast exchange requirement is met easily due to a water exchange rate constant of approximately 8×10^9 s^{-1} [66].

In a more complex situation with a ligand binding an aquo metal ion, an inner sphere complex can form between the metal and ligand [92]. The ligand then replaces coordinated water and consequently reduces P_M. The binding will also have impact upon the water relaxation time through changes in the dynamics of the remaining water attached to the complex. This usually results in reducing relaxation time because tumbling times, with respect to the field, slow increasing relaxation efficiency. A further consideration is possible paramagnetism from the ligand itself.

Thus within our system we have present: free water, waters within the copper hydration shell, waters associated with the humic (possibly with paramagnetic species), and waters associated with coppers bound to the humic.

It is already evident from experimental runs of blank LHA, blank Cu and the LHA-Copper titrations (Figures 4.4.1.1. – 4.4.1.4.) that signals from all the possible environments are present. This then leads to an extension of equation 4.4.2.1, to take into account the host of influences on the observed relaxation within our system,

$$1/T_{2(obs)} = [(P_{Bulk} / T_{2Bulk}) + (P_{LHA} / T_{2LHA})] + [(P_{Cu} / T_{2Cu}) + (P_{Comp} / T_{2Comp.})] \quad (4.4.2.2.)$$

where the subscripts bulk, Cu, LHA, and Comp represent bulk water, cupric ions, Laurentian humic acid, and copper-LHA complexes respectively. To properly utilize equation 4.4.2.2., it is necessary to obtain reliable experimental values for each of the variables.

For T_{2Bulk}, runs of pure water were performed and P_{Bulk} determined to be unity (the probability of protons being in the bulk solution is unity). For the free copper variables in equation 4.4.2.2., copper blanks were run (Figure 4.4.1.2.). $[Cu(H_2O)_6]^{2+}$ is the general formula for cupric ions in water, implying six waters in the copper inner coordination sphere. Due to Jahn-Teller distortion, the Cu^{2+} axial ligands are bound weakly, which may enable HA functional groups to displace axially coordinated H_2O ligands resulting in the formation of an inner sphere complex [120]. Since Copper does form inner sphere complexes [92], with knowledge of the copper concentration, the number of waters associated with free copper can be calculated. Total waters present in solution (water is 55.5084 M) gives the total number of waters and thus a probability can be calculated for the waters to be in the copper inner co-ordination sphere, P_{Cu}. As an approximation, it is assumed that any binding by the LHA to free Cu^{2+} is bidentate [26](though monodentate and polydentate binding is also possible) and two waters are displaced in the inner coordination sphere. Upon binding, if the number of coppers bound is known, then the P_{Cu} and T_{2Cu} can be calculated from the data in the absence of LHA.

Before a similar strategy can be employed for assigning values for the LHA influence some further experiments are required. Since humics are known to contain stable free radicals [49, 54, 55], often in the form of semiquinone structures, the best way to ascribe paramagnetic effects to LHA moieties would be performing liquid state EPR

experiments to quantify the concentration of free radicals in the LHA solutions. The EPR experimental results have been presented in Section 4.2.

From the EPR data, given the decrease in signal encountered with the increase in moisture content, it is assumed to be a valid assumption that at even the most concentrated experimental concentrations (250 mg/L LHA), no significant free radical population remains within the LHA samples. With this in mind, the decreases observed in the T_2 are consistent with the binding of water on the interior of aggregates and on LHA surfaces analogous to those reported by Todoruk *et al.* [28] with respect to soil components.

For the purpose of assigning values for the LHA terms in equation 4.4.2.2., no contribution from free radical species was assumed. The problem of assigning waters associated with the LHA was then circumvented quite simply. Influences such as bulk water or LHA were not split into components; rather the solutions were used in the following manner,

$$\left[\left(P_{Cu} / T_{2Cu}\right) + \left(P_{Comp} / T_{2Comp.}\right)\right] = 1/T_{2(obs)} - \underbrace{\left[\left(P_{Bulk} / T_{2Bulk}\right) + \left(P_{LHA} / T_{2LHA}\right)\right]}_{\Delta} \quad (4.4.2.3.)$$

where P_{Bulk} will again be approximated as unity. A secondary benefit of treating the system in this manner is that, without taking into account results of the EPR experiments, any small paramagnetic influences within the LHA system are automatically accounted for.

If the observed relaxation frequency ($1/T_2$) from the LHA blank runs, Δ, is subtracted from the observed relaxation frequencies of the Cu – LHA titrations, the influence of the Cu –LHA complex and free Cu is evident. This does not account for the

waters lost from the LHA molecule upon binding however that influence is assumed to be small, as there is no measurable paramagnetic influences (as in the case of Cu^{2+} ions) and binding sites are small (less waters associated with the active binding sites compared to the aggregates as a whole). A rearrangement of the second term in 4.4.2.3. gives,

$$T_{2Comp} = P_{Comp} \cdot T_{2Cu} \; / \; (\Delta \cdot T_{2Cu} - P_{Cu}) \qquad (4.4.2.4.)$$

A few quick tests to ensure the equation makes physical sense are easily performed. When no copper is bound, the P_{Comp} is zero and relation 4.4.2.4. yields a T_{2Comp} of zero. When all copper is bound, P_{Cu} is zero and the denominator of equation 4.4.2.4. remains positive. From these quick checks our relation appears to make physical sense.

Now that the LHA contribution is accounted for, it becomes clear that some secondary measurement is required to quantify the amount of copper that is bound to the LHA and the amount that remains free, as the information is not available from the NMR data alone.

It is important for this secondary measurement to be able to distinguish between ‘free’ and ‘bound’ copper. Labile copper is able to tumble fast enough to still be considered ‘free’ on the NMR time scale. Thus after extensive work on ascertaining the most suitable method for estimating all NMR labile copper concentration, without perturbing the binding equilibrium, the competing ligand exchange method (CLEM), as introduced in section 2.3, using a Chelex ion-exchange resin was used. CLEM is an experimental method that can readily distinguish between ‘free’ copper (copper in the aquo form and highly labile copper) and ‘bound’ (complexed copper closely associated

with the humic as to significantly slow the tumbling time of the waters) and thus suits our needs.

The data from the CLE method was presented in section 4.3. The data in Table 4.4.1.1. was then transferred, along with the data from the copper and LHA blank runs to equation 4.4.2.4.

4.4.3. Transverse Relaxation Times of the Cu – LHA Complexes

The transverse relaxation times of the copper – humic complexes were calculated and plotted with the observed T_2 of both the LHA blank and the Cu^{2+} - LHA titrations. These data are presented in Figures 4.4.3.1. to 4.4.3.9. For pH 4.0 and 7.0, all LHA concentrations are presented with the copper concentrations of 1.0×10^{-4} M to 5.0×10^{-6} M.

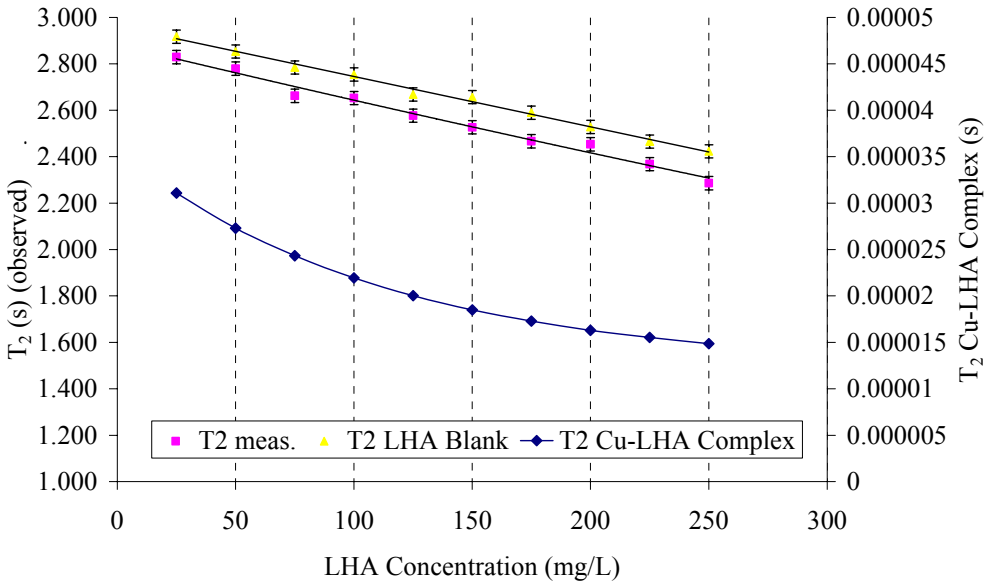

Figure 4.4.3.1. Plot of pH 4.0 5.0×10^{-6} M Cu^{2+}, T_2 for LHA blank and Cu-LHA titration (measured)(left y-axis) and T_2 Cu-LHA complex as a function of LHA concentration. Note: error is significant (Section 5.3.2.)

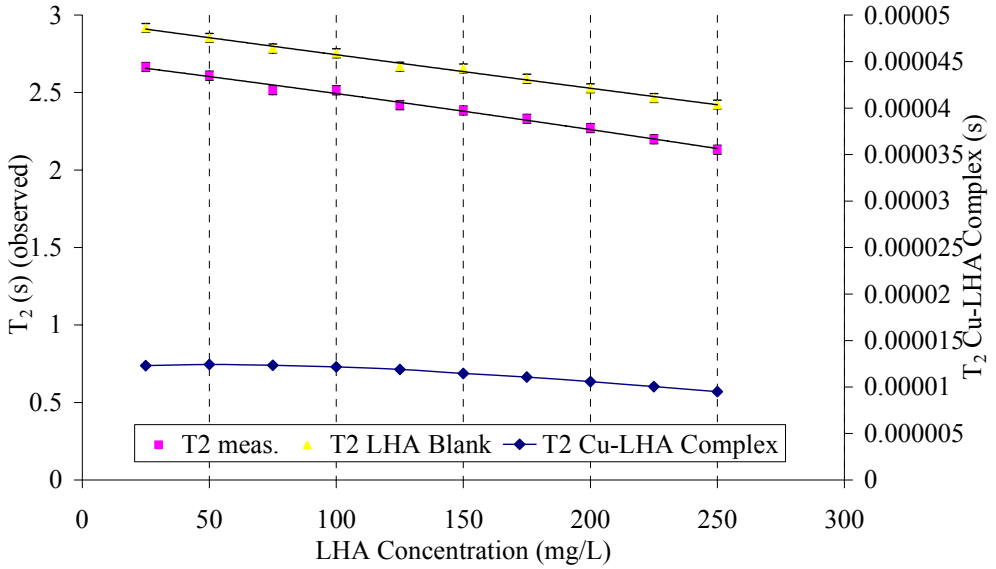

Figure 4.4.3.2. Plot of pH 4.0 1.0 x 10^{-5} M Cu^{2+}, T_2 for LHA blank and Cu-LHA titration (measured)(left y-axis) and T_2 Cu-LHA complex as a function of LHA concentrations. Note: error is significant (Section 5.3.2.)

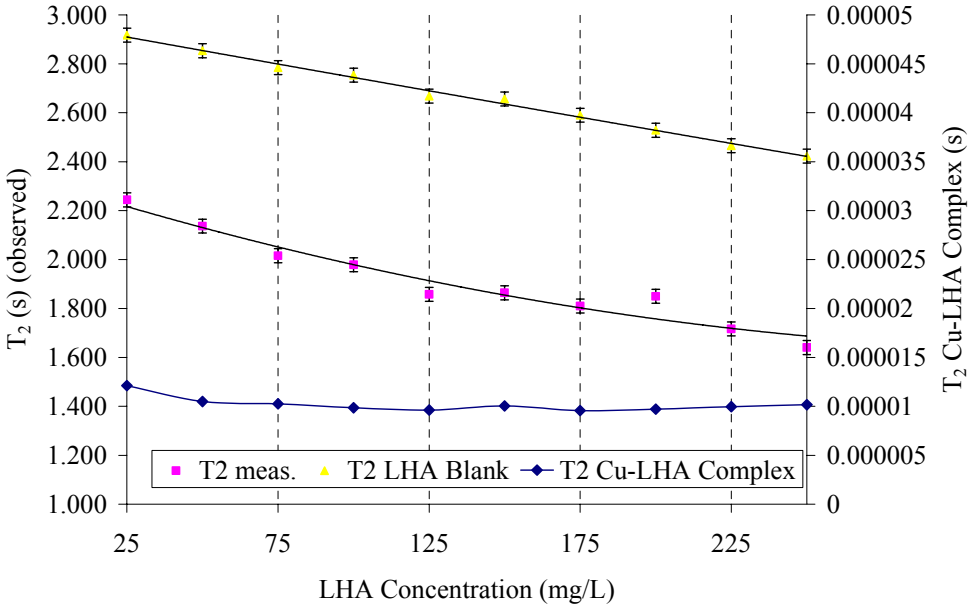

Figure 4.4.3.3. Plot of pH 4.0 5.0 x 10^{-5} M Cu^{2+}, T_2 for LHA blank and Cu-LHA titration (measured)(left y-axis) and T_2 Cu-LHA complex as a function of LHA concentrations. Note: error is significant (Section 5.3.2.)

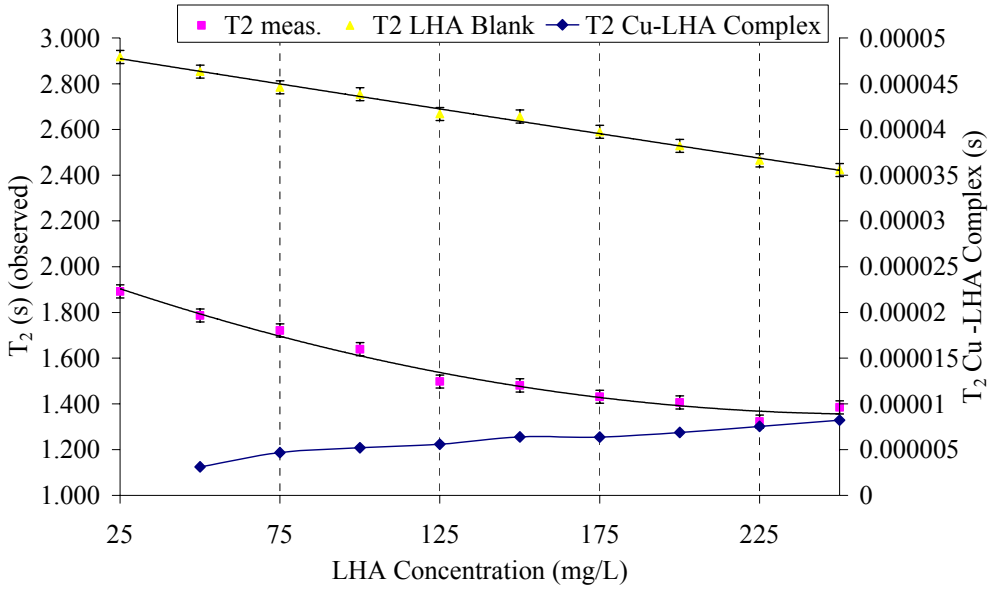

Figure 4.4.3.4. Plot of pH 4.0 1.0 x 10^{-4} M Cu^{2+}, T_2 for LHA blank and Cu-LHA titration (measured)(left y-axis) and T_2 Cu-LHA complex as a function of LHA concentrations. Note: error is significant (Section 5.3.2.)

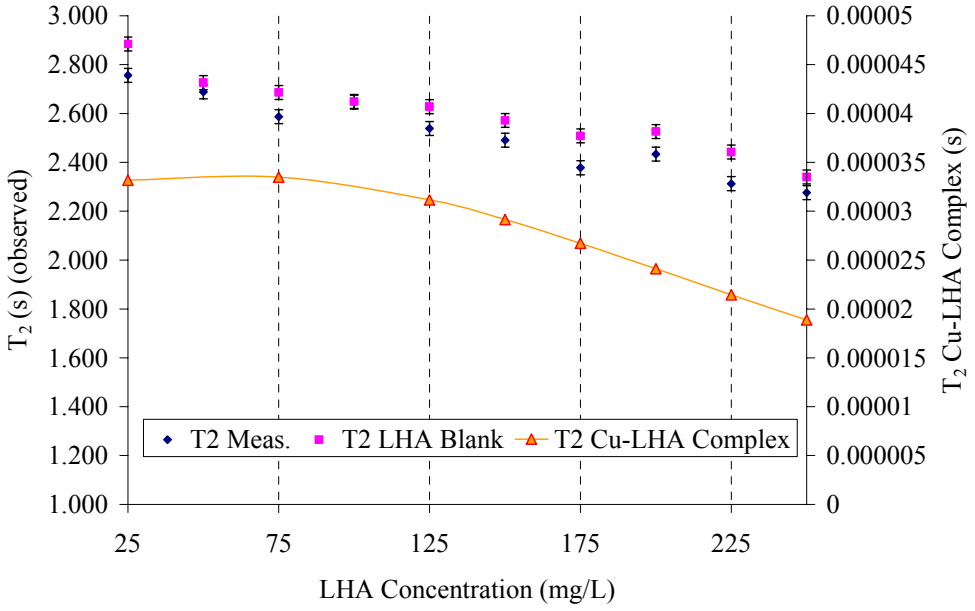

Figure 4.4.3.5. Plot of pH 7.0 5.0 x 10^{-6} M Cu^{2+}, T_2 for LHA blank and Cu-LHA titration (measured)(left y-axis) and T_2 Cu-LHA complex as a function of LHA concentrations. Note: error is significant (Section 5.3.2.)

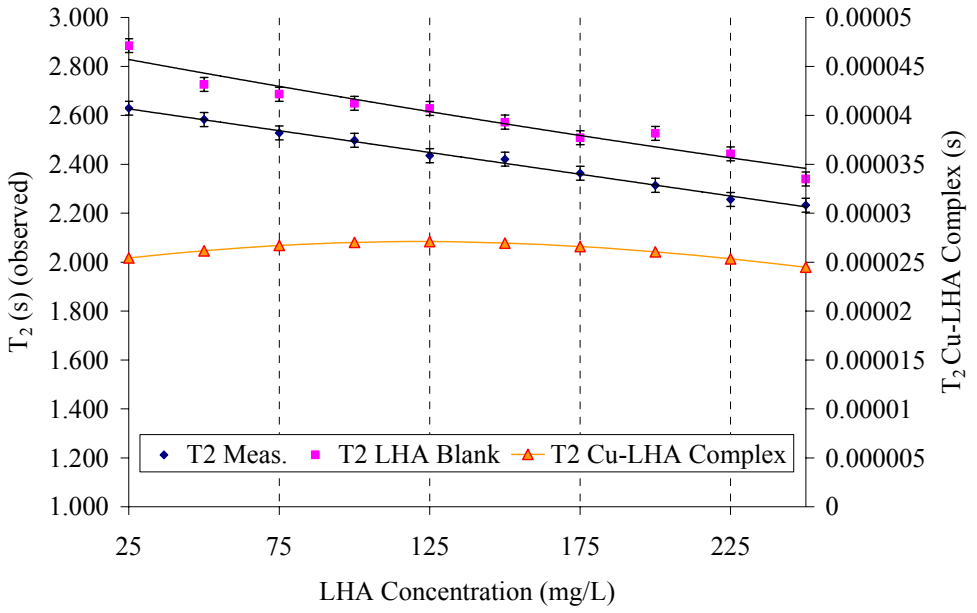

Figure 4.4.3.6. Plot of pH 7.0 1.0 x 10^{-5} M Cu^{2+}, T_2 for LHA blank and Cu-LHA titration (measured)(left y-axis) and T_2 Cu-LHA complex as a function of LHA concentrations. Note: error is significant (Section 5.3.2.)

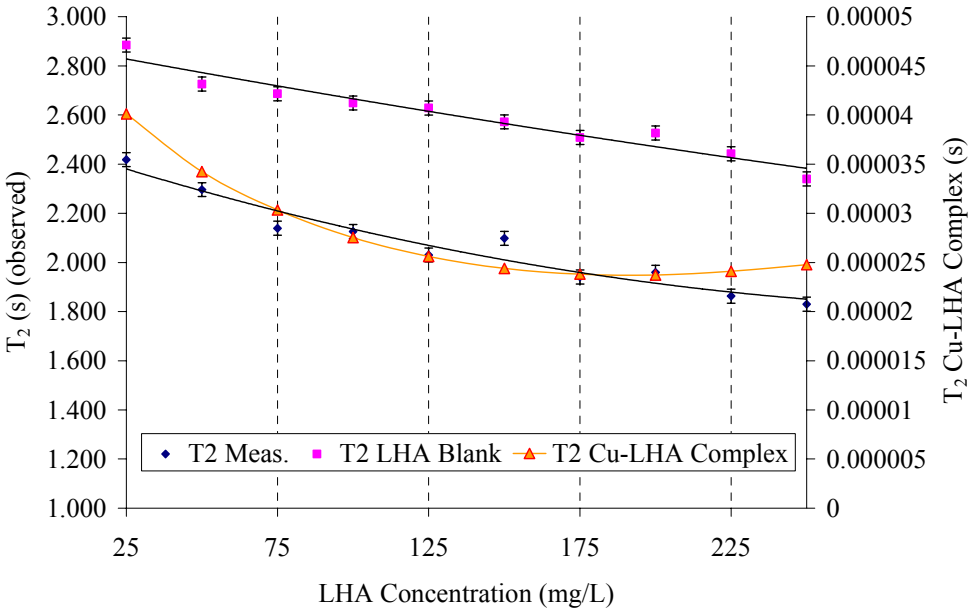

Figure 4.4.3.7. Plot of pH 7.0 5.0 x 10^{-5} M Cu^{2+}, T_2 for LHA blank and Cu-LHA titration (measured)(left y-axis) and T_2 Cu-LHA complex as a function of LHA concentrations. Note: error is significant (Section 5.3.2.)

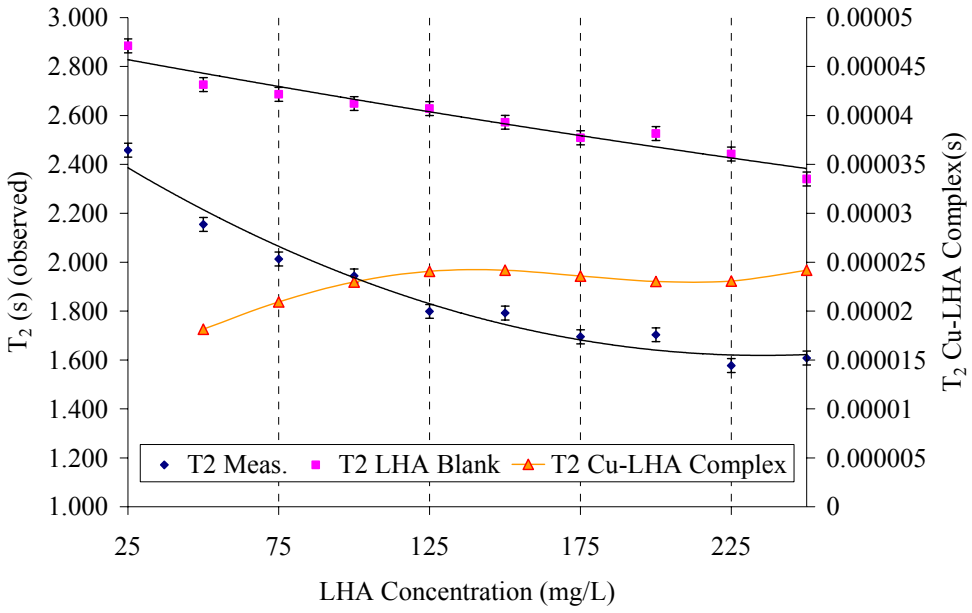

Figure 4.4.3.8. Plot of pH 7.0 1.0 x 10^{-4} M Cu^{2+}, T_2 for LHA blank and Cu-LHA titration (measured)(left y-axis) and T_2 Cu-LHA complex as a function of LHA concentrations. Note: error is significant (Section 5.3.2.)

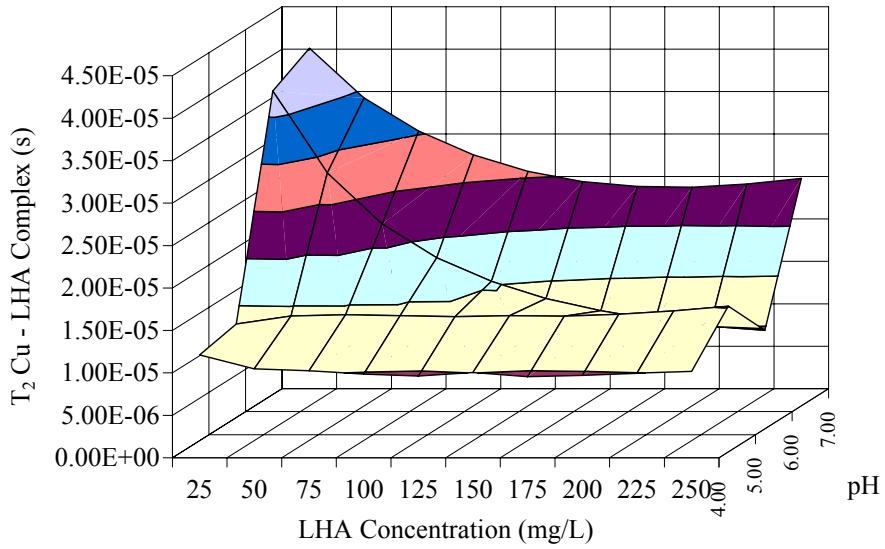

Figure 4.4.3.9. Plot of 5.0 x 10^{-5} M Cu^{2+}, T_2 for LHA blank and Cu-LHA titration (measured)(left y-axis) and T_2 Cu-LHA complex as a function of LHA concentrations and pH. Note: error is significant (Section 5.3.2.)

One of the first observations to be derived from the transverse relaxation times of the Cu-LHA complexes is the relative stability of the relaxation time over large changes in the metal to ligand ratios. As the titration moves from 50 mg/L LHA and 5.0 x 10^{-4} M Cu^{2+} to 250 mg/L LHA and 5.0 x 10^{-6} M Cu^{2+}, it covers a very large range in metal to ligand ratios (a two orders of magnitude difference), yet the T_2 Cu –LHA complex changes very little (less than one order of magnitude). Particularly, there seems to be only a very small range in T_{2bound} when the LHA to metal ratio is large. The variation seen in the data is probably not outside experimental error.

The T_{2bound} for pH 4.0 varies between approximately 5 x 10^{-6} and 2 x 10^{-5} ms, while pH 7.0 varies between 2 x 10^{-5} and 3 x 10^{-5} ms. Thus the pH 4.0 titration data shows more change in the T_{2bound} over the course of the experiments as compared to pH 7.0. It is also relatively flat as the LHA concentration is changed with the exception of the lowest LHA concentrations for 5.0 x 10^{-6} M Cu^{2+}. pH 7.0 data is larger in value and is less stable than pH 4.0 with a changing slope over the course of the LHA concentrations as the copper concentration is changed. The pH 7.0 T_{2bound} is seen to vary more at the lower LHA to metal ratios than pH 4.0 and is relatively constant at large LHA to metal ratios.

The pairing of slopes as the titration moves from low to high LHA concentration in Figure 4.4.3.9. for the pHs 4/5 and 6/7 is evident as it was in Figures 4.4.1.3 and 4.4.1.4. pH 4.0 and 5.0 are lower in magnitude than pH 6.0 and 7.0 for the majority of points. pH 6.0 and 7.0 also shows a decrease to approximately the same value as pH 4/5 in T_{2bound} as the humic acid concentration is raised.

CHAPTER FIVE: DISCUSSION

As demonstrated by the papers of Stenson *et al.* [1] and Cook *et al.* [2] (section 1.1.2), humics are a 'super mixture'. This view has been supported by Piccolo who describes HS as 'supramolecular associations of self-assembling heterogeneous and relatively small molecules deriving from the degradation and decomposition of dead biological material', a conclusion based upon size exclusion chromatography [11]. The evidence presented in the papers of Stenson and Cooper lends a new powerful credibility to the suggestion that HS are comprised of a mixture of small molecules, oligomers (vide infra), and polymers aggregated into functional assemblies by non-covalent forces. The instrumentation used by the authors even permitted structures of 'typical' monomer units to be postulated (Figure 1.2.4.) [3, 19]. These structures, and the information from which they were developed, were provided by high-resolution mass spectrometry that was not available in previous years. The intimacy of the present view of humic material is thus unprecedented and a paradigm shift with regards to how binding is modelled is required.

In a system such as this an improvement in interpretation should be possible if the system is modelled as a Dynamic Combinatorial System (DCS). This interpretation should be able to accurately represent the system upon the introduction of a contaminant, such as metal ions or small organic molecules.

5.1 Dynamic Combinatorial Systems (DCS)

Combinatorial libraries are prevalent in synthesis where many members of the library are constructed of two or more building blocks (a, b, c…). The building blocks are

bound together by covalent bonds that are fixed during synthesis to form different members (M_1 … …M_n). This fixing ensures no post-synthetic interconversion of the building blocks between members (termed a static combinatorial system (SCS)). Dynamic combinatorial chemistry (DCC), however, offers workers a new strategy for the identification of new host and guest compounds with the potential for catalysis and drug activity.

DCC has been largely advanced by the work of J.K.M. Saunders of Cambridge, UK [121-123]. In a dynamic combinatorial library (DCL), the merits of combinatorial chemistry are combined with molecular evolution. A DCS contains building blocks to create supramolecular members, identical to a SCS, however in a DCS the connections between the building blocks are reversible and in flux, continuously able to form and break new members. As a consequence, all the library members are interconverting through exchange processes to give a product distribution which is under thermodynamic control and which may be influenced by the addition of guest molecules. When guest molecules are introduced candidate (host) molecules which bind strongly to guest molecules will become amplified in concentration (assuming that the binding is an advantageous process), while those that exhibit poor binding to the guest molecule will decrease in concentration by virtue of Le Chatelier's principle (Figure 5.1.1.) [121].

With this system in mind, it is a natural progression to envision humic systems as a DCS. Humics are, as previously stated; a complex mixture of small molecules, oligomers, and polymers aggregated into functional assemblies by non-covalent forces, in short a natural DCS.

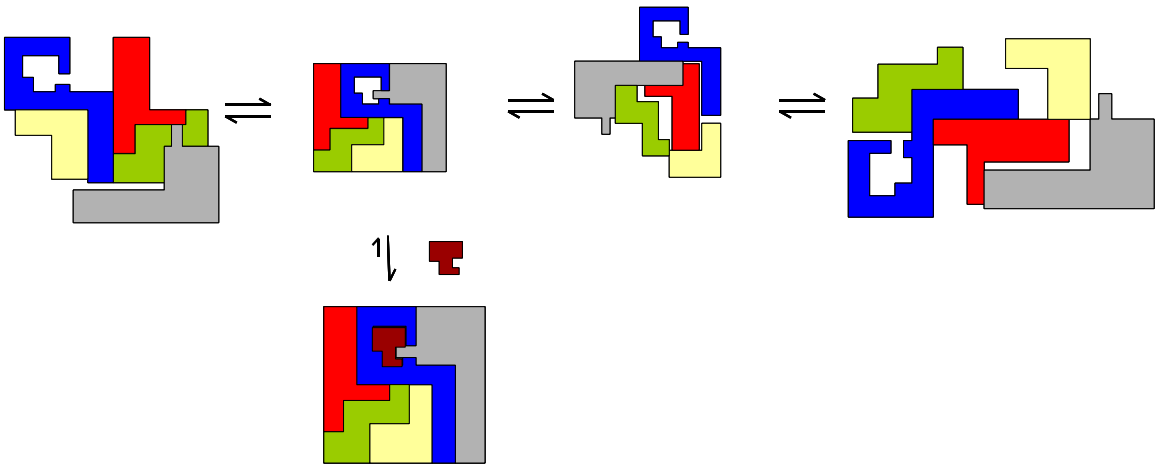

Figure 5.1.1. Pictorial representation of a DCS. This particular system has four members in different concentrations (represented by size). The members are free to interconvert. When a contaminant is introduced (the t shaped object) it binds preferentially and strongly with one of the members. This binding will cause a shift in the library towards the production of the most favourable conformation at the expense of the less favourable three.

This model can be used to offer an explanation for discrepancies in the literature. In 1972, Gamble [124] performed a potentiometric titration with fulvic acid and was required to assume a distribution of binding constants, rather than a discrete number, to interpret his results. This is contrasted with the results presented in numerous papers, by the lab of C.L. Chakrabarti (Table 2.3.1.), in which rate constants for metal dissociation by the CLE method are fitted with 2 – 4 components. These findings can be reasonably explained as a DCS system in which a range of binding constants is expected due to aggregational and conformational shifts in response to the contaminant loading. The sites produced are similar thus the rate constants of dissociation are similar and a discrete number is seen.

The simplest place to start a DCS interpretation of copper to LHA binding interactions, within this thesis, would be dynamic light scattering experiments. DLS can observe any changes in the size of the LHA particles with minimal influence upon the

system as a result of the observations. It is important to ascertain whether size distributions of aggregates reflect changes induced by the redistribution of the library upon addition of a complexing metal ion.

5.2. Dynamic Light Scattering

It is important to recognize the main limitation of dynamic light scattering, which is a bias towards large particles in the presence of a large number of small ones. This is a by-product of the technique's response to a diffusion co-efficient [39].

This limitation impacted upon the results for copper concentrations of 1.0×10^{-3} M. Results were not obtainable for this concentration due in large part to aggregate formation that greatly increased the noise in the experimental data. This is not well modeled by the CONTIN model (see section 2.1.2.) and thus the results were discarded [39]. The aggregation itself is not unexpected. Copper is the second most effective divalent metal cation precipitator of HA after lead [125].

The average size of the particle measured was in the size range of 121 – 250 nm for no copper loading. This value is similar to previous values in the literature. Reid and coworkers [41] reported an average radii of 448 $\pm$ 31 nm for a peat humic acid and 81 $\pm$ 12 nm for a surface water humic acid at pH 7 with 3 mM sodium azide. They found no systematic change in the size of these particles with concentration or ionic strength. Pinheiro *et al.* [39] found an average diameter of 185 $\pm$ 9 nm for a purified peat HA and 148 $\pm$ 9 nm for a commercially available HA (Fluka). The solutions were adjusted to pH 5 and filtered with a 0.45 μm filter. Multiangle laser light scattering was used by Manning and coworkers on a commercially available HA (Aldrich) [36]. They found a root mean square radius of 436 $\pm$ 36 nm with a pH of 6.0. Caceci and Billon used DLS to

determine small but significant amounts of relatively large scatters (50 – 200 nm diameter) in a number of soil, lake, and groundwater HA in 0.01 M $NaClO_4$ [126]. In this study size was not observed to vary as a function of pH (range 4-9) nor ionic strength (0.01 – 0.25 M).

The inherent polydispersity of humic materials tends to render 'average' particle diameters meaningless, unless the polydispersity is reduced by prior size separation [40]. With this in mind the data were analyzed as a distribution of sizes within each pH value and copper concentration. Due to the data analysis technique (Section 3.2.3.), the only observations that can be drawn from the LLS data are qualitative based upon the shape of the plot of summed detector response as a function of particle size.

Data for pH 7.0 exhibited several patterns that are comfortably interpreted as a DCS. Twenty-five mg/L LHA experienced major shifts in distribution as the copper concentration was increased from 0 M to 1.0×10^{-4} M. From a DCS perspective the shifts from a predominance in the lower size classes (1-50 nm, 51-120 nm) towards the high size class (401- 9000 nm) displays the LHA mixture undergoing rearrangement as the most favourable conformation is found for each progressive metal loading. The most favourable conformations likely included inter-particle bridging as the copper loading increased, resulting in the large particle sizes. The higher LHA concentrations show this rearrangement much less, possibly a result of the solution concentration screening conformational changes that are occurring as the system accommodates the binding. Additionally, the higher concentration of LHA could allow for the system to find the most advantageous conformation without a detectable rearrangement of the system. The higher LHA concentration would contain a larger concentration of the most favourable

(or one of similar energy, as there are likely to be several very close in energy) conformation thus large scale conformational changes might not be required. A further possibility is that the rearrangement required is only a small perturbation of the total library as the LHA to metal ratio becomes large. It is interesting to note the onset of coagulation that is occurring at 1.0×10^{-4} M Cu^{2+} and 25 mg/L LHA.

As the pH drops to 4.0, several changes occur within the systems. Intermolecular interactions of the Van der Waal type, interactions between π-electron systems of adjacent molecules, and strong hydrogen bonding all become stronger with decreasing pH [110]. The decreasing ionization of acidic functional groups can decrease particle separation and limit electrostatic repulsion. In a dynamic system such as ours, this will invoke adjustments to the equilibrium state due to the non-covalent basis in which the conformers associate. These changes are evident in the pH 4.0 data as compared to the pH 7.0. The pH 4.0 25 mg/L curve shows very little adjustment in distribution as the copper loading increases. It is only when the copper concentration is 1.0×10^{-4} M that a major shift in the distribution is observed. This lack of rearrangement is a consequence of the increased intermolecular forces. The drive, created by the copper binding, towards rearrangement to a more favourable conformation is balanced by the forces that draw the particles to one another. Results of pH 4.0 are similar to pH 7.0 in that the major shifts in size distribution, as seen in the 25 mg/L results, are minimally visible for LHA concentrations of 125 mg/L and 225 mg/L. This could be a result of screening as mentioned previously for pH 7.0, however major shifts in size distribution for pH 4.0 are not expected to be as large as pH 7.0. Lack of shifts in the size distribution could also be due to, as in pH 7.0, a larger concentration of the favourable conformations making large

scale rearrangements unnecessary. A further possibility, as mentioned previously, is that the rearrangement required is only a small perturbation of the total library as the LHA to metal ratio become large.

The data from pH 5.0 and 6.0 show a continuum in particle distributions from pH 4.0 to pH 7.0, which is a natural progression of the changes that are occurring in the forces between particles. As the pH changes, it will invoke changes in the inter and intramolecular forces that will affect the particle size distribution as demonstrated by pHs 4.0 and 7.0. The distributions did show a more complex pattern but the patterns seen within the pH 4.0 and 7.0 data were still evident.

5.3. EPR

The solid EPR spectra is comprised of a single peak devoid of any splitting which is indicative of the extreme complexity of the sample [127]. The spectral shape and peak centre is typical of many reported in the literature for humic substances with no metals present [47, 50, 115, 128-130] EPR spectra of humic substances are mostly attributed to semiquinone radical units, possibly conjugated to aromatic rings, although contributions from methoxybenzene and nitrogen associated radicals can not be excluded [131]. The humic free radicals content depends on environmental factors influencing its production and stabilization, e.g. origin of material, cropping systems, climate, pollution (sulphur and nitrogen oxides, transition metals) [132], pH and redox conditions, while also depending on laboratory conditions such as pH, temperature, irradiation, solvent, and acid-hydrolysis [115].

The EPR experimental results displayed a decrease in the signal received by the detector as the samples were progressively wetted. These results could be interpreted as a result of dielectric absorption of the microwave radiation by the water. This is not a satisfactory explanation as the samples were run in capillary tubing once they had progressed to a liquid state. This ensures that the water volume was as low as possible, and thus dielectric absorption is not likely to have a major impact upon the sample. Additionally, EPR spectra have appeared using liquid samples in capillary tubes several times in the literature [112, 131, 133-136]. This then leads to an explanation for the disappearance of the signal upon wetting provided by two papers by Uno and coworkers [137, 138]. In these papers the electrophoretic detection of *p*-quinone anion radicals, arising from the electrolysis of benzoquinone (BQ) and chloranil, was achieved in an acetonitrile medium. It was discovered that even very small amounts (less than 1%) of water caused the complete disappearance of the $BQ^{\cdot -}$ radical peak. The disappearance was attributed to the formation of a stable quinhydrone complex (Figure 5.3.1.).

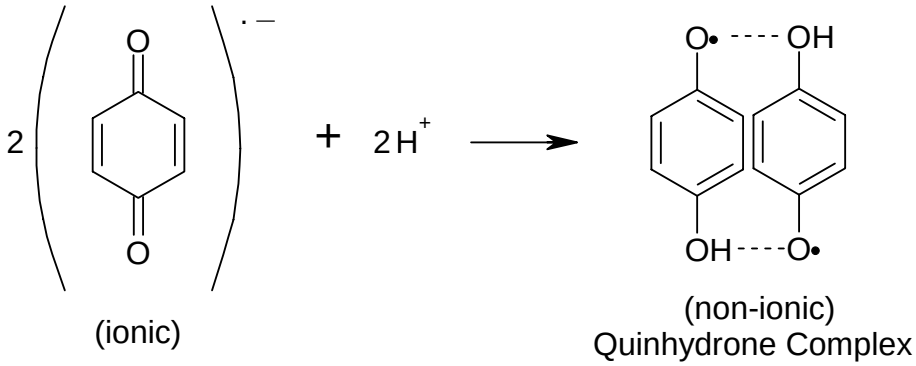

Figure 5.3.1. Formation of the quinhydrone complex from two benzoquinone anion radicals. Adapted from Esaka *et al.* [137]

Within the studied system of Uno *et al.* the quinhydrone complex would have been non-ionic and hence not detectable. Within our LHA, re-arrangement of the system would

allow for the quinone moieties to form such complexes. This is possible due to the rapid tumbling of molecules in liquids, greater freedom of rotation, and lower association with neighbouring molecules than in the solid samples [131]. In contrast, solid samples are unable to rearrange and hence a signal is still apparent for the LHA. An additional explanation is that the solid environment is analogous to that found within the acetonitrile. This environment would have a lower dielectric constant. A diminished EPR signal has been previously reported by Novotny and Martin-Neto in a peat humus [128]. As humidity of the solid sample was increased from 0.8 % to 7.1 % (w / w), the free radicals concentration decreased (which was not totally reversible upon drying). This was attributed to free radicals recombination with the increased molecular mobility. It is assumed that upon drying some of the quinhydrone complexes retained their dimerized conformation and thus the signal for the dimers remained quenched.

Our system allowed for this rearrangement and complex formation, however other humic and fulvic acids have still retained their radicals as is evident by the spectra published. This is likely caused by the individual nature of each HS due to its location and extraction procedures. Many more studies have been able to report only solid sample spectra [47, 50, 53] so our LHA is by no means unique in this respect.

It is also worth noting that any radicals that exist in LHA solution in quantities below detection would likely be destabilized and decreased even further upon the addition of Cu^{2+} ions as was found by Jezierski *et al.*[49, 132]. This interaction was explained by the strong interaction of the metal ions with the active centre responsible for the quinone-hydroquinone-semiquinone equilibria, and/or by the antiferromagnetic interaction between radical spins and metal d orbitals. This was eliminated as possibly

being a redox process after simple 1 M HCl washing out of the copper ions resulted in complete recovery of spin concentration present in the uncomplexed HA [49]

This EPR work very strongly suggests that the concentration of paramagnetic species in the LHA is very small. Due to how equation 4.4.2.4. is arranged, any small amount of paramagnetic influence from the LHA will be accounted for regardless.

5.4 Competing Ligand Exchange Method using Chelex Resin

The initial steep slope on the CLEM experimental curves (Figure 4.3.1 – 4.3.3.) can be attributed to one or several of the following species: copper aqua complexes, quickly dissociating inorganic complexes, and quickly dissociating organic complexes. Within systems with both copper and LHA it is likely that all species are present. However, in blank runs with only buffered copper solutions; aqua and inorganic complexes (buffer anions) are the only possible species. The aqua complexes have been previously reported by Sekaly to possess a resin uptake rate co-efficient of $(2.2 \pm 0.2) \times 10^{-2}\ s^{-1}$ [139] with no reported artifacts in the uptake of the metal aqua complex. Blanks performed here (Figure 4.3.1.) have a rate constant of $(1.9 \pm 0.2) \times 10^{-2}\ s^{-1}$, which is reasonably close to the value of Sekaly. This is important in that it suggests that the Chelex resin cannot experimentally distinguish complexes with dissociation rate coefficients $>10^{-2}\ s^{-1}$. The other limiting case occurs if the lifetimes are much larger than the analytical window (approximately 45 minutes). In between the two extremes resolvable components are to be found.

The vast majority of experiments with the CLEM yielded results that could be fitted well with two components. This is in accordance with Bonafazi *et al.* [140] who

investigated cupric ion binding to LHA using the CLE method with 3-propyl-5-hydroxy-5-(d-arabino-tertahydroxybutyl) thiozolidine-2-thione (PHTTT) as the competing ligand. For pH values of 5 and 6, a very fast unresolved component was evident, and rate constants of 0.093 $\pm$ 0.013 s^{-1} and 0.0077 $\pm$ 0.0008 s^{-1} were determined for the middle and slow components respectively.

Protons determine the state of the functional groups on LHA. At low pH the functional groups are protonated and uncharged, at higher pH the functional groups dissociate and become negatively charged. Thus for a positively charged metal ion in the system, proton competition for binding sites is decreased. Proton competition with copper for binding sites also occurs as pH is decreased. It is then expected that the percent composition of component 1 (fast or NMR labile) decreases as the pH is raised, indicating that more cupric ions are bound by the LHA. Also as the copper concentration increases for a given LHA concentration, the component 1 percentage rises, which is due to more cupric ions being present for the same number of ligands.

5.5 Low-field NMR

5.5.1. Low-field NMR

Ultrapure water showed a relaxation time of 2932 $\pm$ 20 ms which is slightly less than the theoretical longitudional relaxation time of 3000 ms [79]. This is expected as T_2 is always less than or (rarely) equal to T_1 [95].

The relaxation times of the LHA blanks were consistent with water closely associated with the LHA particles through binding on the interior of LHA aggregates and surfaces analogous to soil behaviour reported recently [28]. No distinct paramagnetic

influence is seen in the NMR plots and this is confirmed by the EPR experiments (Section 4.2.). Copper blanks showed very strongly the influence of the waters in the paramagnetic Cu^{2+} ions first coordination sphere. The paramagnetic ions large local magnetic fields cause relaxation efficiency to increase and thus we observe a shortening of relaxation time [97]. This relaxation time decrease is less evident as the pH is raised. This is possibly due to the hydrolysis of Cu^{2+} resulting in the formation of $CuOH^{+}$, which can then dimerize to form $Cu_2(OH)_2$. The dimer formation will result in an even number of electrons and is thus diamagnetic. The increase in $Cu_2(OH)_2$ is pH dependant (Figure 5.5.1.) and with hydrolysis its influence emerges after pH 5.Due to the large local magnetic fields of free cupric ions, small losses to a diamagnetic species could have large effects on the observed NMR signal. The NMR signal is only an average of the effects due to the bulk waters and those in the paramagnetic copper inner sphere (see equation 4.4.2.1.)

The copper – LHA titration's pattern of decreasing T_2 with increasing copper and LHA concentrations is expected due to a larger probability of waters in the highly efficient relaxation environments such as the cupric ion coordination shell, associated with the LHA or the Cu – LHA complex. A grouping of pH 4/5 distinct from pH 6/7 is again evident here. This same grouping was seen in the copper NMR blanks thus it can not be attributed to LHA and is unlikely to be due to the buffer. It is possible that this is then a product of, as previously mentioned, hydrolysis of Cu^{2+} leading to the formation of a non-paramagnetic dimer.

After the data from the NMR titration and CLEM were inserted into equation 4.4.2.4., several patterns were evident. A DCS model provides an interesting choice for interpretation.

5.5.2. Copper – LHA Complex T_2 Calculations

One of the more remarkable aspects of these calculations is that the relaxation times of the Cu – LHA complex does not change significantly at higher LHA to copper ratio over the course of the titration within a pH. Small deviations evident in the curves (Figures 4.4.3.1. – 4.4.3.9.) at higher LHA to copper ratio are within error. The level of error inherent in the calculations should temper any significance attributed to these deviations.

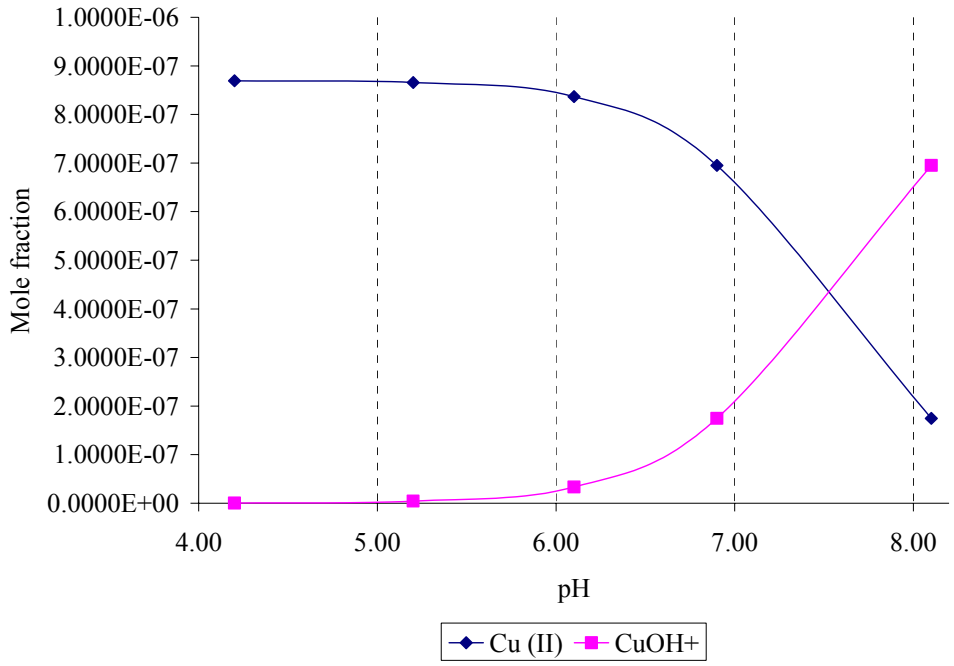

Figure 5.3.1. Copper hydrolysis as a function of pH. (Experimental data provided courtesy of Dr. Don Gamble)

Experimental error can be attributed to two dominant sources; the small difference in the observed T_2 relaxation curves and the kinetic partition of NMR free and bound metal.

If the upward deviation at lower LHA to metal ratio is a real phenomenon, it could be attributed to complexation at weaker sites or systematic error in our kinetic partition of 'NMR' free and bound metal.

The results are as expected for the different pH values possessing different T_{2bound} for identical LHA to metal ratios. This is due to the protonation of functional groups affecting binding as mentioned previously. The consistency in relaxation time of the complex that is seen within the experimental error is consistent with what is expected from a DCS. When the system is at a reasonably high LHA to metal ratio, it is expected that a preferred conformation (or closely related group of conformers) will form the binding site that will give the relaxation signal. When this is the case, changes of the aggregational equilibria will not produce a significant change for the immediate bound copper environment. The system will adjust to provide binding sites for the coppers that are approximately equivalent. This is then what the results indicate.

The spread of relaxation times for pH 4.0 experiments was far larger than that of pH 7.0. This suggests that the pH 4.0 system is more hindered in its adjustments to maintain the 'optimal' binding sites, i.e. the system can not easily adjust its library to produce more of the most favourable conformation. This is substantiated by the DLS data that observed, for pH 4.0, a smaller shift in distribution of particle sizes for comparable copper loadings than pH 7.0. An additional difficulty for binding at low pH is the competition for binding sites from protons within the system.

CHAPTER SIX: CONCLUSIONS AND RECOMMENDATIONS

6.1. Conclusions

Humic substances are extremely complex in nature as is evident from recently available state of the art sample interrogation techniques [1-3]. This information necessitates a new paradigm. The new understanding of HS is that of a collection of monomers, oligomers, and polymers interacting in a complex pattern of labile aggregational and conformational equilibria under the influence of weak forces (H-bonding, hydrophobic interaction, charge transfer complexing). This new structural paradigm then demands a similar shift in present thought on binding of contaminants to humics. The previous models of contaminant binding were based upon an understanding of HS based around a high molecular weight covalently bound polymer [12], thus the time is right for a re-conceptualization.

A dynamic combinatorial system (DCS) model, borrowed from combinatorial synthesis, contains building blocks that are in constant flux, continuously able to form and break new members as they make up non-covalent supramolecular units. With the recent structural evidence, it is a natural progression to envision HS as a DCS. This thesis introduced in Chapter Five the concept of humics as a DCS.

The first major test for the new binding model was whether visible changes can be observed in the size distribution of a humic system subject to varying contaminant loads. The most obvious technique was dynamic laser light scattering (DLS). Light scattering experiments were conducted on a well characterized Laurentian humic acid (LHA) with copper (II) ions in solution. The light scattering results were consistent with predictions

provided by a DCS interpretation. The size distributions shifted as the humic system equilibrium composition adjusted to provide the most advantageous binding sites.

The dynamic combinatorial perspective was then exploited for the interpretation of a copper humic acid titration using a novel low-field nuclear magnetic relaxometery (NMR) technique. Low-field NMR observes the T_2 relaxation time of the solvent protons. The relaxation time is dependant upon the environment to which the proton is exposed. The results from the low-field NMR work supported the results and interpretation of the dynamic light scattering. The decreased aggregational mobility that was evident in the DLS results was also observed in the changing complex relaxation time. The more mobile pH 7.0 demonstrated a more stable T_{2bound} that was indicative of the system adjusting to provide a very similar binding site throughout the course of the titration. The most persuasive support of a DCS system from NMR was the relative stability of the T_2 relaxation time at high LHA to copper ratios. This suggests that the system actively adjusted to the copper introduction by generating binding sites of similar energy to maintain a fairly uniform bound copper environment.

The major contributions of this thesis are two-fold: first, a binding concept that has demonstrated a coherent interpretation of the results presented, while being applicable to the vast multitude of HS interactions with contaminants. As well, low-field NMR has been successfully utilized, for what is believed to be the first time, to study the binding interactions of a humic substance to a metal ion.

6.2. Suggestions for Future Work

This thesis was intended as an exploratory work to determine the feasibility and benefits of a low-field NMR investigation of humic binding interactions with interpretation as a DCS system. It is thus not surprising that a large number of questions are generated from this thesis. This is, in the author's opinion, a good sign. The following is a limited list of possible future directions.

- As a further test of a DCS interpretation workers may re-exam HS literature with DCS interpretations. Instances where the interpretation is acknowledged to be problematic could be a testing ground to gauge improvements afforded by the DCS model.
- Computational modelling utilizing structures of proposed humic components (Figure 1.1.2.3.) could aid in model validation. A DCS would be very difficult to examine with a model solution of any complexity, thus a computational method presents a desirable alternative. The molecules could be modelled as monomers, dimers, and trimers then made to interact with contaminants. This work has already been initiated in our lab.
- Further DLS studies using different contaminants and HSs to attempt to witness the changes to the distribution as loading is increased. Are the changes similar for different starting materials?
- Low-field NMR experiments with other paramagnetic species and LHA could be performed. It would be very interesting to investigate if the system adjustments are similar for another paramagnetic species compared to those of copper.

- Thermostated T_2 dependence runs could be used to investigate the thermodynamic rearrangements of the system.

This list of possible future directions is not overly specific and by no means exhaustive, but intended to demonstrate the many possible directions for further work to add supplementary validation to both the DCS binding model and the low-field NMR binding probe. The possible applications of both model and probe appear very promising.

APPENDICES

Appendix One

Table A.1. DLS confidence intervals (90% and 95%) for pH 4.0 and 7.0 LHA and Cu (II) titration

pH	LHA Concentration (mg/L	Copper Concentration (M	Diameter Interval (nm)	Normalized summed detector response	Confidence Interval 90%	95%
4.00	25	0	1-50	11.9	1.6	1.9
			51-120	45.1	1.8	2.1
			121-250	100.0	1.2	1.4
			251-400	44.4	2.8	3.3
			401-9000	2.3	2.0	2.4
		1.00E-06	1-50	23.6	1.9	2.3
			51-120	68.4	7.0	8.3
			121-250	100.0	2.6	3.1
			251-400	59.0	1.9	2.3
			401-9000	15.2	4.1	4.8
		1.00E-05	1-50	28.4	3.7	4.5
			51-120	67.9	7.5	8.9
			121-250	100.0	3.3	4.0
			251-400	74.5	2.5	3.0
			401-9000	18.1	4.7	5.6
		1.00E-04	1-50	33.8	1.5	1.8
			51-120	11.8	3.7	4.4
			121-250	100.0	2.1	2.5
			251-400	65.8	1.8	2.2
			401-9000	37.2	6.0	7.1
4.00	125	0	1-50	8.1	1.9	2.3
			51-120	36.6	4.5	5.3
			121-250	100.0	2.1	2.5
			251-400	40.3	4.0	4.8
			401-9000	0.0	0.0	0.0
		1.00E-06	1-50	6.4	1.3	1.5
			51-120	42.2	5.6	6.6
			121-250	100.0	3.0	3.6
			251-400	55.5	2.1	2.6
			401-9000	11.2	2.8	3.3
		1.00E-05	1-50	12.3	1.5	1.8
			51-120	41.8	4.1	4.9
			121-250	100.0	1.9	2.3
			251-400	44.1	3.1	3.7
			401-9000	4.6	2.7	3.3

pH	LHA Concentration (mg/L	Copper Concentration (M	Diameter Interval (nm)	Normalized summed detector response	Confidence Interval 90%	95%
4.00	225	0	1-50	13.5	2.6	3.1
			51-120	38.8	7.5	9.0
			121-250	100.0	4.4	5.2
			251-400	43.9	5.4	6.4
			401-9000	11.6	5.8	6.9
		1.00E-06	1-50	7.3	1.4	1.7
			51-120	26.1	0.0	0.1
			121-250	100.0	0.6	0.7
			251-400	19.9	2.9	3.5
			401-9000	0.0	0.0	0.0
		1.00E-05	1-50	15.0	2.0	2.4
			51-120	49.8	6.0	7.2
			121-250	100.0	3.2	3.8
			251-400	56.8	3.2	3.8
			401-9000	14.5	3.9	4.7
		1.00E-04	1-50	13.3	1.7	2.0
			51-120	43.3	4.7	5.6
			121-250	100.0	1.9	2.2
			251-400	55.3	3.7	4.5
			401-9000	4.0	1.7	2.0
7.00	25	0	1-50	98.7	5.0	6.0
			51-120	100.0	2.9	3.5
			121-250	81.3	1.8	2.2
			251-400	40.7	3.1	3.7
			401-9000	5.4	2.7	3.2
		1.00E-06	1-50	31.6	5.2	6.2
			51-120	100.0	3.0	3.6
			121-250	91.1	1.2	1.5
			251-400	36.4	1.9	2.3
			401-9000	20.9	3.1	3.6
		1.00E-05	1-50	32.9	1.0	1.2
			51-120	43.1	1.0	1.2
			121-250	100.0	2.0	2.4
			251-400	45.6	1.0	1.1
			401-9000	31.0	2.7	3.2
		1.00E-04	1-50	2.0	2.0	2.3
			51-120	13.8	3.2	3.9
			121-250	46.2	4.0	4.7
			251-400	35.6	3.4	4.0
			401-9000	100.0	5.4	6.4

pH	LHA Concentration (mg/L	Copper Concentration (M	Diameter Interval (nm)	Normalized summed detector response	Confidence Interval 90%	95%
7.00	125	0	1-50	10.6	1.9	2.2
			51-120	60.4	3.0	3.6
			121-250	100.0	0.9	1.1
			251-400	18.4	3.0	3.5
			401-9000	3.3	2.7	3.2
		1.00E-06	1-50	12.4	3.9	4.7
			51-120	96.6	6.6	7.9
			121-250	100.0	5.7	6.8
			251-400	50.0	4.2	4.9
			401-9000	22.3	5.0	6.0
		1.00E-05	1-50	12.8	2.6	3.1
			51-120	58.2	3.6	4.3
			121-250	100.0	2.2	2.6
			251-400	32.4	3.7	4.4
			401-9000	13.5	4.0	4.8
		1.00E-04	1-50	10.9	0.9	1.1
			51-120	42.8	2.3	2.7
			121-250	100.0	0.9	1.0
			251-400	29.1	0.4	0.5
			401-9000	0.3	1.1	1.3
7.00	225	0	1-50	3.2	2.5	3.0
			51-120	50.0	5.0	5.9
			121-250	100.0	3.6	4.3
			251-400	14.2	2.3	2.7
			401-9000	1.5	2.1	2.5
		1.00E-06	1-50	9.5	0.7	0.9
			51-120	63.7	3.2	3.9
			121-250	100.0	1.7	2.0
			251-400	47.0	1.5	1.8
			401-9000	16.3	1.8	2.2
		1.00E-05	1-50	6.2	1.8	2.1
			51-120	61.9	3.0	3.6
			121-250	100.0	0.4	0.5
			251-400	36.5	1.8	2.2
			401-9000	12.8	3.7	4.4
		1.00E-04	1-50	10.7	3.7	4.4
			51-120	69.3	6.0	7.1
			121-250	100.0	2.5	3.0
			251-400	18.9	6.2	7.4
			401-9000	5.3	2.8	3.4

Appendix Two

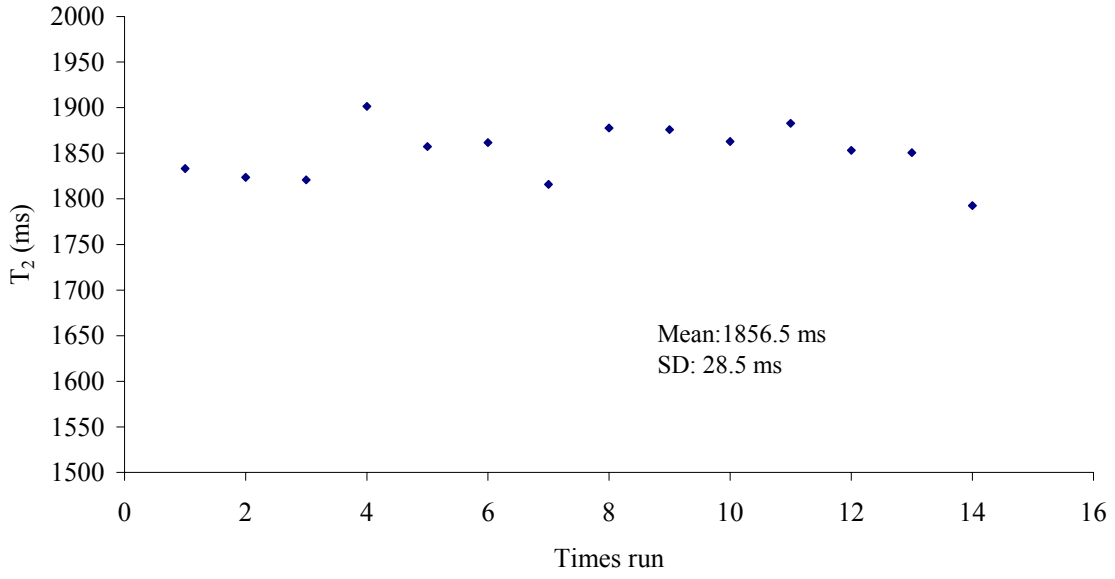

Figure A.2. Plot of 1.0 x 10^{-4} M Cu^{2+} standard T_2 observed as a function of times run. Sample was run at the start of each session.

Appendix Three

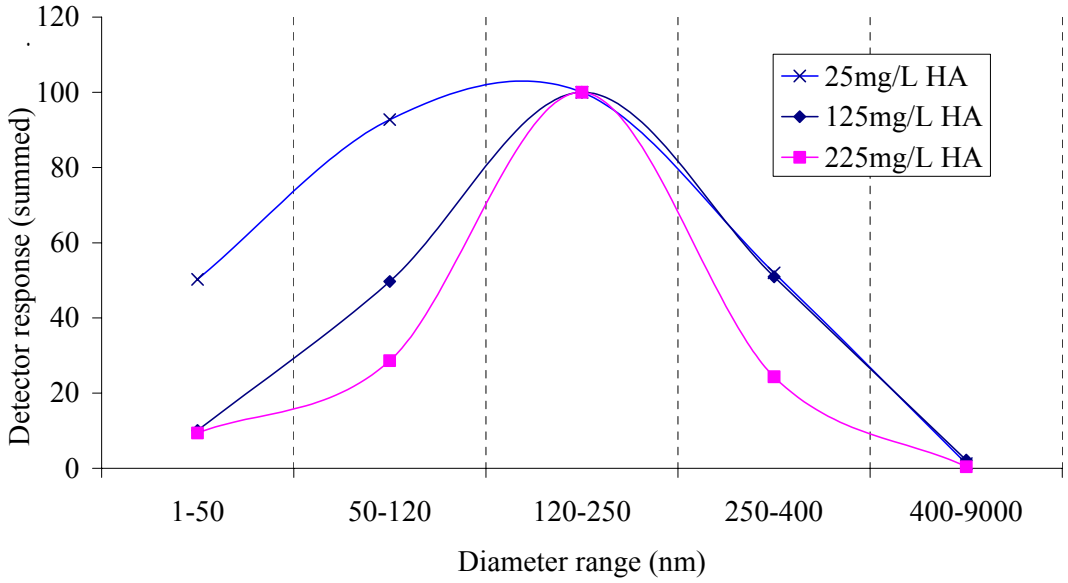

Figure A.3.1. DLS plot of summed size distributions for pH 5.0 25 mg/L, 125 mg/L, and 225 mg/L LHA with no Cu^{2+} added.

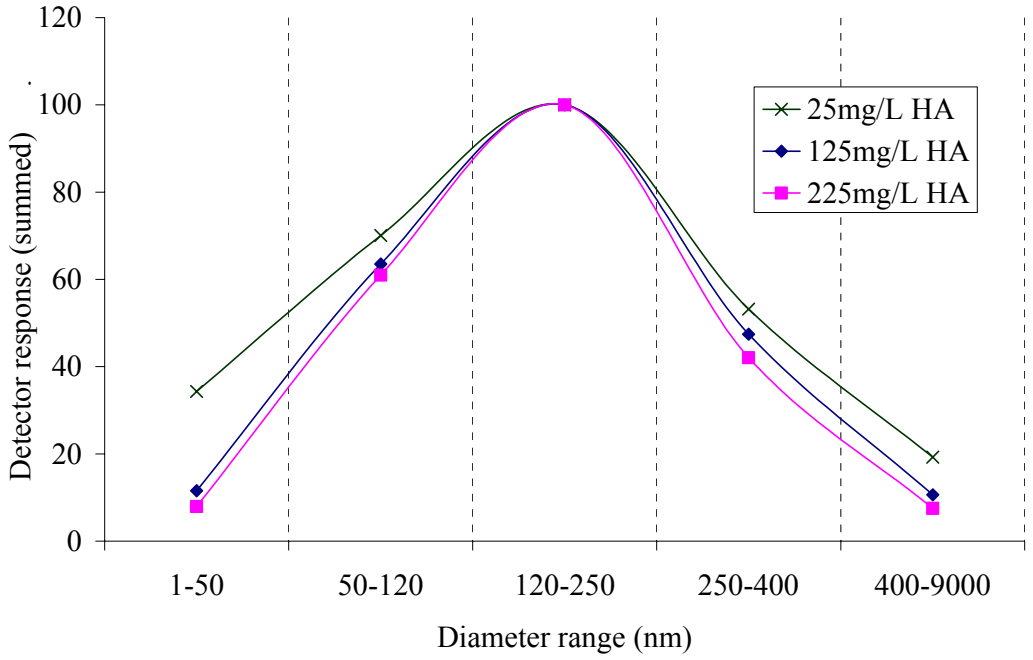

Figure A.3.2. DLS plot of summed size distributions for pH 5.0 25 mg/L, 125 mg/L, and 225 mg/L LHA with 1.0 x 10^{-6} M Cu^{2+} added.

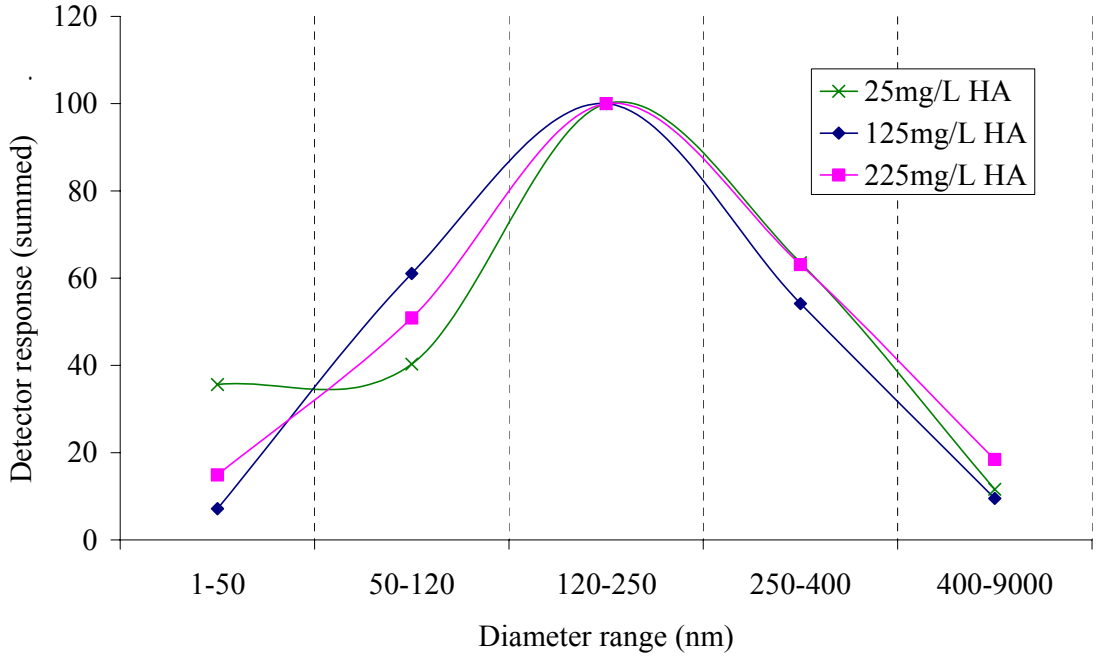

Figure A.3.3. DLS plot of summed size distributions for pH 5.0 25 mg/L, 125 mg/L, and 225 mg/L LHA with 1.0 x 10^{-5} M Cu^{2+} added.

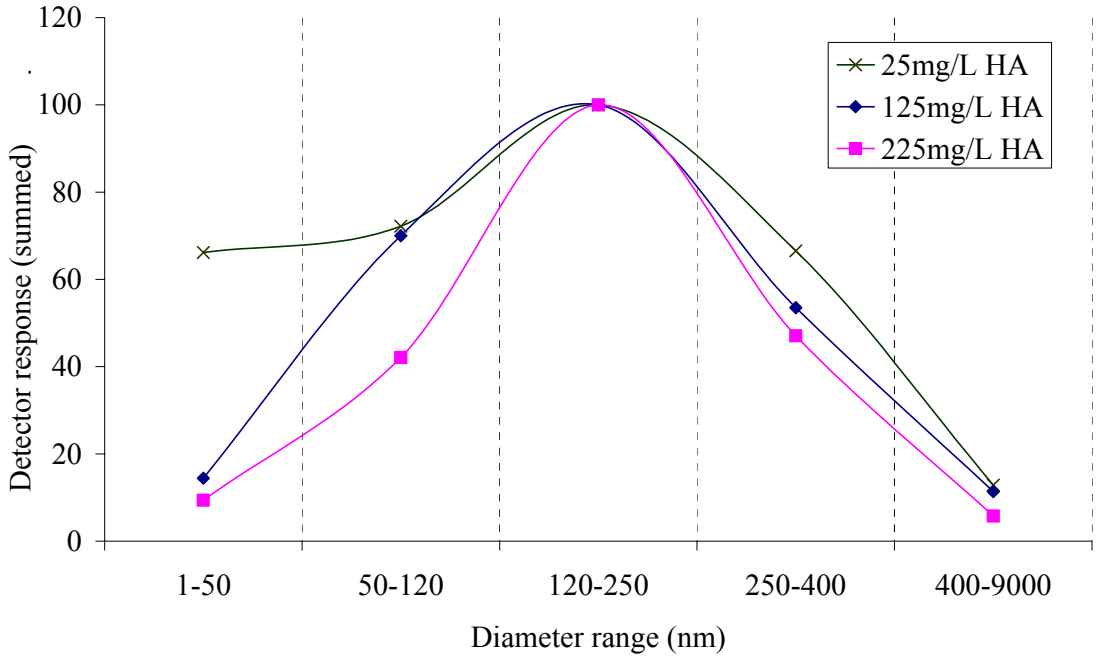

Figure A.3.4. DLS plot of summed size distributions for pH 5.0 25 mg/L, 125 mg/L, and 225 mg/L LHA with 1.0 x 10^{-4} M Cu^{2+} added.

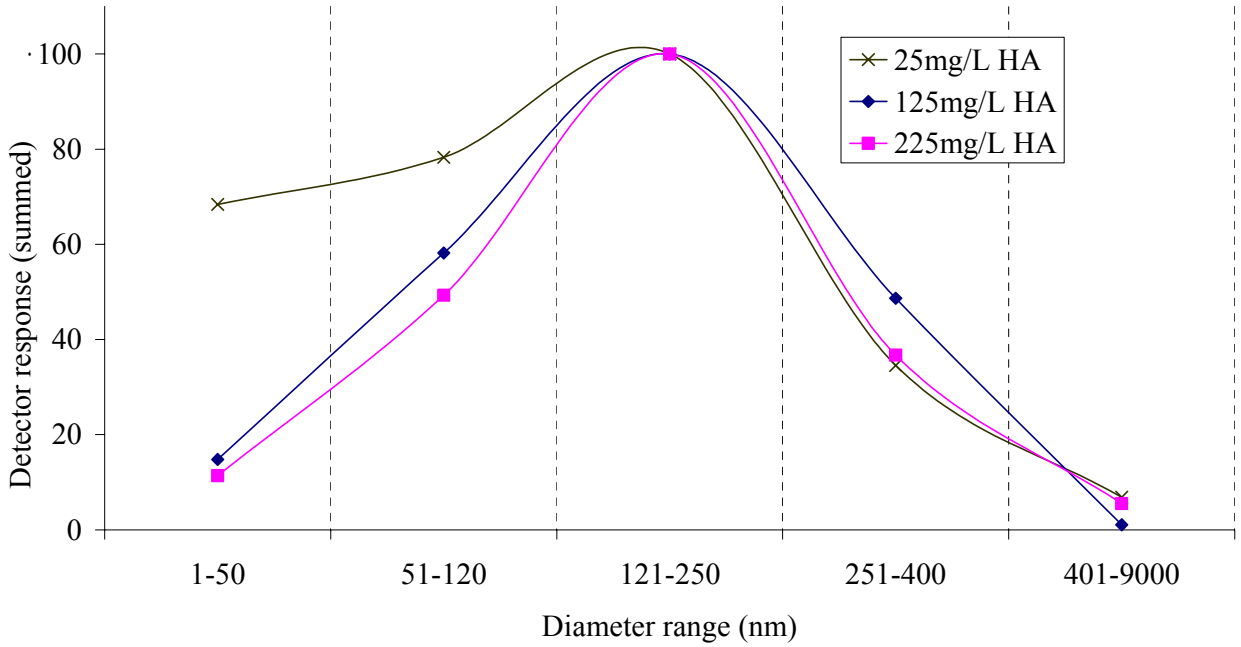

Figure A.3.5. DLS plot of summed size distributions for pH 6.0 25 mg/L, 125 mg/L, and 225 mg/L LHA with no Cu^{2+} added.

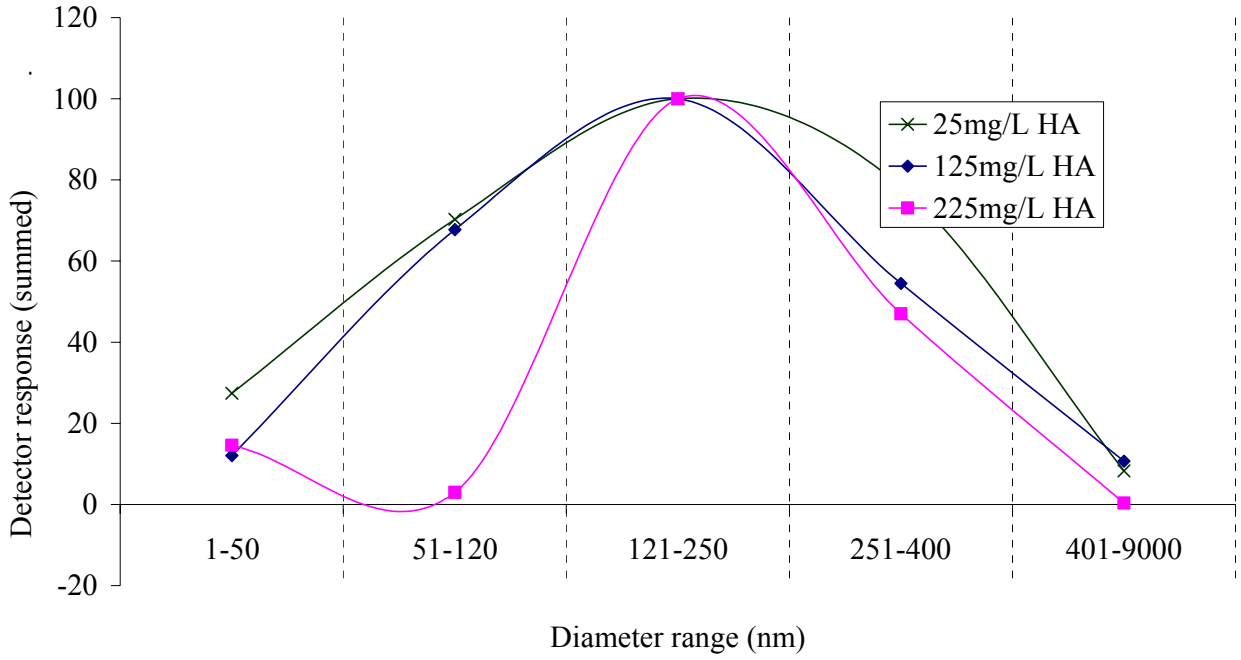

Figure A.3.6. DLS plot of summed size distributions for pH 6.0 25 mg/L, 125 mg/L, and 225 mg/L LHA with 1.0 x 10^{-6} M Cu^{2+} added.

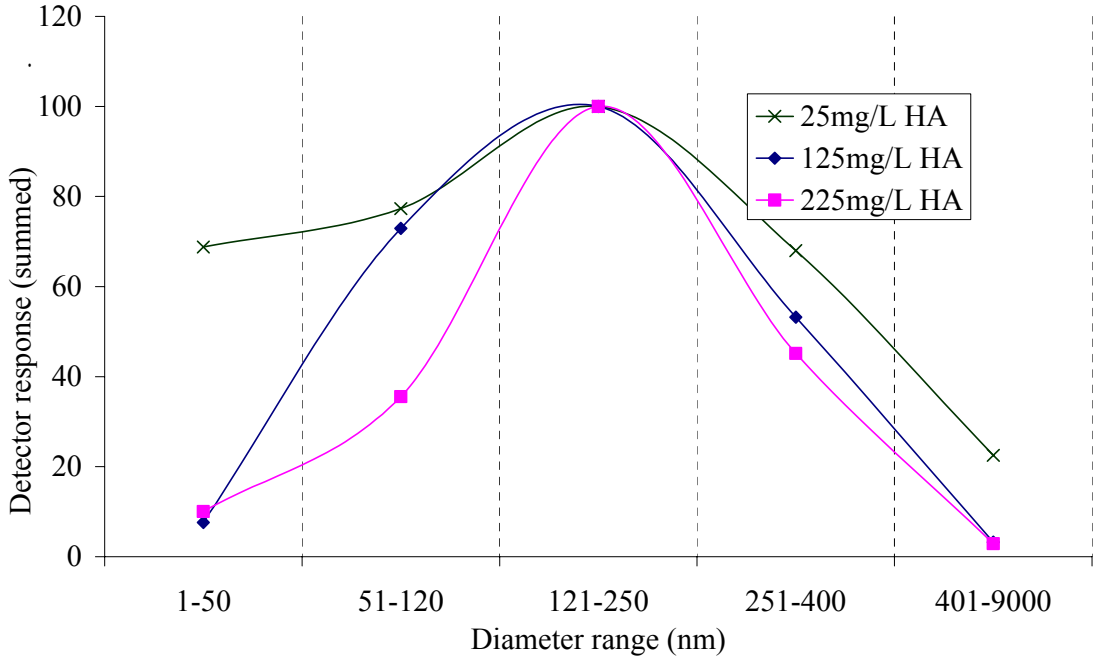

Figure A.3.7. DLS plot of summed size distributions for pH 6.0 25 mg/L, 125 mg/L, and 225 mg/L LHA with 1.0 x 10^{-5} M Cu^{2+} added.

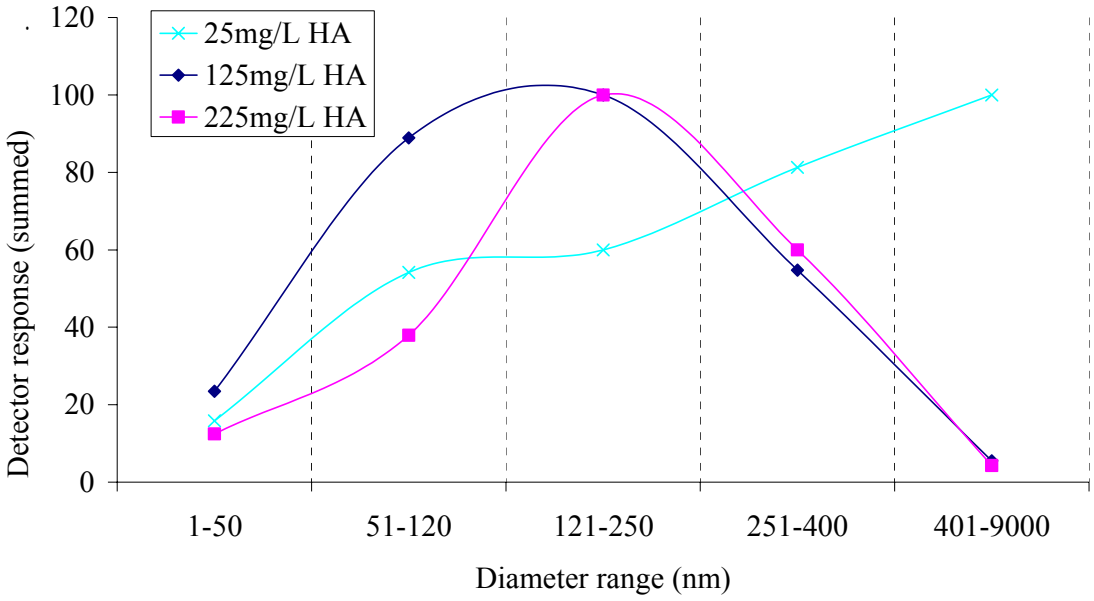

Figure A.3.8. DLS plot of summed size distributions for pH 6.0 25 mg/L, 125 mg/L, and 225 mg/L LHA with 1.0 x 10^{-4} M Cu^{2+} added.

REFERENCES

1. Stenson, A. C., A. G. Marshall, and W. T. Cooper, Anal. Chem., 2003. **75**(6): p. 1275-1284.
2. Cook, R. L., D. D. McIntyre, C. H. Langford, and H. J. Vogel, Enviro. Sci. & Tech, 2003. **37**(17): p. 3935-3944.
3. Cooper, W. T., L. Milligan, J. Chanton, T. Dittmar, and T. Filley. *Ultrahigh Resolution Mass Spectrometry of Aquatic Humic Substances: They Really Are Geopolymers*. in *Humic Substances Seminar VII*. 2004. Boston. In Press
4. Piccolo, A., *Humus and Soil Conservation*, in *Humic Substances in Terrestrial Ecosystems*, A. Piccolo, Editor. 1996, Elsevier: Amsterdam. p. 225-264.
5. Tipping, E., *Cation Binding by Humic Substances*. 1st ed. Cambridge Environmental Chemistry Series, ed. P.G.C. Campbell, R.M. Harrison, and S.J. de Mora. 2002, Cambridge: Cambridge University Press. p. 4-50, 103-170, 262-297.
6. Hoch, A. R., M. M. Reddy, and G. R. Aiken, Geochim. Cosmochim. Acta, 2000. **64**: p. 61-72.
7. Lovely, D. R., J. D. Coates, E. L. Blunt-Harris, E. J. P. Phillips, and J. C. Wormwood, Nature, 1996. **382**: p. 445-448.
8. Slaveykova, V. I., K. J. Wilkinson, A. Ceresa, and E. Pretsch, Environ. Sci. & Tech, 2003. **37**(6): p. 1114-1121.
9. Marinsky, J. A., S. Gupta, and P. Schindler, J. Coll. Inter. Sci, 1982. **89**(2): p. 401-411.
10. Schnitzer, M., Soil Sci., 1991. **151**: p. 41-58.
11. Piccolo, A., Soil Sci., 2001. **166**(11): p. 810-832.
12. Stevenson, F. J., *Humus Chemistry: Genesis, Composition, Reactions*. 2nd ed. 1994, New York: Wiley. p. 3-111.
13. Aiken, G. R., D. M. McKnight, R. L. Wershaw, and P. MacCarthy, *Humic Substances in Soil, Sediment, and Water*. Humic Substances. 1985, New York: Wiley. p.34-132.
14. Hayes, M. H. B., P. MacCarthy, R. L. Malcolm, and R. S. Swift, *The Search for Structure: Setting the Scene*, in *Humic Substances II: In Search of Structure*, M.H.B. Hayes, P. MacCarthy, R.L. Malcolm, and R.S. Swift, Editors. 1989, John Wiley and Sons: Chichester. p. 3-33.
15. Malcolm, R. L., Anal. Chim. Acta, 1990. **232**(1): p. 19-30.
16. Simpson, A. J., Mag. Reson. In Chem., 2002. **40**: p. s72-s82.
17. Thurman, E. M., *Organic Geochemsitry of Natural Waters*. 1985, Dordrecht: Martinus Nijhoff/Dr. W. Junk Publishers. p.1-21.
18. MacCarthy, P. and J. A. Rice, *An Ecological Rationale for the Heterogeneity of Humic Substances: A Holistic Perspective of Humus*, in *Scientists on Gaia*, S.H. Schneider and P.J. Boston, Editors. 1991, MIT Press: Cambridge MA. p. 339-345.
19. These, A. and T. Reemstma. *New Results and Old Questions on Fulvic and Humic Acid Structures Obtained by SEC-ESI-MS* in *Humic Substances Seminar VII*. 2004. Boston. In Press.
20. Sigg, L., *Metal Transfer Mechanisms in Lakes; the Role of Settling Particles*, in *Chemical Processes in Lakes*, W. Stumm, Editor. 1985, John Wiley and Sons: New York. p. 283-310.

21. Henderson, P., *Inorganic Geochemistry*. 1982, Oxford: Pergamon Press. pp. 343.
22. Christensen, J. B., D. L. Jensen, and T. H. Christensen, Water Res., 1996. **30**(12): p. 3037-3049.
23. Rate, A. W., R. G. McLauren, and R. S. Swift, Environ. Sci. & Tech, l992. **26**(12): p. 2477-2483.
24. Singer, P. C., *Trace Metals and Metal-Organic Interactions in Natural Waters*. 1973, Ann Arbor, Michigan: Ann Arbor Science.
25. Glaus, M. A., W. Hummel, and L. R. Van Loon, Environ. Sci. & Tech, 1995. **29**(8): p. 2150-2153.
26. Robertson, A. P. and J. O. Leckie, Environ. Sci. & Tech, 1999. **33**(5): p. 786-795.
27. Todoruk, T. R. PhD Thesis, 2003, University of Calgary: Calgary. p. 43-60.
28. Todoruk, T. R., C. H. Langford, and A. Kantzas, Environ. Sci. & Tech, 2003. **37**: p. 2707-2713.
29. Berne, B. J. and R. Pecora, *Dynamic Light Scattering with Applications to Chemistry, Biology, and Physics*. 1st ed. Wiley-Interscience Publication. 1976, New York: John Wiley and Sons, Inc. p. 1-53.
30. Chu, B., *Laser Light Scattering*. Quantum Electronics: Principles and Applications. 1974, New York: Academic Press. p.9-62.
31. Provencher, S. W., Biophys. J., 1976. **16**: p. 27-41.
32. Provencher, S. W., Comp. Phys. Comm., 1982. **27**: p. 213-227.
33. Black, A. P. and R. F. Christman, J. Amer. Water Works Assoc, 1963. **55**: p. 897.
34. Underdown, A. W., C. H. Langford, and D. S. Gamble, Anal. Chem, 1981. **53**(13): p. 2139-2140.
35. Gamble, D. S., C. H. Langford, and A. W. Underdown, Org. Geochem, 1985. **8**: p. 35-39.
36. Manning, T. J., T. Bennett, and D. Milton, Science Total Environ., 2000. **257**: p. 171-176.
37. Wagoner, D. B. and R. F. Christman, Acta Hydrochim. Hydrobiol, 1998. **26**(3): p. 191-195.
38. Kretzschmar, R., H. Holthoff, and H. Sticher, J. Coll Inter Sci, 1998. **202**: p. 95-103.
39. Pinheiro, J. P., A. M. Mota, J. M. R. d'Oliveira, and J. M. G. Martinho, Anal Chim Acta, 1996. **329**: p. 15-24.
40. Wagoner, D. B., R. F. Christman, G. Cauchon, and R. Paulson, Environ. Sci. & Tech, 1997. **31**(3): p. 937-941.
41. Reid, P. M., A. E. Wilkinson, E. Tipping, and M. N. Jones, J. Soil Sci, 1991. **42**: p. 259-270.
42. Palmer, N. E. and R. von Wanduszka, Fresenius J. Anal. Chem, 2001. **371**: p. 951-954.
43. Zavoisky, E., J of Phys. U.S.S.R., 1945. **9**(211): p. 245.
44. Blume, R. J., Phys. Rev., 1958. **109**: p. 1867.
45. Keijzers, C. P., E. J. Reijerse, and J. Schmidt, *Pulsed EPR: A New Field of Applications*. 1989, North Holland: Koninklijke Nederlandse Akademie van Wetenschappen. p. 1-17.
46. Boyd, S. A., L. E. Sommers, D. W. Nelson, and D. X. West, Soil Sci. Soc. Amer. J., 1981. **45**: p. 745-749.

47. Chen, J., B. Gu, E. J. LaBoeuf, H. Pan, and S. Dai, Chemosphere, 2002. **48**: p. 59-68.
48. Cheshire, M. V., D. B. M^{c}Phail, and M. L. Berrow, Sci. Tot. Environ, 1994. **152**: p. 63-72.
49. Jerzykiewicz, M., A. Jezierski, F. Czechowski, and J. Drozd, Org. Geochem, 2002. **33**: p. 265-268.
50. Jezierski, A., F. Czechowski, M. Jerzykiewicz, and J. Drozd, App. Magn. Reson., 2000. **18**: p. 127-136.
51. Goodman, B. A. and M. V. Cheshire, Nature New Biol., 1973. **244**: p. 158-159.
52. Paciolla, M. D., G. Davies, and S. A. Jansen, Environ. Sci. & Tech, 1999. **33**: p. 1814-1818.
53. Tipikin, D. S., G. G. Lazarev, V. A. Zhorin, and Y. S. Lebedev, Russ. J. Phys. Chem., 1993. **67**(9): p. 1834-1838.
54. Rex, R. W., Nature, 1960. **188**: p. 1185-1186.
55. Steelink, C. and G. Tollin, Biochim. Biophys. Acta, 1962. **59**: p. 25-34.
56. Jezierski, A., F. Czechowski, M. Jerzykiewicz, Y. Chen, and J. Drozd, Spectrochim. Acta Part A, 2000. **56**: p. 379-385.
57. Jezierski, A., F. Czechowski, M. Jerzykiewicz, I. Golonka, J. Drozd, E. Bylinska, Y. Chen, and M. R. D. Seaward, Spectrochim. Acta Part A, 2002. **58**: p. 1293-1300.
58. Pake, G. E. and T. L. Estle, *The Physical Principles of Electron Paramagnetic Resonance*. 2nd ed. Frontiers in Physics, ed. D. Pines. 1973, Reading, Massachusetts: W.A. Benjamin Inc. p.1-13.
59. Carrington, A. and A. D. McLachlan, *Introduction to Magnetic Resonance*. 1979, London: Chapman and Hall. 1-263.
60. Garmon, R. G. and C. N. Reilley, Anal. Chem., 1962. **34**(6): p. 600-607.
61. Schechter, I., Anal. Chem., 1992. **64**(7): p. 729-737.
62. Langford, C. H. and R. L. Cook, The Analyst, 1995. **120**(3): p. 591-596.
63. Schechter, I., Anal. Chem., 1991. **63**(13): p. 1303-1307.
64. Langford, C. H. and D. W. Gutzman, Anal. Chim. Acta, 1992. **256**(1): p. 183-201.
65. Buffle, J., *Complexation Reactions in Aquatic Systems: An Analytical Approach*. 1988, Chichester: Ellis Horwood. p. 81-89.
66. Sekaly, A. L., J. Murimboh, N. M. Hassan, R. MAndal, M. E. Ben Younes, C. L. Chakrabarti, and M. H. Back, Environ. Sci. & Tech., 2003. **37**(1): p. 68-74.
67. Chakrabarti, C. L., Y. Lu, D. C. Gregoire, M. H. Back, and W. H. Schroeder, Environ. Sci. & Tech, 1994. **28**(11): p. 1957-1967.
68. Cheng, J., C. L. Chakrabarti, M. H. Back, and W. H. Schroeder, Anal. Chim. Acta, 1994. **288**: p. 141-156.
69. Fasfous, I. I., T. Yapici, N. M. Hassan, C. L. Chakrabarti, and M. H. Back, Environ. Sci. & Tech., 2004. **In Press**
70. Lu, Y., C. L. Chakrabarti, M. H. Back, D. C. Gregoire, and W. H. Schroeder, Anal. Chim. Acta, 1994. **293**: p. 95-108.
71. Florence, T. M., Water Res., 1977. **11**(8): p. 681-687.
72. Campbell, P. G. C., M. Bisson, R. Bougie, A. Tessier, and J.-P. Villeneuve, Anal. Chem., 1983. **55**(14): p. 2246-2252.
73. Rocha, J. C., I. A. S. Toscano, and P. Burba, Talanta, 1997. **44**: p. 69-74.

74. Jansen, S., R. Blust, and H. P. van Leeuwen, Environ. Sci. & Tech, 2002. **36**(2164-2170).
75. van Leeuwen, H. P., Environ. Sci & Tech, 1999. **33**(21): p. 3743-3748.
76. Morel, F. M. M. and J. G. Hering, *Principles and Applications of Aquatic Chemistry*. 1993, New York: John Wiley. p. 323-325, 398-403.
77. Hering, J. G. and F. M. M. Morel, Environ. Sci. & Tech, 1988. **22**: p. 1469-1478.
78. Freeman, R., *A Handbook of Nuclear Magnetic Resonance*. 2nd ed. 1997, Essex: Addison Wesley Longman. p.1-22.
79. Bloch, F., W. W. Hanson, and M. E. Packard, Phys. Rev., 1946. **69**: p. 127.
80. Purcell, E. M., H. C. Torrey, and R. V. Pound, Phys. Rev., 1946. **69**: p. 37.
81. Belliveau, S. M., K. Mirotchnik, and A. Kantzas, Graduate Course Notes, 1996. p. 1-19.
82. Schnitzer, M. and D. H. R. Barton, Nature, 1963. **198**: p. 217
83. Lentiz, H., H. D. Ludemann, and W. Ziechmann, Geoderma, 1977. **18**: p. 325.
84. Wilson, M. A., *NMR Techniques and Applications in Geochemistry and Soil Chemistry*. 1984, Oxford, UK: Pergamon Press. p.1-32.
85. Wershaw, R. L. and M. A. Mikita, eds. *NMR of Humic Substances and Coal. Techniques, Problems and Solutions*. 1987, Lewis Publishers: Chelsea MI.
86. Kleinberg, R. L. and H. Vinegar, The Log Analyst, 1996. **7**(6): p. 20-32.
87. Straley, C., D. Rossini, H. Vinegar, P. Tutunjian, and C. Morriss, The Log Analyst, 1997. **8**(2): p. 84-94.
88. Brosio, E., G. Altobelli, and A. Di Nola, J. Food Tech, 1984. **19**: p. 103-108.
89. Lambelet, P., F. Renevey, C. Kaabi, and A. Raemy, J. Agric. Food Chem, 1995. **43**: p. 1462-1466.
90. Eisinger, J., R. G. Shulman, and W. E. Blumberg, Nature, 1961. **192**: p. 963-964.
91. Gamble, D. S., C. H. Langford, and J. P. K. Tong, Can. J. Chem, 1976. **54**(8): p. 1239-1245.
92. Deczky, K. and C. H. Langford, Can. J Chem, 1978. **56**: p. 1947-1951.
93. Martin, M. L., J.-J. Delpuech, and G. J. Martin, *Practical NMR Spectroscopy*. 1980, London: Heyden & Son Ltd. p. 1-29.
94. van der Klink, J. J. and H. B. Brom, Progress in Nuclear Magnetic Resonance Spectroscopy, 2000. **36**: p. 89-201.
95. Hornack, J. P., *The Basics of MRI*, in *http://www.cis.rit.edu/htbooks/nmr/bnmr.htm*. 2002: Rochester. Accessed May 11 2004.
96. Brown, M. A. and R. C. Semelka, *MRI: Basic Principals and Applications*. 1995, Toronto: Wiley-Liss. p. 25.
97. Wehrli, F. W., *Principles of Magnetic Resonance*, in *Magnetic Resonance Imaging*, D.D. Stark and W.G. Bradley, Editors. 1988, C.V. Mosby Company: Toronto. p. 3-47.
98. Jepsen, S. M., H. T. Pedersen, and S. B. Engelsen, J. of Sci. Food Agric., 1999. **79**: p. 1973.
99. Bhattacharyya, K., Acc. Chem. Res., 2003. **36**(2): p. 95-101.
100. Hahn, E. L., Phys. Rev, 1950. **80**: p. 580.
101. Carr, H. Y. and E. M. Purcell, Phys. Rev, 1954. **94**: p. 630.
102. Meiboom, S. and D. Gill, Rev. Sci. Instrum, 1958. **29**: p. 688.

103. Xu, X. and L. A. Davis, SPE On-line Journal, 1999: p. Paper No. SPE 56800.
104. Bruccoleri, A. G., B. C. Pant, D. K. Sharma, and C. H. Langford, Environ. Sci. & Tech, 1993. **27**(5): p. 889-894.
105. Wang, Z., D. S. Gamble, and C. H. Langford, Environ. Sci. & Tech, 1992. **26**(3): p. 560-565.
106. Cook, R. L. PhD Thesis, 1997, University of Calgary: Calgary. p. 185.
107. Wang, Z., B. C. Pant, and C. H. Langford, Anal. Chim. Acta, 1990. **232**(1): p. 43-49.
108. Wang, Z., PhD Thesis, 1989, Concordia University: Montreal.
109. Kerndorff, H. and M. Schnitzer, Geochim. Cosmochim. Acta, 1980. **44**: p. 1701-1708.
110. Senesi, N., Y. Chen, and M. Schnitzer, *Aggregation-Dispersion Phenomena in Humic Substances*, in *Soil Organic Matter Studies: Proceedings of a Symposium on Soil Organic Matter Studies*. 1976: Vienna. p. 143-155.
111. Ariese, F., S. van Assema, C. Gooijer, A. G. Bruccoleri, and C. H. Langford, Aqua. Sci., 2004. **66**(1): p. 89-94.
112. Senesi, N. and M. Schnitzer, Soil Sci., 1977. **123**(4): p. 224-234.
113. Olson, D. L. and M. S. Shuman, Anal. Chem., 1983. **55**(7): p. 1103-1107.
114. Shuman, M. S., B. J. Collins, P. J. Fitzgerald, and D. L. Olson, in *Aquatic and Terrestrial Humic Materials*, R.F. Christman and E.T. Gjessing, Editors. 1983, Ann Arbour Science: Ann Arbour, MI. p. 349-370.
115. Senesi, N., Anal. Chim. Acta, 1990. **232**: p. 51-75.
116. Mildvan, A. S. and M. Cohn, Adv. Enzym., 1970. **33**: p. 1-65.
117. McConnell, H. M., J. Chem. Phys., 1958. **28**(3): p. 430-431.
118. Kaplan, J. I. and G. Fraenkel, *NMR of Chemically Exchanging Systems*. 1st ed. 1980, New York: Academic Press. 163.
119. Langford, C. H. and T. R. Stengle, *Solvation and the Second Coordination Sphere*, in *NMR of Paramagnetic Molecules*, 1973, Editors. LaMar, G., W. Horrocks, R. Holm p. 372-386.
120. McBride, M. B., Soil Sci., 1978. **126**: p. 200-209.
121. Cousins, G. R. L., S.-A. Poulsen, and J. K. M. Saunders, Curr. Opin. Chem. Biol., 2000. **4**: p. 270-279.
122. Otto, S., R. L. E. Furlan, and J. K. M. Saunders, Drug Disc. Today, 2002. **7**(2): p. 117-125.
123. Otto, S., R. L. E. Furlan, and J. K. M. Saunders, Science, 2002. **297**(5581): p. 590-594.
124. Gamble, D.S. Can. J. Chem., 1972, **50**(16):p.2680-2690.
125. Pagenkopf, G. K. and C. Whitworth, J. Inorg. Nuc. Chem, 1981. **43**: p. 1219-1222.
126. Caceci, M. S. and A. Billon, Geochem., 1990. **15**(3): p. 335-350.
127. Riffaldi, R. and M. Schnitzer, Soil Sci. Soc. Amer. J. Div. S-3 Soil Microbio. Biochem, 1972. **36**: p. 301-305.
128. Novotny, E. H. and L. Martin-Neto, Geoderma, 2002. **106**: p. 305-317.
129. Klucakova, M., P. Pelikan, L. Lapcik, B. Lapcikova, J. Kucerik, and M. Kalab, J. Poly. Mat, 2000. **17**: p. 337-356.

130. Martin-Neto, L., O. R. Nascimento, J. Talamoni, and N. R. Poppi, Soil Sci., 1991. **151**(5): p. 369-376.
131. Senesi, N. *Application of Electron Spin Resonance and Fluorescence Spectroscopies to the Study of Soil Humic Substances*. in *10th symposium humus et planta*. 1991. Prague: Elsevier.
132. Jezierski, A., J. Drozd, M. Jerzykiewicz, Y. Chen, and K. J. Kaye, App. Magn. Reson, 1998. **14**: p. 275-282.
133. Ariese, F., S. van Assema, C. Gooijer, A. G. Bruccoleri, and C. H. Langford, Aqua. Sci., 2004. 66(1): p.89-94.
134. Scott, D. T., D. M. McKnight, E. L. Blunt-Harris, S. E. Kolesar, and D. R. Lovely, Environ. Sci. & Tech, 1998. **32**(19): p. 2984-2989.
135. Ghosh, K. and M. Schnitzer, Soil Sci. Soc. Amer. J., 1980. **44**: p. 975-978.
136. Varadachari, C., A. K. Barman, and K. Ghosh, J. Indian Soc. Soil Sci., 1983. **31**: p. 28-30.
137. Esaka, Y., N. Okumura, B. Uno, and M. Goto, Anal. Sci., 2001. **17**: p. 99-102.
138. Okumura, N. and B. Uno, Bull. Chem. Soc. Japan, 1999. **72**: p. 1213-1217.
139. Sekaly, A. L., PhD Thesis 2000, Carelton University: Ottawa.
140. Bonifazi, M., B. C. Pant, and C. H. Langford, Environ. Tech, 1996. **17**: p. 885-890.